bushfire&natural
HAZARDSCRC

A CHARACTERISATION OF SYNOPTIC WEATHER FEATURES OFTEN ASSOCIATED WITH EXTREME EVENTS IN SOUTHEAST AUSTRALIA

Stage 1 – Common features of recent events

Peter Love, Paul Fox-Hughes, Tom Remenyi, Nick Earl, Dean Rollins, Gabi Mocatta and Rebecca Harris

University of Tasmania & Bureau of Meteorology

UNIVERSITY *of* TASMANIA

Australian Government
Bureau of Meteorology

Version	Release history	Date
1.0	Initial release of document	23/07/2021

TABLE OF CONTENTS

EXECUTIVE SUMMARY

Negatively tilted upper-tropospheric troughs are a synoptic weather pattern that have been associated with the development of thunderstorms and severe weather, including extreme fire weather and tornadoes. While various case studies and some preliminary climatological analysis have been conducted in the past, a thorough investigation of the development of these synoptic features during extreme weather events has not yet been done in Australia or elsewhere. This study aimed to identify how often negatively tilted troughs occur and how often they are associated with extreme storms and fire weather.

The objectives of the project were to:

- identify the extent to which negatively tilted troughs are associated with recent extreme weather events across southeast Australia;

- assess the relationship between the occurrence of negatively tilted troughs and on-ground conditions such as elevated fire danger, high winds and/or dangerous thunderstorms;

- assess seasonality of negatively tilted troughs and any potential link with large-scale climate drivers such as the Southern Annular Mode (SAM) and Indian Ocean Dipole (IOD).

The major components of the project were:

- a review of previously documented cases of negatively tilted upper-tropospheric troughs associated with severe weather;

- a detailed case study of the role of a negatively tilted upper-tropospheric trough in the extreme fire weather during the January 2003 Canberra bushfires;

- a detailed case study of the role of a negatively tilted upper-tropospheric trough in the development of a tornado outbreak in Perth in July 2014;

- a climatology of negatively tilted upper-tropospheric troughs in southern Australia for the period 1990-2018 and their relationship with severe weather reported in the Bureau of Meteorology Severe Storms Archive.

REVIEW OF PREVIOUSLY DOCUMENTED CASES

- A wide range of locations, dates, impacts and morphologies of negatively tilted upper-tropospheric troughs was observed, establishing a very broad scope for the climatological analysis.

JANUARY 2003 CANBERRA BUSHFIRES

- This event showed similar characteristics to the negatively tilted upper-tropospheric troughs associated with three other severe fire weather events in southeast Australia.

- The negatively tilted upper-tropospheric trough occurred a long way to the south but strong evidence was found that an associated upper-tropospheric dry air intrusion could have reached well over the continent

and played a role in the sudden drying event observed in Canberra on the day.

- Interactions between the negatively tilted upper-tropospheric trough and a weaker trough to the northwest were likely the origin of a broad dry band positioned over Bass Strait during the fire event and which was connected at low levels to the dry intrusion and dry air over the continent.

JULY 2014 PERTH TORNADOES

- Strong upper-tropospheric divergence associated with a negatively tilted upper-tropospheric trough and its interaction with another trough to the northeast resulted in ascending air over southwest Western Australia.

- This vertical circulation reinforced strong dynamic forcing at the surface favourable for the formation of tornadoes.

- Gravity wave processes in the upper-tropospheric jet at the apex of the negatively tilted upper-tropospheric trough could have played a role in coupling lower- and upper-tropospheric circulation in the frontal zone.

CLIMATOLOGY

- Several distinct patterns of negatively tilted upper-tropospheric trough development in southern Australia were evident.

- Negatively tilted upper-tropospheric trough were present in the region close to 7 % of the time, or roughly 2.5 times per month.

- There was a strong semi-annual cycle peaking in June-July and November-January.

- Over 40 % of the 862 negatively tilted upper-tropospheric trough events identified over the 1990-2018 period in the BARRA dataset were associated with a report in the Bureau of Meteorology Severe Storms Archive

- Severe weather was nearly twice as likely to occur when a negatively tilted upper-tropospheric trough was present.

- The two peaks in the semi-annual cycle appear to be the combination of anti-phased annual cycles in different regimes of northern and southern subregions, related to the annual migration of the subtropical ridge.

- Statistically significant preferences for negatively tilted upper-tropospheric trough occurrence was observed during the negative phase of the Southern Annular Mode (SAM) and during the negative and neutral phases of the Indian Ocean Dipole (IOD).

- There was an indication of a reduction in negatively tilted upper-tropospheric trough occurrence during El Niño, however, these differences were not statistically significant.

- Other biases towards negatively tilted upper-tropospheric trough occurrence were associated with more complicated combinations of season with the states of multiple regional climate drivers.

While modern numerical weather prediction (NWP) systems are increasingly capable of resolving the surface weather parameters associated with severe weather events, there are known deficiencies. An example of this is the over-estimation of low winds and under-estimation of high winds common to numerous models. Better understanding of the role of features such as NTT in generating surface weather helps interpretation and refinement of the NWP output, particularly for users of weather data such as emergency services agencies.

Furthermore, as products from NWP such as sub-seasonal to seasonal outlooks become more refined, there is value in recognising the occurrence of potential impacts of NTT that may be resolved at the synoptic or sub-synoptic scale in such model configurations even if the potential severity of the weather parameters are note explicitly resolved. For example, if a sub-seasonal to seasonal model ensemble shows a high probability of a NTT occurrence in a particular region a certain number of weeks in advance, that is useful information for planning and preparedness for emergency services managers.

Thus, this sort of synoptic climatological study in combination with detailed analyses of particular events continues to be of great relevance to natural hazard prediction and management.

FUTURE WORK

- The material in the case studies and climatology sections of this report would each form the basis for manuscripts to be published in peer-reviewed literature for the benefit of enhanced scrutiny, credibility and broad dissemination of the results.

- Climatological analysis of numerical severe weather indicators using BARRA, in combination with the NTT climatology compiled in this study, would establish more specific relationships between particular severe weather phenomena with the distinct NTT morphologies and locations observed.

- Similar climatological analysis could be applied to regional climate projections to assess projected changes to NTT occurrence in the future.

- A climatology of vertical motions across the entire BARRA-R domain was compiled during the project. The climatology is to be shared with the meteorological community and would make a valuable subject of further publications in peer-reviewed literature.

END-USER STATEMENT

Sandra Whight, *Community Services, Bureau of Meteorology, Tasmania*

Negatively tilted troughs are associated with a range of severe weather in Australia and more generally. While meteorologists are aware of the potential for them to deliver impactful events, it is valuable to have a better understanding of the mechanisms by which these events occur, and their frequency and distribution. This project has examined several significant NTT case studies, including fire and severe thunderstorm events, and has compiled the first Australian climatology of the occurrence of NTTs. As such, it provides a useful reference to operational meteorologists, and context for further study of this phenomenon.

Eddie Staier, *Fire Management Office, Tasmanian Parks and Wildlife Service, Tasmania*

As a fire practitioner and fire behaviour analyst it is very important to have a good understanding about the weather drivers that will impact on fire behaviour. As a Fire Duty Officer planning and preparing for response it is important to have an understanding of the predicted weather influencers and how they might change the forecast. The work on Negatively Tilted Troughs and their influence on extreme weather gives us a better understanding of when and how we can expect conditions to vary from the forecast and gives us the opportunity to put trigger's in place to react to any variance.

Chris Irvine, *Flood Policy Unit, Tasmania State Emergency Service, Tasmania*

This project has provided an important insight into the role Negatively Tilted Troughs can play in the development of extreme weather events in south east Australia and Tasmania. The State Emergency Service (SES) is working with the Bureau of Meteorology to incorporate this knowledge into the weather briefing services provided by the Bureau to SES. This knowledge will be used by the State Emergency Service to inform its operational preparedness and public information messaging prior to forecast and expected extreme weather events in Tasmania.

1 INTRODUCTION

Negatively tilted upper-tropospheric troughs have been associated with the development of thunderstorms and severe weather, including extreme fire weather and tornadoes. Although relatively rare events, preliminary assessments suggest they may have been associated with many of the major disasters that have occurred in Australia such as the Canberra bushfires of 2003 (Fox-Hughes, 2015), the Cobbler Rd, NSW, grassfire of 2013 (Bureau of Meteorology, 2017), and the Hobart Cup Day thunderstorm of 2014 (Fox-Hughes, 2014).

Various case studies of severe weather events in Australia have noted the presence of negatively tilted upper-tropospheric troughs and their likely role in the occurrence of particular surface weather phenomena. Some climatological studies of severe weather phenomena have also inferred the association of negatively tilted upper-tropospheric troughs. In relation to tornadoes, Fox-Hughes et al. (1996, 2018) describe two events in northern Tasmania, while composite upper-tropospheric synoptic patterns associated with tornadoes derived by Hanstrum et al. (2002) exhibited the characteristics of negatively tilted upper-tropospheric troughs.

In a case study of extreme fire weather in southeast Tasmania, Fox-Hughes (2012) examined the role of a negatively tilted upper-tropospheric trough, and similar to Hanstrum et al. (2002), the composite synoptic analysis of days associated with sudden spikes in fire danger in Tasmania by Fox-Hughes (2015) revealed a negatively tilted upper-tropospheric trough pattern.

Similar studies have been carried out in other regions around the world, most notably in North America. The regionally based climatological studies mention above were preceded by statistical analyses of upper-tropospheric tilt associated with convection in the eastern Great Plains region (MacDonald and Ward, 1974; MacDonald, 1976; Glickmann et al., 1977). Evenson and Johns (1995) generated composite analyses associated with severe weather reports in northwest USA and identified negatively tilted upper-tropospheric troughs as one of three characteristic patterns that resulted.

Speer and Leslie (2000) assessed the phase of the Indian Ocean Dipole (IOD) at the time of the negatively tilted upper-tropospheric trough events noted in their study. However, they considered only three events and in each case the IOD phase was different. No other attempts to characterise the relationship of negatively tilted upper-tropospheric troughs with Australian regional climate drivers were identified during the literature survey.

A thorough investigation of the development of these synoptic features during extreme weather events has not yet been done in Australia or elsewhere. Furthermore, while climatological studies such as Hanstrum et al. (2002), Fox-Hughes (2015) and Evenson and Johns (1995) implicate negatively tilted upper-tropospheric troughs in relation to certain reported extreme weather events, they do not address the frequency with which they occur in the absence of reports. This limits the ability to generalise to new places and events and predict which events have the potential to escalate to dangerous weather events. This will become even more important in the future, as extreme events are projected to

increase in frequency and intensity across Australia as the climate continues to change.

The objectives of the project are to:

- identify the extent to which negatively tilted troughs are associated with recent extreme weather events across southeast Australia;

- assess the relationship between the occurrence of negatively tilted troughs and on-ground conditions such as elevated fire danger, high winds and/or dangerous thunderstorms;

- assess seasonality of negatively tilted troughs and any potential link with large-scale climate drivers such as the Southern Annular Mode (SAM) and Indian Ocean Dipole (IOD).

This will provide important information of relevance to fire managers and emergency services managing extreme storm impacts, for government and the broader community. This study aims to identify how often negatively tilted troughs occur and how often they are associated with extreme storms and fire weather. If they are associated with large scale climate drivers, there may be a possibility of improving seasonal forecasts of some extreme events.

The remainder of this report is structured as follows. Section 2 gives a brief description of the main datasets used in this study. Section 3 provides an overview of negatively tilted upper-tropospheric troughs in the Australian region, introducing some definitions and reviewing the literature discussing severe weather events associated with this weather pattern. A detailed investigation of some case studies of negatively tilted upper-tropospheric troughs associated with severe weather events is given in section 4. The development and analysis of a climatology of negatively tilted upper-tropospheric troughs and their association with severe weather is described in section 5. Finally, section 6 is a summary of the main results, implications and pathways for future research on negatively tilted upper-tropospheric troughs (hereafter NTT).

2 DATA

2.1 AUSTRALIAN REGIONAL REANALYSIS

The Australian Bureau of Meteorology (BoM) Atmospheric high-resolution Regional Reanalysis for Australia (BARRA) (Su et al., 2019) is a gridded dataset describing the weather of the Australian region from 1990 to 2019. As with other reanalysis products, BARRA is created by rerunning a numerical weather forecast model constrained by atmospheric observations over the historical period to create a consistent climate record. The high-resolution gridded output represents the best estimate of the state of the atmosphere based on the combination of atmospheric observations and the dynamical relations governing the Earth system. BARRA uses the Unified Model version 10.2 forecast model (Davies et al. 2005) and the UKMO VAR 4-dimensional variational data assimilation system (Rawlins et al., 2007). Observations ingested are those employed by BoM's operational numerical weather prediction system. ERA-Interim global reanalysis provides initial and lateral boundary conditions.

The BARRA model domain covers Australia, New Zealand, the maritime continent, the Southern Ocean south of Australian and much of the Indian Ocean to the west. Gridded outputs are provided at 12 km horizontal resolution on 21 pressure levels with hourly temporal resolution. Additionally, the outputs have been dynamically downscaled over four subdomains over southern Australia to produce further outputs at 1.5 km horizontal resolution. The regional 12 km domain outputs are referred to as BARRA-R while the four subdomains are BARRA-TA (Tasmania), BARRA-AD (South Australia), BARRA-SY (eastern NSW) and BARRA-PH (southwest Western Australia) as depicted in Figure 2-1.
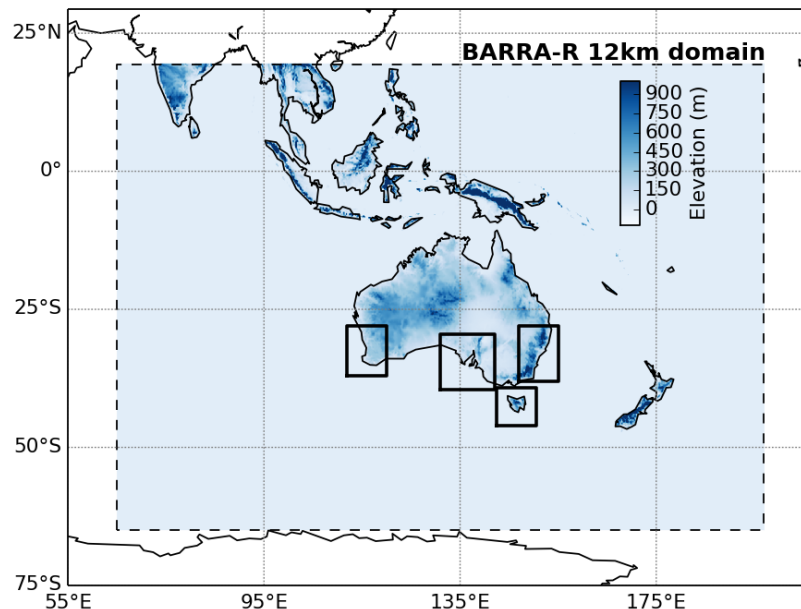
FIGURE 2-1 AUSTRALIAN BUREAU OF METEOROLOGY ATMOSPHERIC HIGH-RESOLUTION REGIONAL REANALYSIS FOR AUSTRALIA (BARRA) SPATIAL DOMAIN AND NESTED SUBDOMAINS.

2.2 SEVERE STORMS ARCHIVE

The BoM Severe Storms Archive is a database of severe weather reports contributed by BoM weather observers as well as subjective reports from members of the public. Reports describe the date/time, location and type of severe weather events, usually accompanied by plain language descriptive comments. The "severe phenomena" recorded in the database are:

- Severe wind gusts (> 90 km/h)

- Damaging hail (diameter > 2 cm)

- Tornadoes

- Heavy rainfall conducive to flash flooding

- Lightning resulting in serious injury or death

- Waterspouts

- Damaging dust-devils

Severe phenomena are grouped by "event" which is the development, lifetime and decay of an individual thunderstorm or squall line. Natural hazards explicitly excluded from the database are:

- Most phenomena directly related to tropical cyclones

- Severe winds at sea (except waterspouts near the shore)

- Fire weather events

- Riverine flooding

- Non-severe events

- Extreme temperature events

- Earthquakes, tsunamis & landslides

The nature of reporting for the database leads to known biases. There is an increasing trend in the number of events that results from increases in population and the spread of population. Additionally, the spatial distribution of events over the country is influenced by the distribution of the population, leading to more recorded events in regions of higher population density. Since this study is concerned primarily with the overall statistics during the reanalysis period, and considers regional variations on very large scales, these limitations on the database are considered acceptable for achieving a broad perspective.

2.3 REGIONAL CLIMATE DRIVER INDICES

The variability in various large-scale atmospheric and oceanic circulations is known to have direct influences on Australian climate. The principal examples of these regional climate drivers are the Southern Annular Mode (SAM), the Indian Ocean Dipole (IOD) and the El Niño Southern Oscillation (ENSO). A range of quantitative measures exists that describe the variability of these phenomena, typically as a time series index with temporal resolutions between daily and monthly.

2.3.1 Southern Annular Mode

The SAM describes the latitudinal variability of the mid- to high-latitude band of westerly winds in the southern hemisphere. This variation affects the paths of weather systems across southern Australia causing a range of impacts on rainfall and temperature (Hendon et al., 2007), and was anticipated to have the strongest relationship with NTT. It is characterised by the difference in zonal mean sea level pressure between 40°S and 65°S (Gong and Wang, 1999). The index used to describe the SAM in this study was the Antarctic Oscillation (AAO) obtained from the US National Weather Service (NWS) Climate Prediction Center (CPC) (https://www.cpc.ncep.noaa.gov/products/precip/CWlink/daily_ao_index/aao/aao.shtml). Monthly mean values of the index were used to describe the phase of the SAM as either positive or negative.

2.3.2 Indian Ocean Dipole

The IOD describes the east-west sea surface temperature (SST) difference and associated atmospheric circulation in the northern Indian Ocean. When SST northwest of Australia is warmer than usual (negative IOD phase) there is greater moisture availability generally resulting in increased rainfall across parts of southern Australia. When the SST is cooler than usual (positive IOD phase) the opposite is generally true resulting in lower rainfall. The IOD index used in this study was the Dipole Mode Index (DMI) provided by the US National Oceanic and Atmospheric Administration (NOAA) Physical Sciences Laboratory, which is based on the HadISST1.1 SST dataset (https://psl.noaa.gov/gcos_wgsp/Timeseries/Data/dmi.had.long.data). Positive and negative IOD phases are characterised by DMI values greater or less than 0.5 standard deviations of the full time series for at least 3 months (Saji and Yamagata, 2003).

2.3.3 El Niño Southern Oscillation

The El Niño Southern Oscillation refers to the changes between El Niño and La Niña conditions, characterised by warm and cool (respectively) temperature anomalies in the eastern equatorial Pacific Ocean and the variation of surface pressure between Darwin and Tahiti. During El Niño conditions eastern Australia frequently receives lower than average winter-spring rainfall while winter-spring rainfall is typically above average in eastern and central Australia during La Niña conditions. Various indices describing ENSO are readily available, three of which were applied in the present study as described below.

Southern Oscillation Index

The Southern Oscillation Index (SOI) describes the difference in surface pressure between Darwin and Tahiti. Variations in the SOI give a good indication of El Niño and La Niña event development and intensity. The monthly SOI data applied in the present study were provided by BoM (ftp://ftp.bom.gov.au/anon/home/ncc/www/sco/soi/soiplaintext.html).

NIÑO Sea Surface Temperatures

The NIÑO indices directly measure sea surface temperatures associated with ENSO by averaging SST over defined regions of the tropical Pacific Ocean, or combinations of those regions. The NIÑO1+2, NIÑO3, NIÑO3.4 and NIÑO4 indices were used in this study. The monthly average NIÑO SST data were taken from the US NWS CPC Optimum Interpolation OISST.v2 dataset (https://www.cpc.ncep.noaa.gov/data/indices/sstoi.indices).

Oceanic Niño Index

The Oceanic Niño Index (ONI) is a 3-month running mean of the SST in the NIÑO3.4 region of the central equatorial Pacific Ocean, as calculated from the Extended Reconstructed SST (ERSSTv5) dataset. El Niño and La Niña episodes are defined by the ONI exceeding ±0.5 for 5 consecutive months. The ONI data were provided by the US NWS CPC (https://www.cpc.ncep.noaa.gov/data/indices/oni.ascii.txt).

3 NEGATIVELY TITLED UPPER-TROPOSPHERIC TROUGHS

3.1 DEFINITIONS

Troughs and ridges are defined in any number of reference texts, for example, Milrad (2018) states that: "On upper-tropospheric height charts, troughs are axes of geopotential height minima, while ridges are axes of geopotential maxima." Milrad (2018) goes on to define the trough axis or equivalently the trough line thus: "Trough axes should be drawn through the line of maximum positive curvature such that geopotential heights on either side of the trough axis are larger than along the axis itself."

Previous studies of NTT have not always assumed the strict definition. MacDonald and Ward (1974), MacDonald (1976) and Glickman et al. (1977) took a simpler approach, presumably to speed up the processing of hundreds of charts: "The trough lines ... were determined by connecting the points on each height contour ... where the respective contour reached its lowest latitude in and around the area of the study."

Machta (1949) introduced a new solution to the plane nondivergent vorticity equation (Rossby, 1939) in which trough and ridge lines could assume an arbitrary angle, or "tilt", from meridians. This model was able to explain the net midlatitude poleward flux of absolute angular momentum, that Jeffreys (1926) had noted must be present, through the asymmetry in troughs and ridges as proposed by Starr (1948). The mathematical convention of this model was chosen such that, in the northern hemisphere, the more frequently observed northeast to southwest tilted troughs which were responsible for the positive northward angular momentum flux were associated with a positive angle describing the tilt of the troughs. Thus, a northern hemisphere trough line oriented northwest to southeast was associated with a negative angle and hence negative tilt (and a negative, or equatorward, angular momentum flux). In the southern hemisphere the convention is reciprocated so that a trough oriented from southwest to northeast has a negative angle and is referred to as negatively tilted. Troughs with axes that are oriented along meridians, that is with zero angle, are referred to as neutral or neutrally tilted.

An example of a negatively tilted upper-tropospheric trough in the BARRA-R 300 hPa geopotential height field for the Australian region is given in Figure 3-1 where the trough axis is indicated by a red line. Characterising the tilt in a trough axis is not always as straight forward as it is in this example, as an axis can exhibit considerable curvature and include regions of positive, neutral and negative tilt.
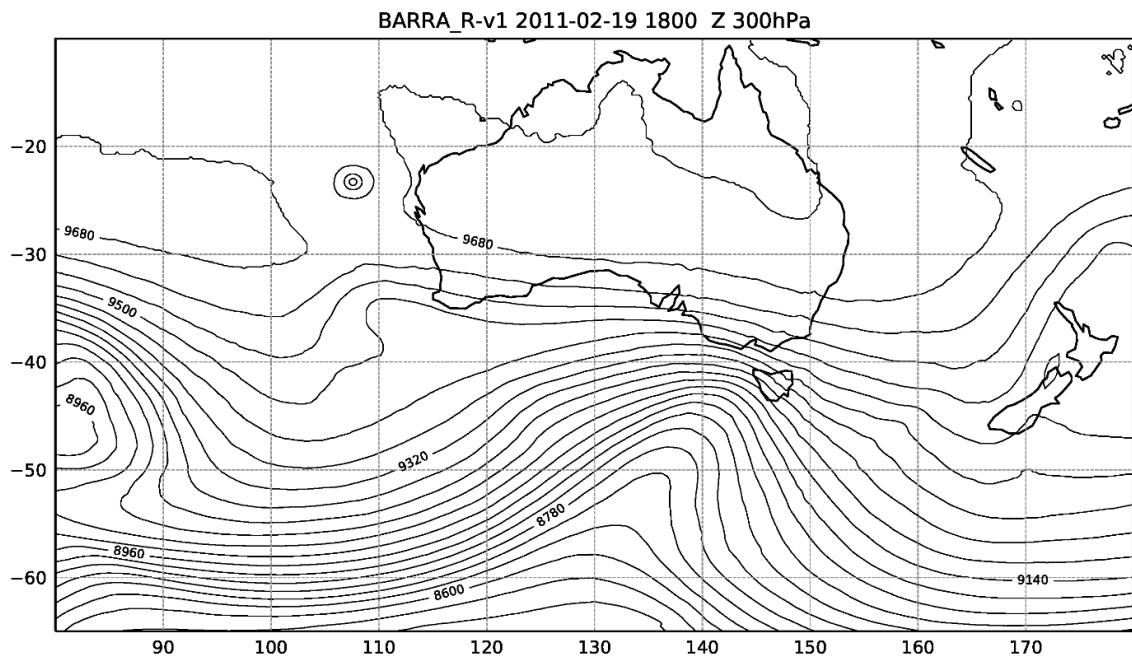
FIGURE 3-1 BARRA-R GEOPOTENTIAL HEIGHT CONTOURS (METRES) AT 300 HPA ON 19 FEBRUARY 2011. THE NEGATIVELY TILTED TROUGH AXIS IS INDICATED BY THE RED LINE

3.2 DOCUMENTED SEVERE WEATHER EVENTS RELATED TO NTT

In order to understand the range of impacts incurred by NTT and assist in the characterisation of NTT in the historical record, a review of NTT events during the 1990-2018 period that have been documented in peer reviewed literature was conducted. The list of events documented in this section is almost certainly not comprehensive and is separated into two parts. The first includes events where a NTT has been identified explicitly in a study describing a severe weather event. Publications that describe severe weather events that are known anecdotally or otherwise to be associated with NTT, but where NTT are not mentioned explicitly are listed in the second part. Each case is accompanied by a visual reassessment of the upper-tropospheric synoptic situation with the BARRA-R 300 and 500 hPa geopotential height fields. Also plotted in these fields are the locations where severe weather has been recorded in the SSA. The times chosen for the plots are intended to best represent the characteristics of the NTT involved and so do not always coincide exactly with the associated surface impacts, hence, some plots do not feature any severe weather markers.

3.2.11 NTT Directly Implicated

1990-04-19 Floods over eastern Australia

During the period of 17-22 April 1990 heavy rain occurred over much of eastern Australia. The event was associated with an upper-tropospheric cut-off low as described in detail by Mills and Russell (1992). On 19 April the well developed upper cut-off low narrowed and began to assume a negative tilt with significantly decreasing wavelength to the downstream ridge. The onset of negative tilting in the cut-off low can be seen in the BARRA-R geopotential height at 300 hPa in Figure 3-2. As the negative tilt progressed, the peak in the subgeostrophic flow around the apex of the trough moved around to the northeast side of the trough at the same time as the supergeostrophic flow associated with the increasing anticyclonic curvature of the downstream ridge was also increasing in strength and proximity. This resulted in a localised region of strong divergence over NSW. Cyclogenesis downstream of an inverted trough in the surface easterlies over eastern Australia at the time was associated with this strong upper-tropospheric divergence (lee-trough effects due to the easterly flow over the Great Dividing Range also played a role in enhancing surface convergence). Mills and Russell (1992) note that this pattern is consistent with Bjerknes (1954) and shares similar characteristics with previous case studies (Moore and Abeling, 1988; Uccellini et al., 1984; Velden and Mills, 1990).

Speer and Leslie (2000) also note an NTT associated with an east coast low and extended heavy rainfall at Coffs Harbour, NSW, in April 1990, however, they do not specify the exact date. They cite an accumulated rainfall of 296 mm over a three-day period, which according to BoM records occurred on 4-6 April. This does coincide with a broad shallow NTT over central eastern Australia, however, there is no indication of an ECL at that time so there is some ambiguity as to whether they are referring to the early April event or the ECL that developed as described in Mills and Russell (1992).

FIGURE 3-2 BARRA-R GEOPOTENTIAL HEIGHT CONTOURS (METRES) AT 300 HPA (LEFT) AND 500 HPA (RIGHT) ON 19 APRIL 1990 AT 1200 UTC. SEVERE

WEATHER REPORTED IN THE BUREAU OF METEOROLOGY SEVERE STORMS ARCHIVE DURING THE FOLLOWING 6 HOURS IS INDICATED BY THE MARKERS DEFINED IN THE LEGEND AT TOP RIGHT.

1922-11-22 Tornadic thunderstorm in Smithton, Tasmania

Widespread high winds and damage to property was reported across southeast Australia on 21-22 November 1992, including the occurrence of an F3 tornado passing through Smithton in northwest Tasmania. The tornado occurred following the passage of a cold front across the region, with a strong jet streak positioned over northern Tasmania as described by Fox-Hughes et al. (1996). A narrow NTT with a sharp apex in the vicinity of Bass Strait was situated on the northeast flank of a longwave trough south of Western Australia, as shown in Figure 3-3 several hours prior to the tornado. Following the passage of the surface front, very cold middle to upper-level air advected from higher latitudes by the longwave trough moved over Tasmania with the passage of the NTT at the same time as lower-level air over northern Tasmania was warming, leading to significant instability just prior to the tornado. The exact nature of the thunderstorm was not be determined by Fox-Hughes et al. (1996) due to the lack of observations and the low resolution modelling performed at the time, with various factors suggesting the occurrence or otherwise of a supercell thunderstorm.

FIGURE 3-3 BARRA-R GEOPOTENTIAL HEIGHT CONTOURS (METRES) AT 300 HPA (LEFT) AND 500 HPA (RIGHT) ON 21 NOVEMBER 1992 AT 1200 UTC. SEVERE WEATHER REPORTED IN THE BUREAU OF METEOROLOGY SEVERE STORMS ARCHIVE DURING THE FOLLOWING 6 HOURS IS INDICATED BY THE MARKERS DEFINED IN THE LEGEND AT TOP RIGHT.

1998-12-26 Sydney to Hobart yacht race

During the 1998 Sydney to Hobart yacht race, storm force winds on 27 December caused many of the yachts to retire, sink, or be abandoned with many crew requiring rescue and six crew losing their lives. Mills (2001) describes the complicated evolution of this event in detail. Briefly, the synoptic development of the event is characterised by a strong upper-tropospheric trough south of the Great Australian Bight which became negatively tilted and cut off (Figure 3-4). A surface low formed over Victoria in association with the upper-level cut-off low

and deepened into a major cyclone as it moved through eastern Bass Strait and merged with southwestward moving low at lower latitude in the Tasman Sea. Mills (2000) suggests that the vertical circulation resulting from an isentropic potential vorticity filament associated with the NTT was responsible for the development of a secondary low which in turn was the cause of the storm force winds.

FIGURE 3-4 BARRA-R GEOPOTENTIAL HEIGHT CONTOURS (METRES) AT 300 HPA (LEFT) AND 500 HPA (RIGHT) ON 26 DECEMBER 1998 AT 0600 UTC. SEVERE WEATHER REPORTED IN THE BUREAU OF METEOROLOGY SEVERE STORMS ARCHIVE DURING THE FOLLOWING 6 HOURS IS INDICATED BY THE MARKERS DEFINED IN THE LEGEND AT TOP RIGHT.

2002-11-07 Extreme fire weather in southeast Tasmania

The forest fire danger index (FFDI) at Hobart Airport on 7 November 2002 exceeded 24 (fire danger rating of "very high") in the early afternoon, increasing throughout the afternoon and spiking to well over 100 in the early evening just prior to the passage of two fronts. A second peak in FFDI occurred later in the evening. Fox-Hughes (2012) investigated the causes of the event and found that a band of warm dry air ahead of the fronts originated in the middle-troposphere south of Western Australia several days earlier. After following a descending trajectory northeast over south coast the air mass subsided further as it was advected southeastward over Tasmania where thermal mixing and föehn effects brought the dry air to the surface. At the time of the event an NTT was situated southwest of Tasmania (Figure 3-5). The vertical circulation associated with a jet entrance on the northeast flank of the NTT was likely responsible for the descent of dry high-momentum air from the upper troposphere near the trough apex down to the top of the mixed layer over Tasmania where it was subject to mixing down to the surface.

FIGURE 3-5 BARRA-R GEOPOTENTIAL HEIGHT CONTOURS AT 300 HPA (LEFT) AND 500 HPA (RIGHT) ON 7 NOVEMBER 2002 AT 0600 UTC. SEVERE WEATHER REPORTED IN THE BUREAU OF METEOROLOGY SEVERE STORMS ARCHIVE DURING THE FOLLOWING 6 HOURS IS INDICATED BY THE MARKERS DEFINED IN THE LEGEND AT TOP RIGHT.

2003-10-25 Extensive intense thunderstorm activity over NSW-QLD.

In their analysis of east Australian severe thunderstorms associated with satellite detection of enhanced-V features, Feren (2008) notes several cases where the synoptic situation featured NTTs. The first of these was during a widespread outbreak of very severe weather along the east coast of New South Wales and Queensland. An NTT over southeast Australia at the exit of an upper-level jet was approaching a slow-moving ridge to the east. The NTT and its association with widespread severe hail and rain reports are shown in Figure 3-6. This pattern bears similarities to the April 1990 flooding case described above, with Feren (2008) comparing the event to the same prior studies cited by Mills and Russell (1992). Accordingly, it was speculated that strong divergence occurred downstream of the trough enhancing convection in the region.
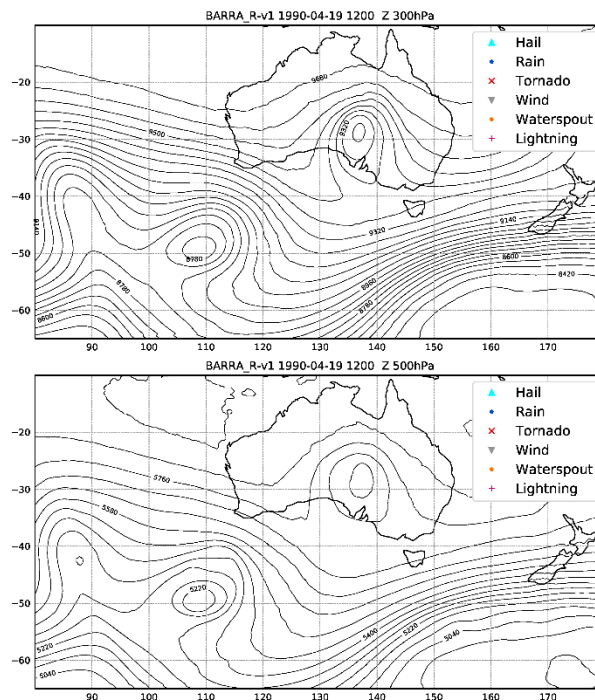
FIGURE 3-6 BARRA-R GEOPOTENTIAL HEIGHT CONTOURS AT 300 HPA (LEFT) AND 500 HPA (RIGHT) ON 25 OCTOBER 2003 AT 0000 UTC. SEVERE WEATHER REPORTED IN THE BUREAU OF METEOROLOGY SEVERE STORMS ARCHIVE DURING THE FOLLOWING 6 HOURS IS INDICATED BY THE MARKERS DEFINED IN THE LEGEND AT TOP RIGHT.

2005-01-11 Wangary Eyre Peninsula severe bushfire.

On 11 January 2005 a severe bushfire occurred on Eyre Peninsula, South Australia, causing extensive damage to property and loss of livestock. In a pattern similar to the 2002 Hobart event described by Fox-Hughes (2012) a dramatic increase in FFDI occurred prior to the passage of a cold front with a second spike following the front. Mills (2008a) attribute rapid surface drying and strong winds to vertical circulations associated with a strong NTT southwest of the affected area and a subtle short-wave trough over the west of South Australia. The NTT can be seen Figure 3-7 south of the continent with some similarity to the 2002 Hobart event although much larger in scale. Mills (2008a) infers that the interaction of the strong jet wrapping around the apex off the NTT with a smaller jet associated with the short-wave trough (not discernible in Figure 3-7) lead to convergence and descent of upper-tropospheric air to the top of the mixed layer ahead of the front. Subsequent mixing by dry convection, possibly assisted by the descent associated with acceleration in the entrance region of a low-level prefrontal jet, brought this dry high-momentum air to the surface. A sloping region of descending, very dry air connected the upper-tropospheric jet in the region of the NTT apex with the descending region of the cross-frontal circulation, causing the post-frontal surface drying.
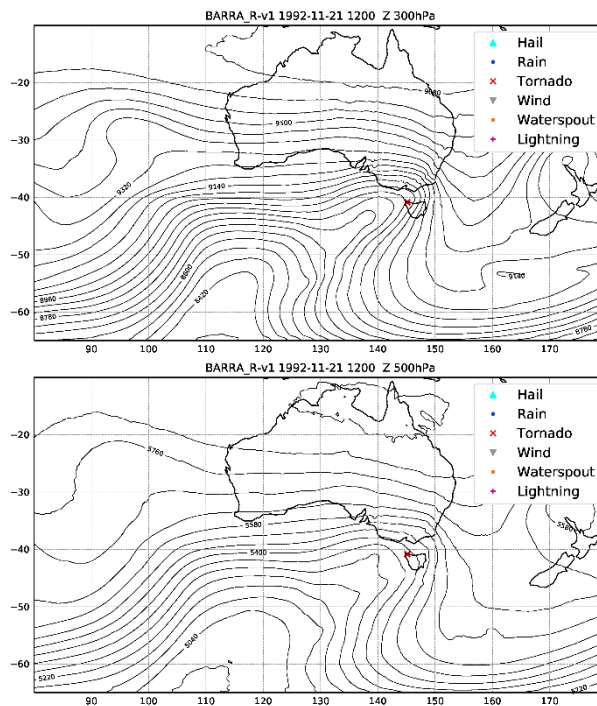
FIGURE 3-7 BARRA-R GEOPOTENTIAL HEIGHT CONTOURS (METRES) AT 300 HPA (LEFT) AND 500 HPA (RIGHT) ON 11 JANUARY 2003 AT 0000 UTC. SEVERE WEATHER REPORTED IN THE BUREAU OF METEOROLOGY SEVERE STORMS ARCHIVE DURING THE FOLLOWING 6 HOURS IS INDICATED BY THE MARKERS DEFINED IN THE LEGEND AT TOP RIGHT.

2005-10-24 Large hail on New South Wales-Queensland coast

Feren (2008) describes another large outbreak of severe thunderstorms that caused large hail along the coast of New South Wales and Queensland on 24 October 2005. A cut-off upper-tropospheric low centred over the South Australian-Victorian coast had become negatively tilted as it moved slowly eastward (Figure 3-8). A localised region of strong divergence was identified in the highly diffluent region downstream of the NTT, within which most of the severe thunderstorms occurred.
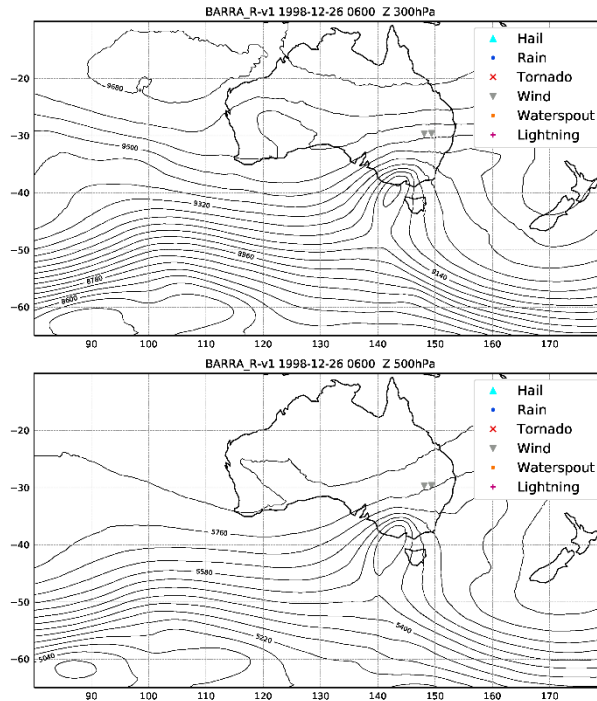

FIGURE 3-8 BARRA-R GEOPOTENTIAL HEIGHT CONTOURS (METRES) AT 300 HPA (LEFT) AND 500 HPA (RIGHT) ON 24 OCTOBER 2005 AT 0600 UTC. SEVERE

WEATHER REPORTED IN THE BUREAU OF METEOROLOGY SEVERE STORMS ARCHIVE DURING THE FOLLOWING 6 HOURS IS INDICATED BY THE MARKERS DEFINED IN THE LEGEND AT TOP RIGHT.

2005-11-27 Brisbane tornado

An F2 tornado and large hail occurred in the outer suburbs of Brisbane on 11 November 2005, with large hail also reported in nearby coastal regions. Again sharing similarities with previous cases in the region, the associated thunderstorms occurred in a region of strong divergence in a jet propagating around the apex of an intensifying trough towards a shortwave ridge to the east, as described by Feren (2008). The trough can be seen over southeast Australia in Figure 3-9 in relation to the location of the tornado and hail reports, several hours before the tornado occurred and as the trough was in the process of becoming negatively tilted.

FIGURE 3-9 BARRA-R GEOPOTENTIAL HEIGHT CONTOURS (METRES) AT 300 HPA (LEFT) AND 500 HPA (RIGHT) ON 27 NOVEMBER 2005 AT 0600 UTC. SEVERE WEATHER REPORTED IN THE BUREAU OF METEOROLOGY SEVERE STORMS ARCHIVE DURING THE FOLLOWING 6 HOURS IS INDICATED BY THE MARKERS DEFINED IN THE LEGEND AT TOP RIGHT.

2005-12-06 East Victoria severe thunderstorm outbreak, large hail

An outbreak of severe thunderstorms over eastern Victoria resulted in large hail reports across the region on 7 December 2005. The hail fell in the early morning, a rare event in eastern Australia. Feren (2008) notes that the event was associated with a fast moving short-wave NTT, which can be seen in Figure 3-10 extending from Bass Strait across the Victorian coast and inland from the New South Wales coast. The NTT was positioned in the exit region of an upper-level jet with strong divergence ahead of the NTT and low inertial stability in the anticyclonic exit region of the jet.
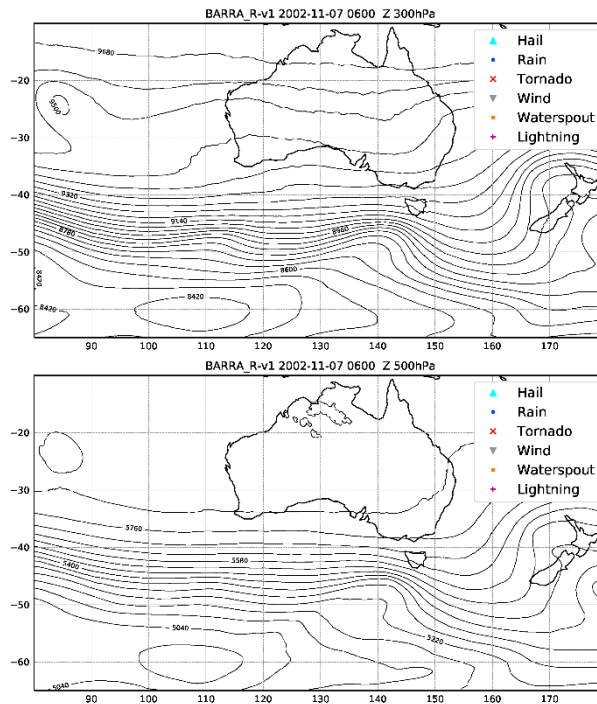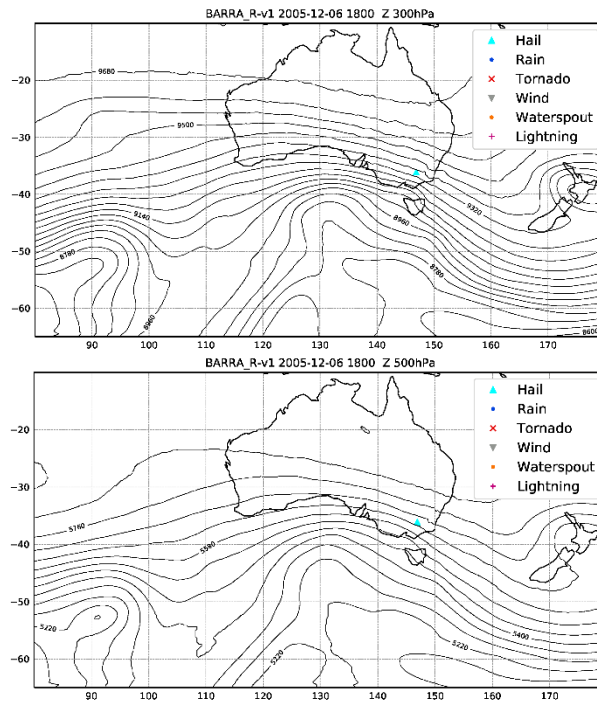
FIGURE 3-10 BARRA-R GEOPOTENTIAL HEIGHT CONTOURS (METRES) AT 300 HPA (LEFT) AND 500 HPA (RIGHT) ON 6 DECEMBER 2005 AT 1800 UTC. SEVERE WEATHER REPORTED IN THE BUREAU OF METEOROLOGY SEVERE STORMS ARCHIVE DURING THE FOLLOWING 6 HOURS IS INDICATED BY THE MARKERS DEFINED IN THE LEGEND AT TOP RIGHT.

2009-04-15 Scottsdale tornado

During the morning of 15 April 2009 a squall line crossed northern Tasmania resulting in widespread damage to houses, power infrastructure and trees. Damage patterns and one witness report were consistent with the occurrence of several tornadoes. The squall line was associated with a strong NTT extending from deep in the Southern Ocean to the south coast of Australia just west of Tasmania (Figure 3-11). The weather and damage observations of this event along with a summary of the synoptic and mesoscale situation at the time is described by Fox-Hughes et al. (2018).

FIGURE 3-11 BARRA-R GEOPOTENTIAL HEIGHT CONTOURS (METRES) AT 300 HPA (LEFT) AND 500 HPA (RIGHT) ON 14 APRIL 2009 AT 1800 UTC. SEVERE WEATHER REPORTED IN THE BUREAU OF METEOROLOGY SEVERE STORMS ARCHIVE DURING THE FOLLOWING 6 HOURS IS INDICATED BY THE MARKERS DEFINED IN THE LEGEND AT TOP RIGHT.

2011-03-22 Wilsons Prom extreme rainfall

Extreme rainfall causing flooding and landslide occurred at Wilsons Promontory, Victoria, on 22-23 March 2011. Taylor et al. (2013) describe how warm air advection associated with low pressure centres along the southeast coast of Australia combined with orographic lifting of gale force easterly winds to produce the heavy rainfall. These processes were enhanced by divergence associated with a shallow cut-off upper-tropospheric low to the west. The negative tilt in this low can be seen at 300 hPa in Figure 3-12. A further contribution to the upper-tropospheric divergence occurred in the exit region of a jet streak over southern New South Wales.
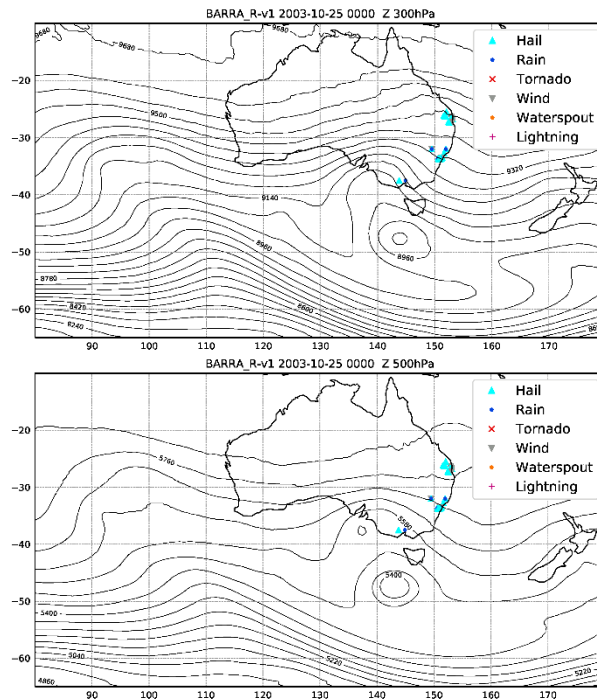
FIGURE 3-12 BARRA-R GEOPOTENTIAL HEIGHT CONTOURS (METRES) AT 300 HPA (LEFT) AND 500 HPA (RIGHT) ON 14 APRIL 2009 AT 1800 UTC. SEVERE WEATHER REPORTED IN THE BUREAU OF METEOROLOGY SEVERE STORMS ARCHIVE DURING THE FOLLOWING 6 HOURS IS INDICATED BY THE MARKERS DEFINED IN THE LEGEND AT TOP RIGHT.

2013-01-08 Cobbler Road fire, NSW

A fire in rural New South Wales on 8-9 January 2013 caused significant damage and loss of livestock. The fire danger at the time was extreme and eased little overnight. Bureau of Meteorology (2017) describe the meteorological conditions in relation to comparative fire spread simulations of the event. A heat trough running the continent from northwest to southeast passed over the area late in the afternoon ahead of a weak cold front. A very deep mixed layer had the potential to mix strong winds from the middle-troposphere to the surface. An upper-tropospheric trough also passed over the region overnight, becoming negatively tilted later on 9 January. Noting previous studies of such phenomena, Bureau of Meteorology (2017) speculate that the NTT likely played a role in maintaining the elevated fire danger overnight.

Unlike the NTT associated with fire events discussed in previous sections, the upper-tropospheric trough was positively tilted when upstream of the fire location, as seen late in the evening of 8 January in Figure 3-13. While the base of the trough exhibits some suggestion of negative tilt at around 50 °S, the main axis of the trough did not assume a negative tilt until around 9 January 0000 UTC at which point it was positioned well out into the Tasman Sea.
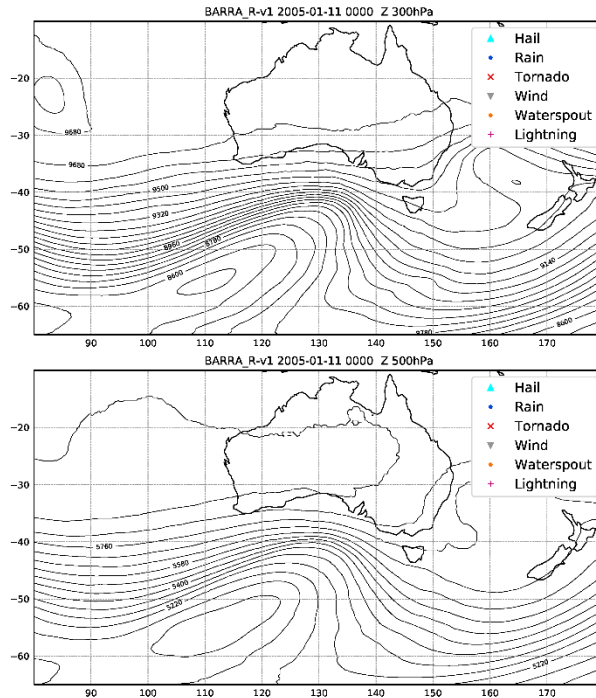
FIGURE 3-13 BARRA-R GEOPOTENTIAL HEIGHT CONTOURS (METRES) AT 300 HPA (LEFT) AND 500 HPA (RIGHT) ON 8 JANUARY 2013 AT 1200 UTC. SEVERE WEATHER REPORTED IN THE BUREAU OF METEOROLOGY SEVERE STORMS ARCHIVE DURING THE FOLLOWING 6 HOURS IS INDICATED BY THE MARKERS DEFINED IN THE LEGEND AT TOP RIGHT.

2013-02-23 NSW south coast tornadoes

Several tornadoes up to strength EF2 occurred in the evening of 23 February 2013 along the New South Wales south coast causing damage across the region, particularly in Kiama. The timing and synoptic conditions were atypical for tornado occurrence in the region as noted in Louis (2018). In the days preceding the event, an east coast low (ECL) formed off the coast of Queensland. The ECL moved south and across the New South Wales north coast and inland to the southwest. A period of intensification of the ECL off the coast of the Queensland-New South Wales border was attributed by Louis (2018) to a very broad NTT centred over northeast South Australia (Figure 3-14).
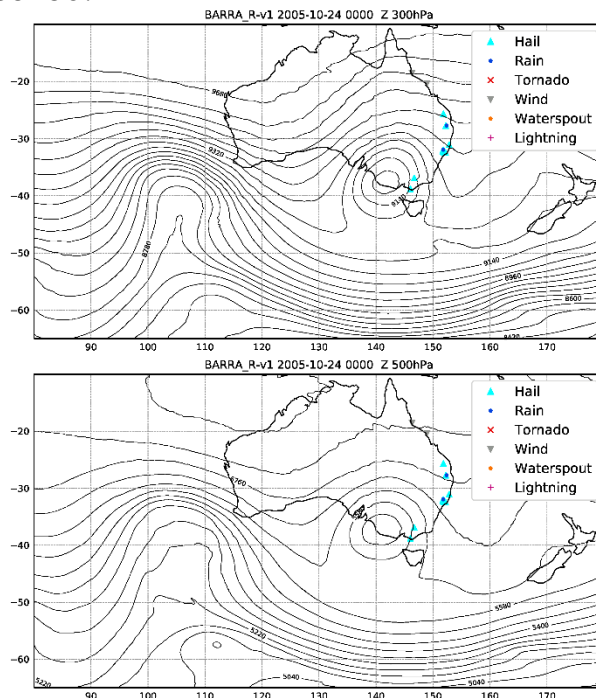
FIGURE 3-14 BARRA-R GEOPOTENTIAL HEIGHT CONTOURS (METRES) AT 300 HPA (LEFT) AND 500 HPA (RIGHT) ON 22 FEBRUARY 2013 AT 0600 UTC. SEVERE WEATHER REPORTED IN THE BUREAU OF METEOROLOGY SEVERE STORMS ARCHIVE DURING THE FOLLOWING 6 HOURS IS INDICATED BY THE MARKERS DEFINED IN THE LEGEND AT TOP RIGHT.

2014-10-27 Ballandean fire, QLD

In another fire spread simulation case study, Bureau of Meteorology (2017) examine a fire near Ballandean near the New South Wales-Queensland border. A trough across northern Australia generated thunderstorms which ignited the fire on 27 October 2014. A second trailing trough extended southwards down the east coast towards a front extending from deep in the Southern Ocean. A strong NTT associated with the surface trough and front also passed through southeast Australia, likely contributing to vertical circulations associated with the lightning activity. Surface and upper air observations also strongly indicate that following the passage of the troughs, an intrusion of very dry upper-tropospheric air associated with the NTT reached the surface, as seen in the Hobart and Wangary events described above.
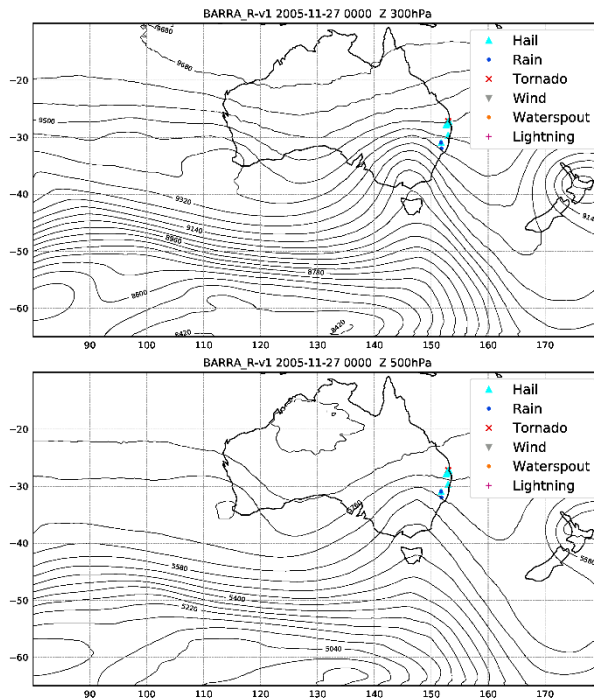
FIGURE 3-15 BARRA-R GEOPOTENTIAL HEIGHT CONTOURS (METRES) AT 300 HPA (LEFT) AND 500 HPA (RIGHT) ON 27 OCTOBER 2014 AT 0000 UTC. SEVERE WEATHER REPORTED IN THE BUREAU OF METEOROLOGY SEVERE STORMS ARCHIVE DURING THE FOLLOWING 6 HOURS IS INDICATED BY THE MARKERS DEFINED IN THE LEGEND AT TOP RIGHT.

2016-06-02-07 East coast rainfall event

Over the period of 2-7 June 2007 an ECL event brought significant rain, gale force winds and very large waves along a large stretch of the New South Wales coast, which combined with a king tide brought significant damage over the extensive region. The event is described by Bureau of Meteorology (2016a) and Louis et al. (2016). From 2 June an upper-tropospheric trough over South Australia became negatively tilted leading to the development of a low pressure centre at the surface over southern Queensland. The NTT continued to strengthen and become progressively more negatively tilted, extending across the Queensland coast (Figure 3-16) with an upper-tropospheric low cutting off from the apex of the trough late on 4 June. This resulted in the development of a series of low pressure centres in the surface trough off the north coast of New South Wales. The intense pressure gradient from the resulting ECL southeastward across the Tasman Sea towards a strong blocking high over New Zealand brought gale

force winds, storm surge and very large waves to much of the New South Wales coast.
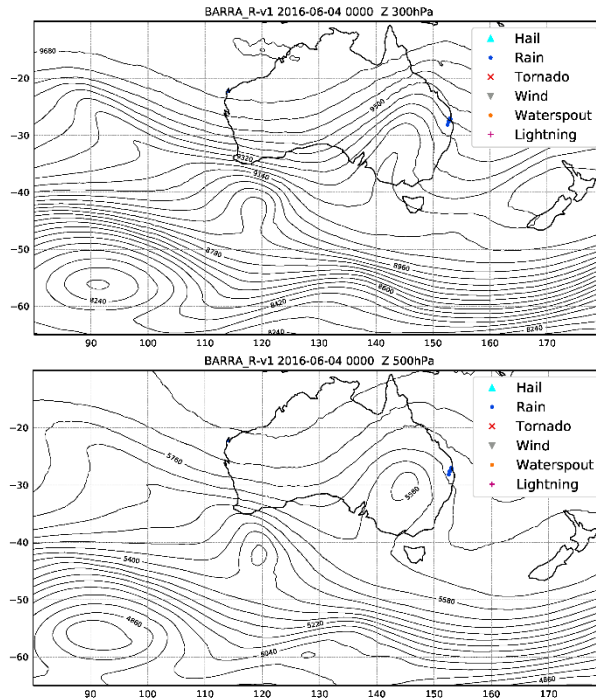
FIGURE 3-16 BARRA-R GEOPOTENTIAL HEIGHT CONTOURS (METRES) AT 300 HPA (LEFT) AND 500 HPA (RIGHT) ON 4 JUNE 2016 AT 0000 UTC. SEVERE WEATHER REPORTED IN THE BUREAU OF METEOROLOGY SEVERE STORMS ARCHIVE DURING THE FOLLOWING 6 HOURS IS INDICATED BY THE MARKERS DEFINED IN THE LEGEND AT TOP RIGHT.

2016-09-28 SA tornado outbreak

An outbreak of supercell thunderstorms across South Australia on 28 September 2016 caused numerous tornadoes, heavy rain and large hail resulting in severe damage to power infrastructure causing a statewide power outage. Bureau of Meteorology (2016b) and Sgarbossa et al. (2018) describe the event, beginning with the development of an upper-tropospheric trough south of Western Australia than became negatively tilted and cut off from the long-wave trough to the south (Figure 3-17). Moving eastward along the south coast the upper-level cut-off low caused explosive cyclogenesis in the associated surface low which produced a cold front crossing the state.
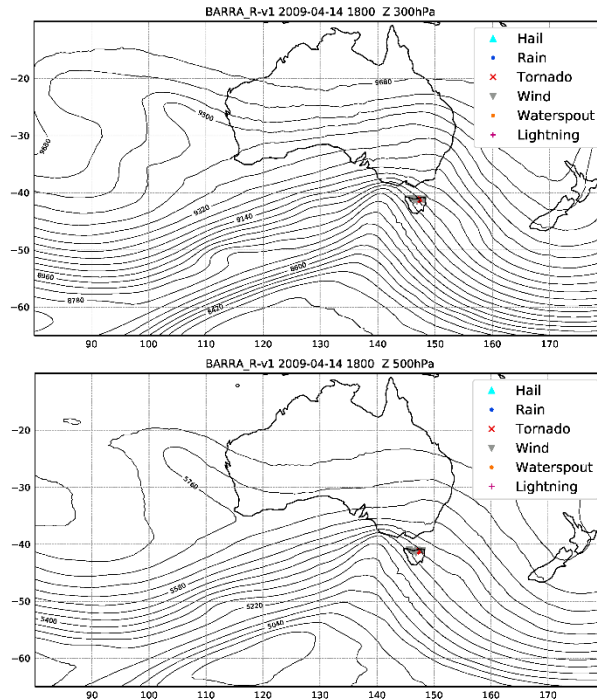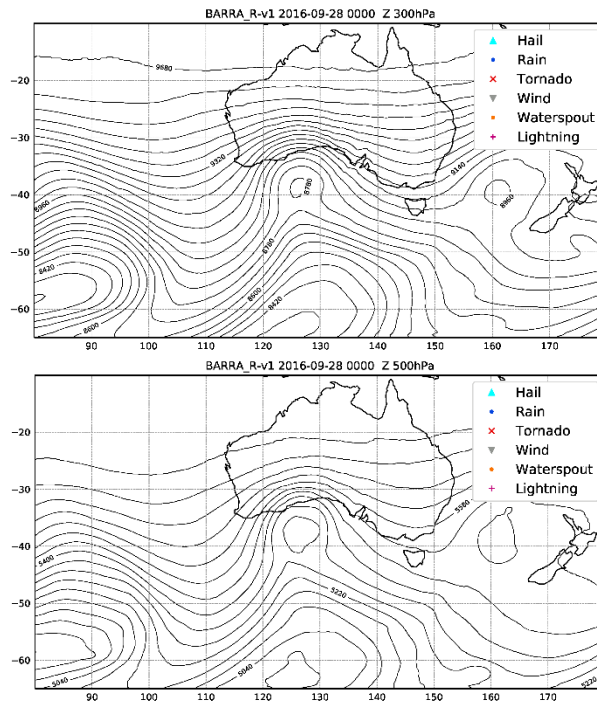
FIGURE 3-17 BARRA-R GEOPOTENTIAL HEIGHT CONTOURS (METRES) AT 300 HPA (LEFT) AND 500 HPA (RIGHT) ON 28 SEPTEMBER 2016 AT 0000 UTC. SEVERE WEATHER REPORTED IN THE BUREAU OF METEOROLOGY SEVERE STORMS ARCHIVE DURING THE FOLLOWING 6 HOURS IS INDICATED BY THE MARKERS DEFINED IN THE LEGEND AT TOP RIGHT.

3.2.2 NTT indirectly implicated

2003-01-08 Lightning fire ignitions across SE Australia

In his analysis of sudden surface drying events across southern Australia, Mills (2008b) notes that a drying event with strong spatial coherence across southeast Australia over 6-7 January 2003 might have preconditioned fuel for ignition during a widespread lightning event on 8 January. While not noted explicitly by Mills (2008b), a strong upper-tropospheric trough developing south of Western Australia and propagating eastwards during this time could have been associated with the drying event. The trough sharpened as it approached the southeast coast and extended northwards over the continent as it became negatively tilted on 8 January (Figure 3-18), the day of the lightning event. This event set off the extensive bushfires across southeast Australia including the devastating Canberra bushfires.
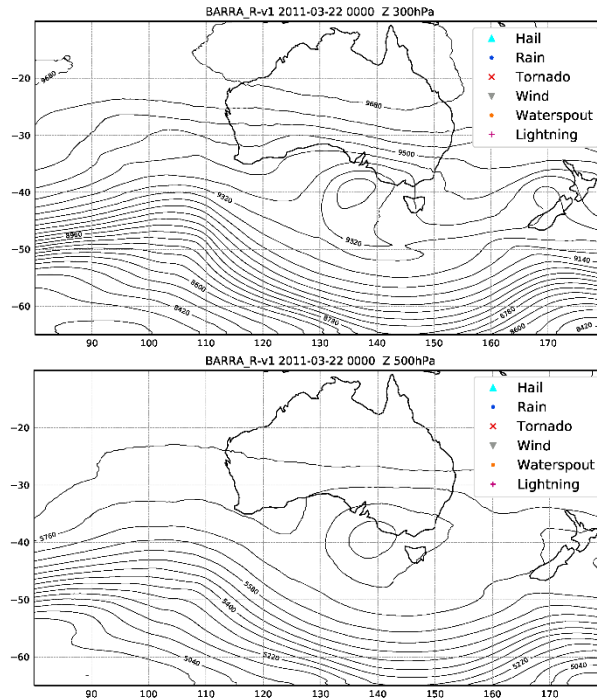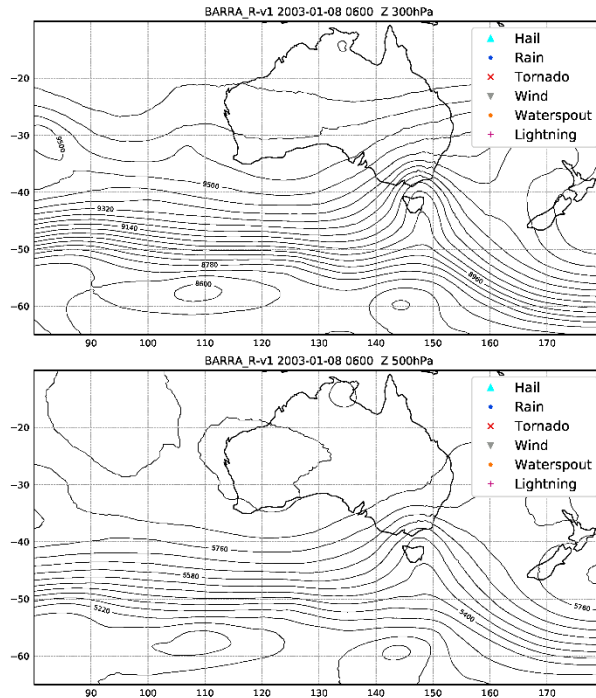
FIGURE 3-18 BARRA-R GEOPOTENTIAL HEIGHT CONTOURS (METRES) AT 300 HPA (LEFT) AND 500 HPA (RIGHT) ON 8 JANUARY 2003 AT 0600 UTC. SEVERE WEATHER REPORTED IN THE BUREAU OF METEOROLOGY SEVERE STORMS ARCHIVE DURING THE FOLLOWING 6 HOURS IS INDICATED BY THE MARKERS DEFINED IN THE LEGEND AT TOP RIGHT.

2003-01-18-23 Canberra bushfires

Bushfires caused severe damage to suburbs of Canberra and large areas of the Australian Capital Territory during 18-23 January 2003. The meteorological conditions associated with the fires on 18 January are described by Mills (2005) who describes two sudden surface drying episodes attributed to transport to the surface of middle to upper-tropospheric air, similar to the previous fire events described above. The role of a strong NTT to the south of Australia at the time (Figure 3-19) was not discussed by Mills (2005) and will be the subject of further investigation in section 4.1.
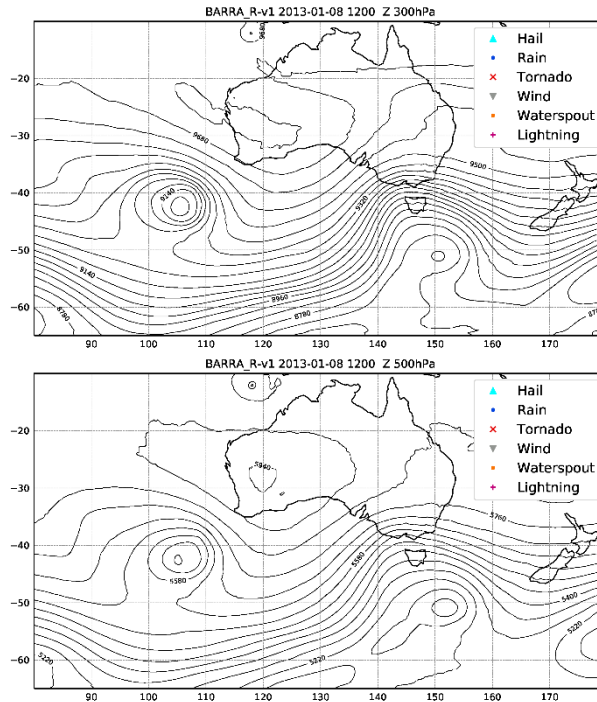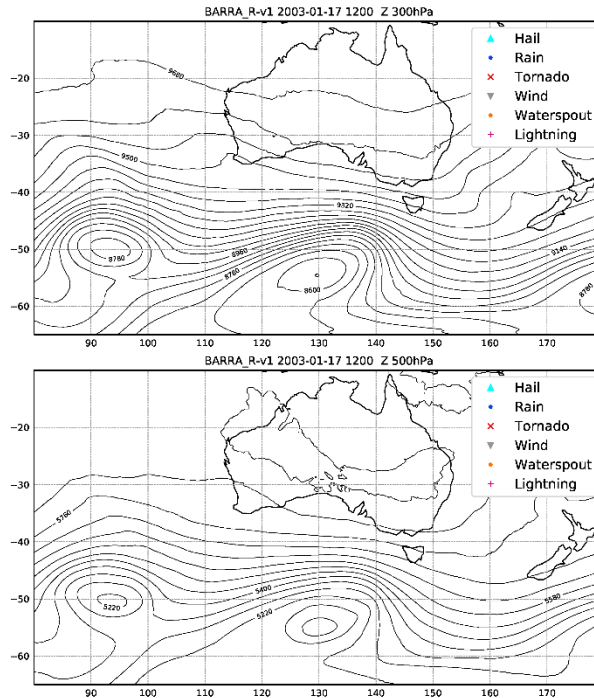
FIGURE 3-19 BARRA-R GEOPOTENTIAL HEIGHT CONTOURS (METRES) AT 300 HPA (LEFT) AND 500 HPA (RIGHT) ON 18 JANUARY 2003 AT 1200 UTC. SEVERE WEATHER REPORTED IN THE BUREAU OF METEOROLOGY SEVERE STORMS ARCHIVE DURING THE FOLLOWING 6 HOURS IS INDICATED BY THE MARKERS DEFINED IN THE LEGEND AT TOP RIGHT.

2007-12-06 Kangaroo Island fire

During December 2007 bushfires burnt more than 20 % of Kangaroo Island, South Australia. Various aspects of the fires and their interaction with the weather are discussed by Peace et al. (2011) and Peace and Mills (2012) These include ignition of the fires by lightning on 6 December and extreme fire behaviour on 9 December associated with downward entrainment of very dry air above a very strong inversion by penetrative convection of the fire plume itself. The origin of this very dry air is given by Peace and Mills (2012) as descending dry band ahead of an incoming ridge, and while not noted explicitly this converged with a dry band around the apex of a strong upper-tropospheric trough than became negatively tilted as it passed south of Kangaroo Island at the time (Figure 3-20). The day of the lightning ignitions also saw the passage of a smaller scale NTT along the South Australian coast, which was not the subject of either study.
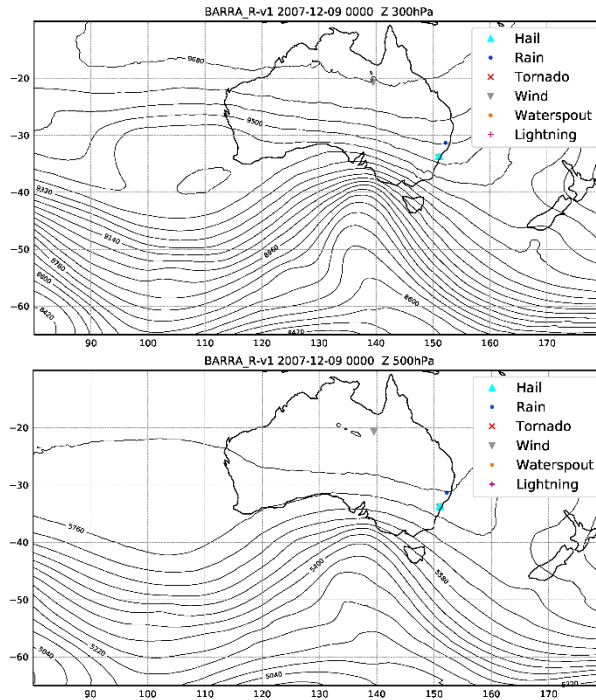
FIGURE 3-20 BARRA-R GEOPOTENTIAL HEIGHT CONTOURS (METRES) AT 300 HPA (LEFT) AND 500 HPA (RIGHT) ON 9 DECEMBER 2007 AT 0000 UTC. SEVERE WEATHER REPORTED IN THE BUREAU OF METEOROLOGY SEVERE STORMS ARCHIVE DURING THE FOLLOWING 6 HOURS IS INDICATED BY THE MARKERS DEFINED IN THE LEGEND AT TOP RIGHT.

2015-10-17 Esperance fires

On 17 November 2015 extreme fire weather resulted in a bushfire near Esperance, Western Australia, causing the loss of four lives as well as extensive damage to property, crops, and livestock. Burrows (2015) describes the event, noting that the fires were ignited by lightning associated with the passage of a trough on 15 November. Although not mentioned by Burrows (2015), this surface trough was associated with a short-wave NTT shown in Figure 3-21. On 17 December an NTT feature was embedded in a long-wave trough to the west of Western Australia which could have played a role in the presence of an extremely dry wedge of air noted by Burrows (2015) in the atmospheric sounding from nearby Albany.
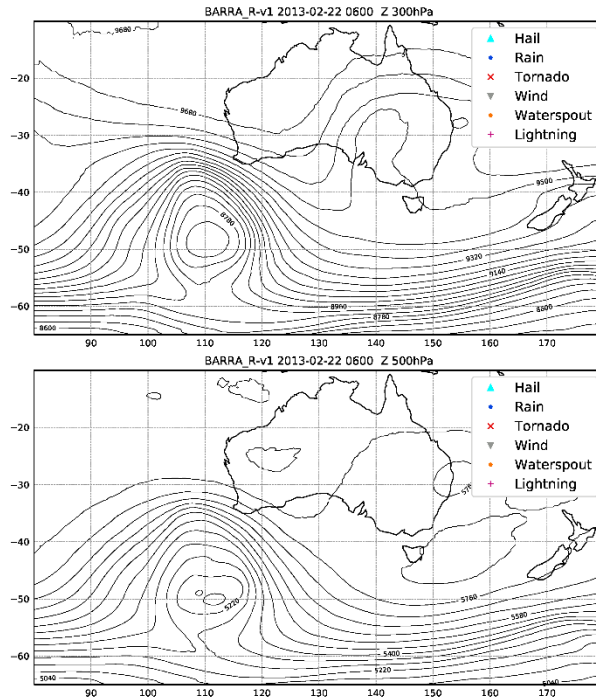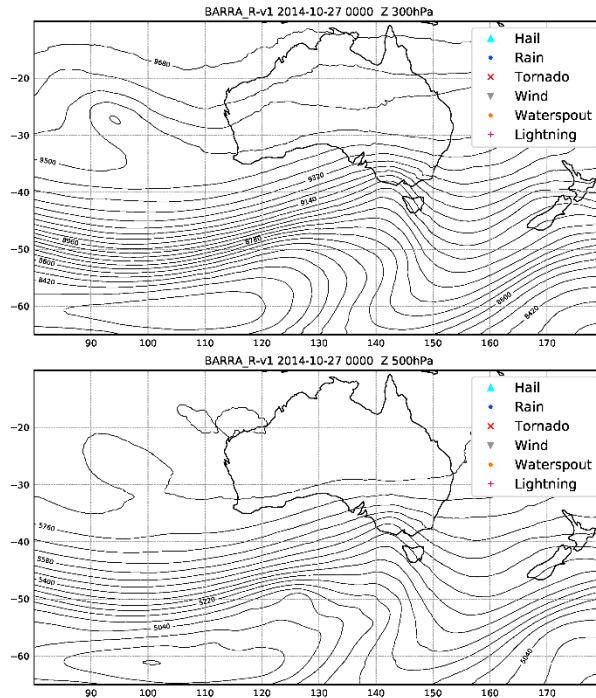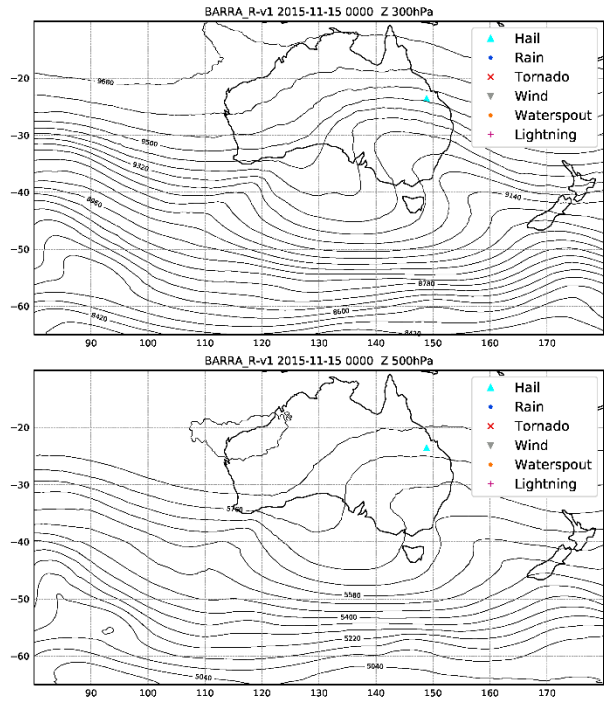
FIGURE 3-21 BARRA-R GEOPOTENTIAL HEIGHT CONTOURS (METRES) AT 300 HPA (LEFT) AND 500 HPA (RIGHT) ON 15 NOVEMBER 2015 AT 0000 UTC. SEVERE WEATHER REPORTED IN THE BUREAU OF METEOROLOGY SEVERE STORMS ARCHIVE DURING THE FOLLOWING 6 HOURS IS INDICATED BY THE MARKERS DEFINED IN THE LEGEND AT TOP RIGHT.

4 CASE STUDIES

4.1 CANBERRA BUSHFIRES 18 JANUARY 2003

4.1.1 Background

In the week prior to 18 January 2003 lightning ignited fires in the forest to the west and southwest of Canberra. By 18 January, the fires were well established and dangerous fire weather on 18 January allowed fire to move rapidly towards Canberra and engulf the outskirts of the city. Some 500 houses were destroyed, four people killed and the historic Mt Stromlo observatory badly damaged (McLeod, 2003). The total cost of the fires was estimated at $300 million. Estimates of the energy released by the fire over ten minutes at the time of peak flaming suggested a value of 3.5 x 1012 kJ, in excess of that generated by the Hiroshima nuclear explosion (Fromm et al., 2006). In addition, pyrocumulonimbus thunderstorms (pyroCb) were triggered by the fire. A fire tornado was documented moving through Canberra suburbs, contributing to the destruction wrought by the fire and black hail (resulting from ash and smoke incorporated into hail generated by the storms) was reported along the storm tracks.

Antecedent hot and very dry conditions over much of southeastern Australia as a result of the 2002-03 El Niño event contributed to conditions that allowed the Canberra fire to ignite and spread. As discussed in section 3.2.2, a large scale drying event across southeastern Australia accompanied a lightning outbreak that ignited numerous bushfires across the region (Mills, 2008b). The possible role of a NTT in the preconditioning of fuels and the lightning ignition event is noted here but will not be investigated in detail. The progress of a trough over the southeast of Australia on 18 January resulted in strong, dry and hot winds that enhanced fire spread into the outskirts of Canberra. Mills (2005) described the mesoscale meteorology of the event in some detail and notes the presence of very dry surface air at times during the fire, suggesting an association with dry mid- to upper-level bands of very dry air visible on satellite water vapour imagery (Figure 4-1). He further identifies such 'water vapour dry slots' as being associated with atmospheric instability. This instability, in addition to potentially contributing to the development of thunderstorms including the Canberra pyroCb, could have assisted the descent of the upper level dry air to the surface.
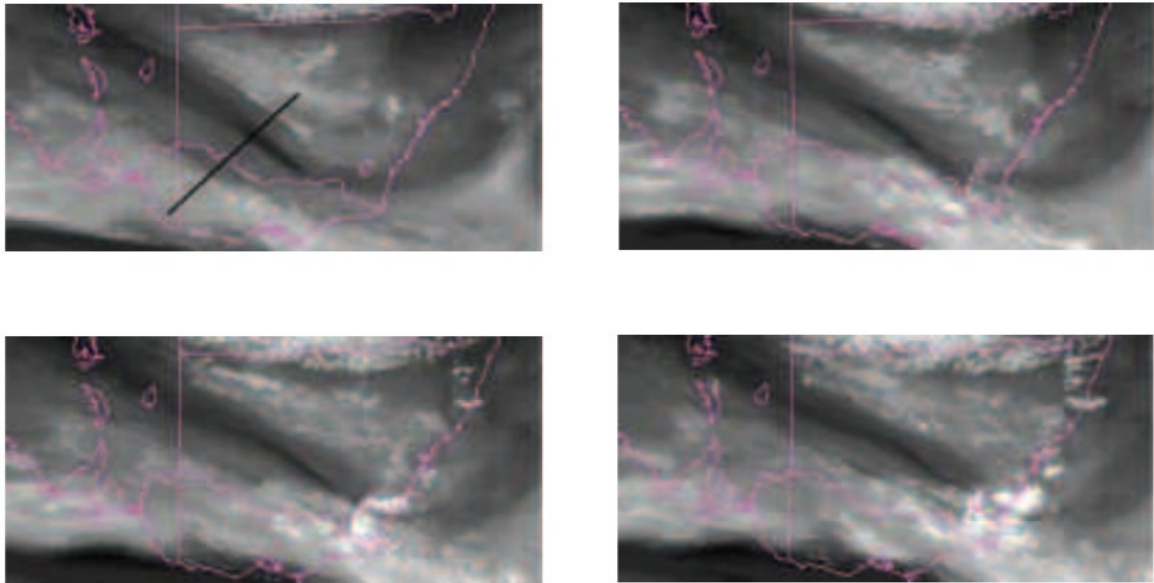
FIGURE 4-22 GMS-5 SATELLITE WATER VAPOUR IMAGERY SEQUENCE DURING THE CANBERRA FIRE AT 2330 UTC 17 JANUARY AND 0230, 0430 AND 0530 UTC 18 JANUARY, SHOWING A DRY SLOT OVER THE REGION (FROM MILLS (2005)).

4.1.2 Synoptic Analysis

The synoptic situation at 300 hPa on 17-18 January is summarised by plots of geopotential height and scalar wind speed in Figure 4-2. A strong NTT was positioned south of Western Australia early on 17 January with a strong jet around its apex. In addition there was a weaker west-northwesterly jet originating downstream of a weaker trough off the west coast and extending across just north of the apex region of the NTT. As the NTT moved east over the subsequent 36 hours the eastern end of the weaker jet moved progressively further north. As the tilt in the NTT became more severe at 1200 UTC on 17 November the jet core strengthened and extended down the northwest flank of the NTT. At this time the jet began to separate in to two around the NTT apex.
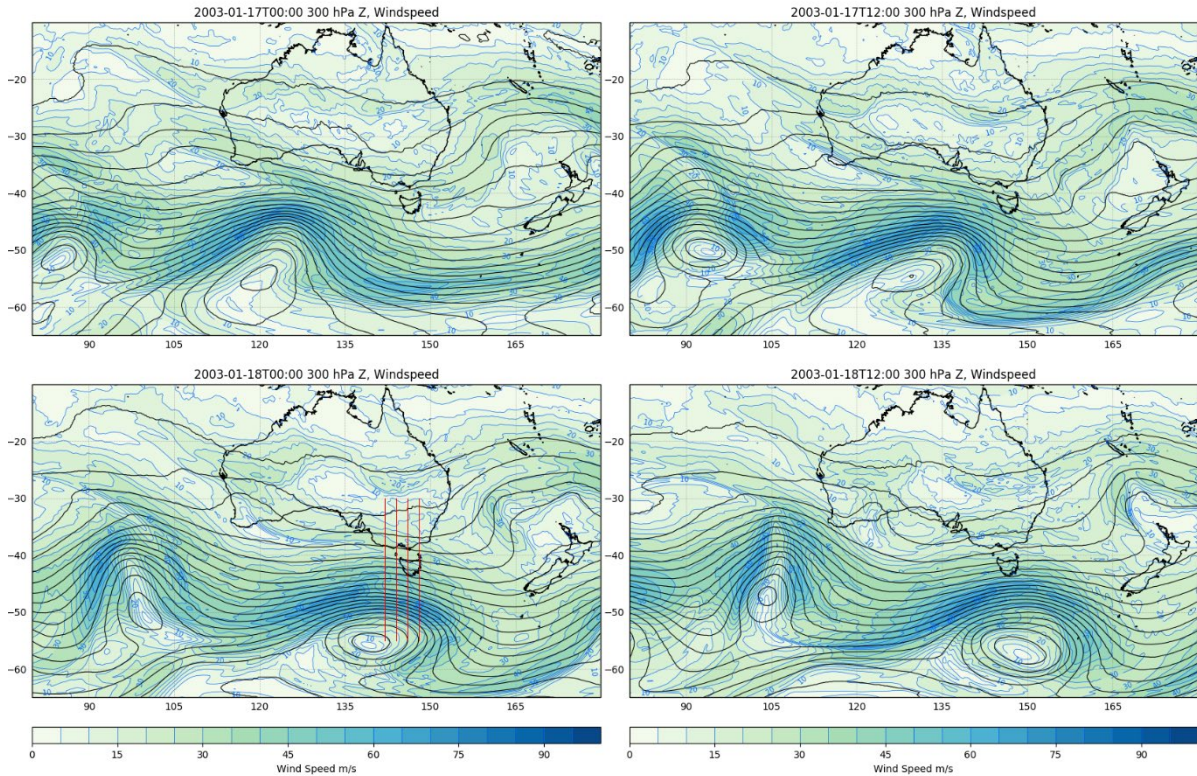
FIGURE 4-23 BARRA-R GEOPOTENTIAL HEIGHT CONTOURS (METRES) AT 300 HPA (BLACK CONTOURS) AND SCALAR WIND SPEED (MS⁻¹) AT 12 HOUR INTERVALS FROM 0000 UTC 17 JANUARY 2003 TO 1200 UTC 18 JANUARY 2003. AT 0000 UTC 17 JANUARY 2003 A NEGATIVELY TILTED TROUGH ORIGINATES SOUTH OF WESTERN AUSTRALIA, EXTENDING TOWARDS THE CENTRAL AUSTRALIAN CONTINENT. RED LINES IN THE BOTTOM LEFT PANEL INDICATE THE LOCATIONS OF THE CROSS SECTIONS IN FIGURE 4-4.

Full disk GMS-5 satellite water vapour imagery in Figure 4-3 shows the broader temporal and spatial context for the dry slot noted by Mills (2005) and shown in Figure 4-1. In the 0000 and 1200 UTC 18 January images a broader dry band extended through the Bass Strait region, the edge of which is visible at the bottom of the images in Figure 4-1. This dry band can be seen in the earlier images to originate southwest of Western Australia.
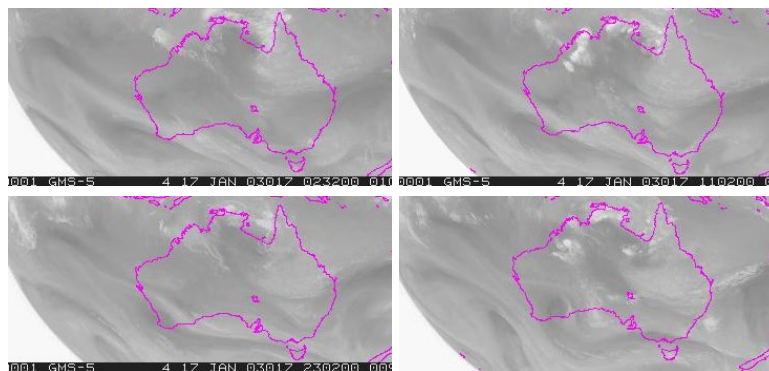
FIGURE 4-24 GMS-5 6.8 MM CHANNEL WATER VAPOUR IMAGERY AT 12 HOUR INTERVALS FROM 0000 UTC 17 JANUARY 2003 TO 1200 UTC 18 JANUARY 2003.

The structure of the troposphere over southeast Australia and the northern Southern Ocean at 0000 UTC 18 January is depicted by a series of meridional cross sections through 142E, 144E, 146E and 148E in Figure 4-4. Potential temperature contours show a strong frontal zone extended from the upper troposphere at around 50 °S northward and downward to the surface over southeast Australia. The upper-tropospheric extent of this region corresponded

to the apex region of the NTT. Along this frontal zone was a region of enhanced potential vorticity (PV), possibly indicating the descent of air along this path. The extremely dry air coincident with the enhanced PV and frontal zone is consistent with descending motion.

A dry region through the depth of the troposphere in the vicinity of 40 °S was coincident with the dry band over Bass Strait as seen in Figure 4-3. The lower regions of the dry band merged with the dry, high PV air in the frontal zone and was connected at lower levels to dry air over the continent. Further north, the dry slot implicated in Mills (2005) can be seen in the upper troposphere. Up stream of Canberra, at 142 °E and 144 °E, it appears that dry air from both the apex region of the NTT and the dry band over Bass Strait could have been propagating northward and downward along isentropes under the moist region above the south coast and well inland.

The 142 °E section of Figure 4-4 (top panel) is plotted again in more detail in the top panel of Figure 4-5 with the addition of meridional-vertical wind vectors. The vertical component of the wind has been scaled by a factor of 300 relative to the meridional component to highlight the overall patterns in the wind field. Northward and downward motion was present all along the frontal zone as far north as 33 °S. Similarly, northward and downward motion was coherent in the Bass Strait dry band and below 700 hPa covered a broad region over the south of the continent, extending all the way down to the surface. The bottom panel of Figure 4-5 shows the dry air masses and tangential cross sectional wind vectors in relation to the zonal wind. In a typical scenario for a dry intrusion, the strong vertical windshear below the upper-tropospheric jet core coincided with a strong horizontal temperature gradient. Conservative transport of potential vorticity along the downward sloping isentropes was favourable in the strong cyclonic shear on the poleward side of the jet.

There was already a broad region of very dry air over southeast Australia at this time as seen in Figure 4-6. The presence of an additional band of very dry air over Western Australia is noteworthy but has not been investigated in the present study.
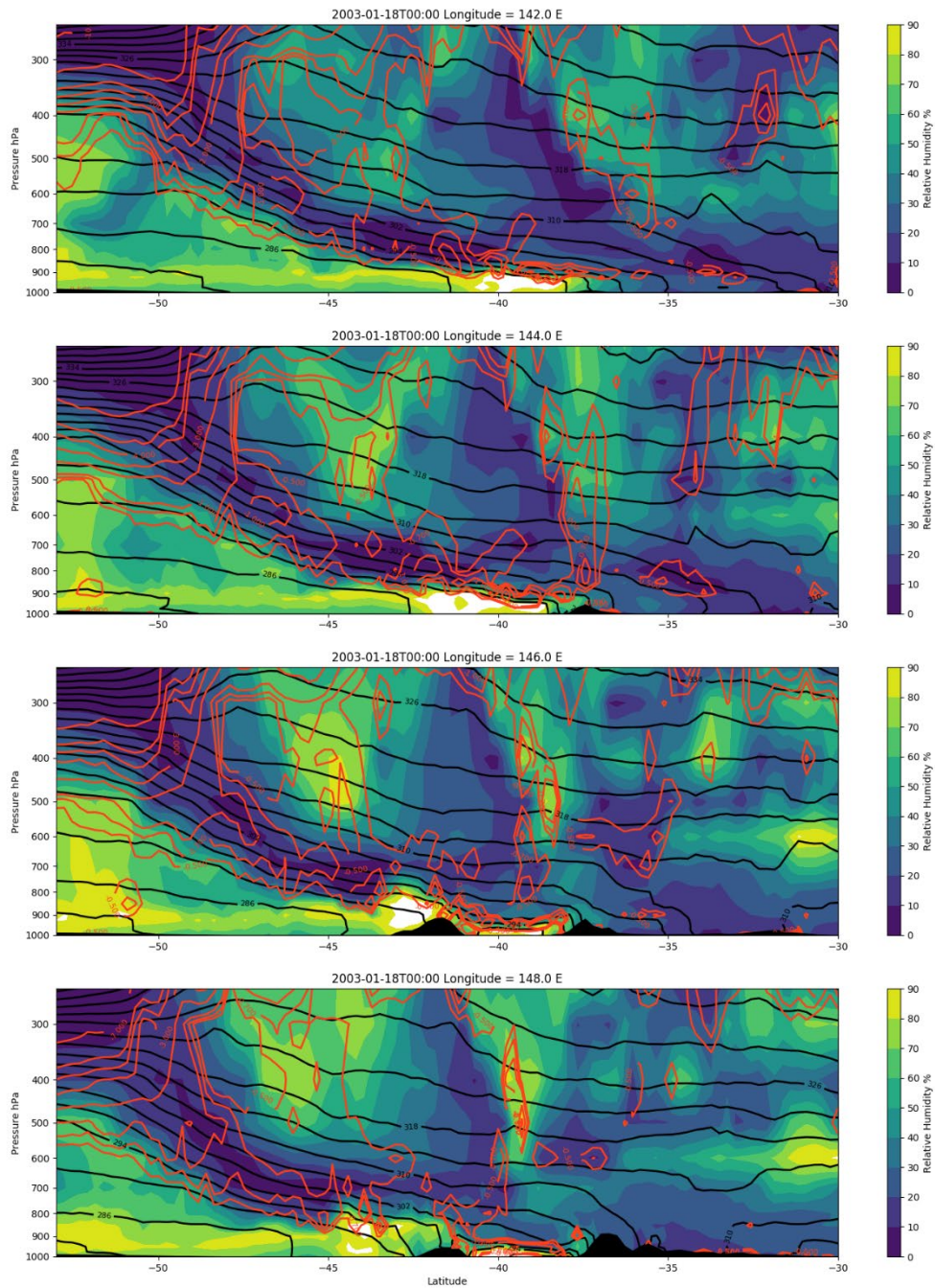
FIGURE 4-25 MERIDIONAL CROSS SECTIONS OF RELATIVE HUMIDITY (SHADED), POTENTIAL TEMPERATURE (BLACK CONTOURS) AND POTENTIAL VORTICITY (RED CONTOURS) AT 142, 144, 146 AND 148 °E AT 0000 UTC 18 JANUARY 2003.
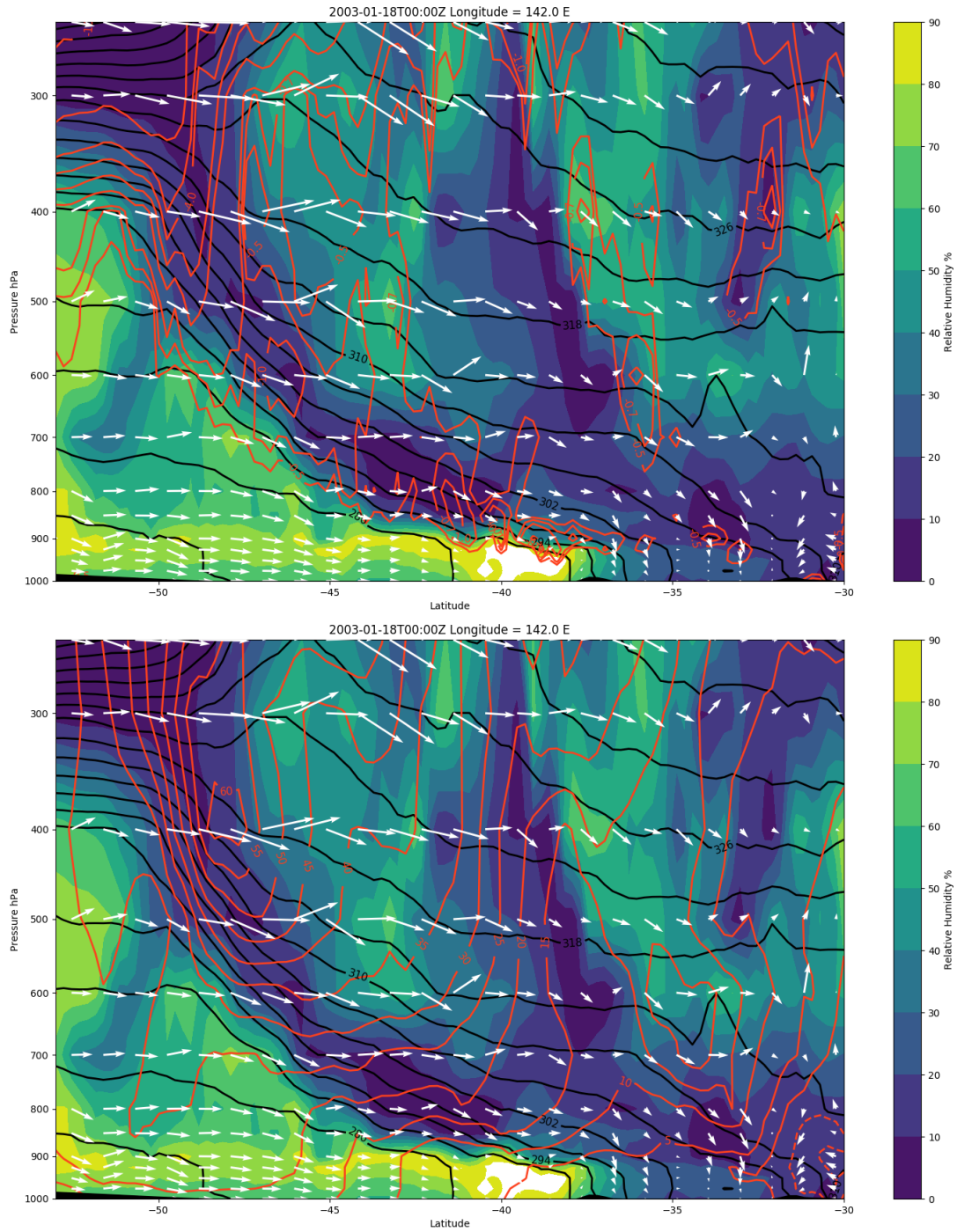
FIGURE 4-26 MERIDIONAL CROSS SECTIONS OF RELATIVE HUMIDITY (SHADED), POTENTIAL TEMPERATURE (K, BLACK CONTOURS) AND MERIDIONAL-VERTICAL WIND VECTORS (WHITE ARROWS) AT 142 °E AT 0000 UTC 18 JANUARY 2003. RED CONTOURS ARE POTENTIAL VORTICITY (PVU, TOP) AND ZONAL WIND (5 MS⁻¹INTERVALS, BOTTOM).
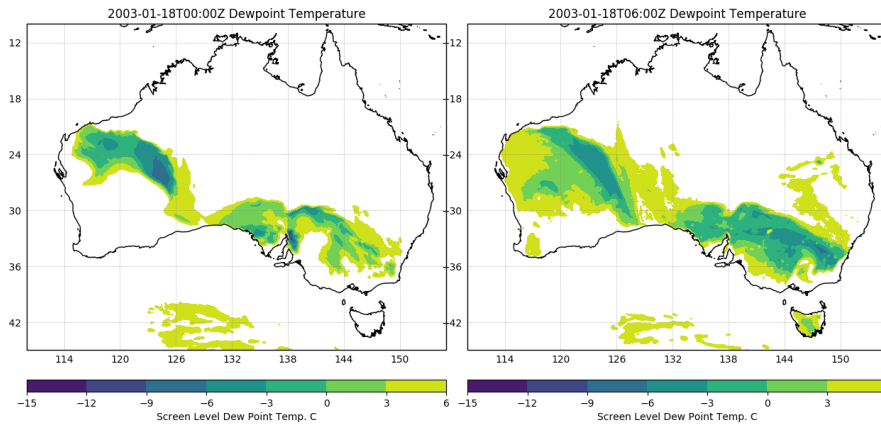
FIGURE 4-27 BARRA-R SCREEN LEVEL DEW POINT TEMPERATURE AT 0000 AND 0600 UTC ON 18 JANUARY 2003.

Figure 4-7 shows that by mid-afternoon a very deep mixed layer had formed over southeast Australia. There was still some northward and downward movement over the south coast and as far north as 35 °S, but further north there was much stronger dry convection through the full depth of the mixed layer to 600 hPa, or probably higher, where the dry slot met the top of the mixed layer.
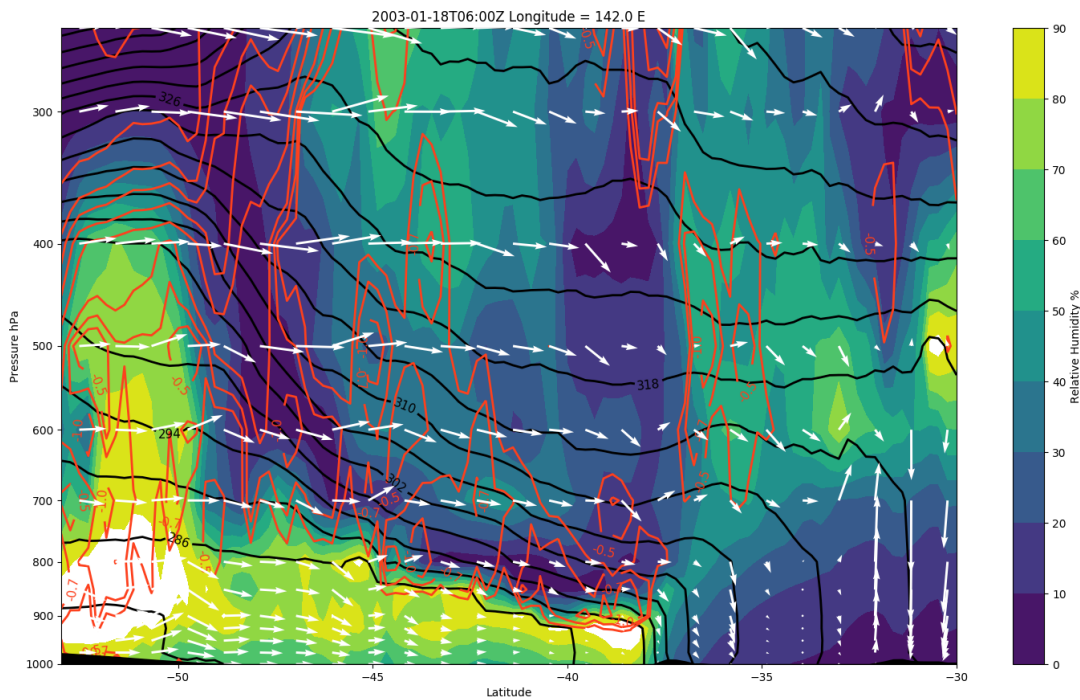
FIGURE 4-28 MERIDIONAL CROSS SECTIONS OF RELATIVE HUMIDITY (SHADED), POTENTIAL TEMPERATURE (K, BLACK CONTOURS) POTENTIAL VORTICITY (PVU, RED CONTOURS) AND MERIDIONAL-VERTICAL WIND VECTORS (WHITE ARROWS) AT 142 °E AT 0600 UTC 18 JANUARY 2003.

The other cross sections given in Figure 4-8 show this to be a rather coherent picture. The dry slot was more pronounced and coherent over the full longitudinal extent, propagating southward with increasing longitude until it was positioned directly over Canberra at 35 °S (just east of the last section). As discussed in Mills (2005), this position was favourable for the entrainment of air from the dry slot into the mixed layer and down to the surface. At this time, the extremely dry surface region north of 35 °S covered a very large region of southeast Australia (Figure 4-6).
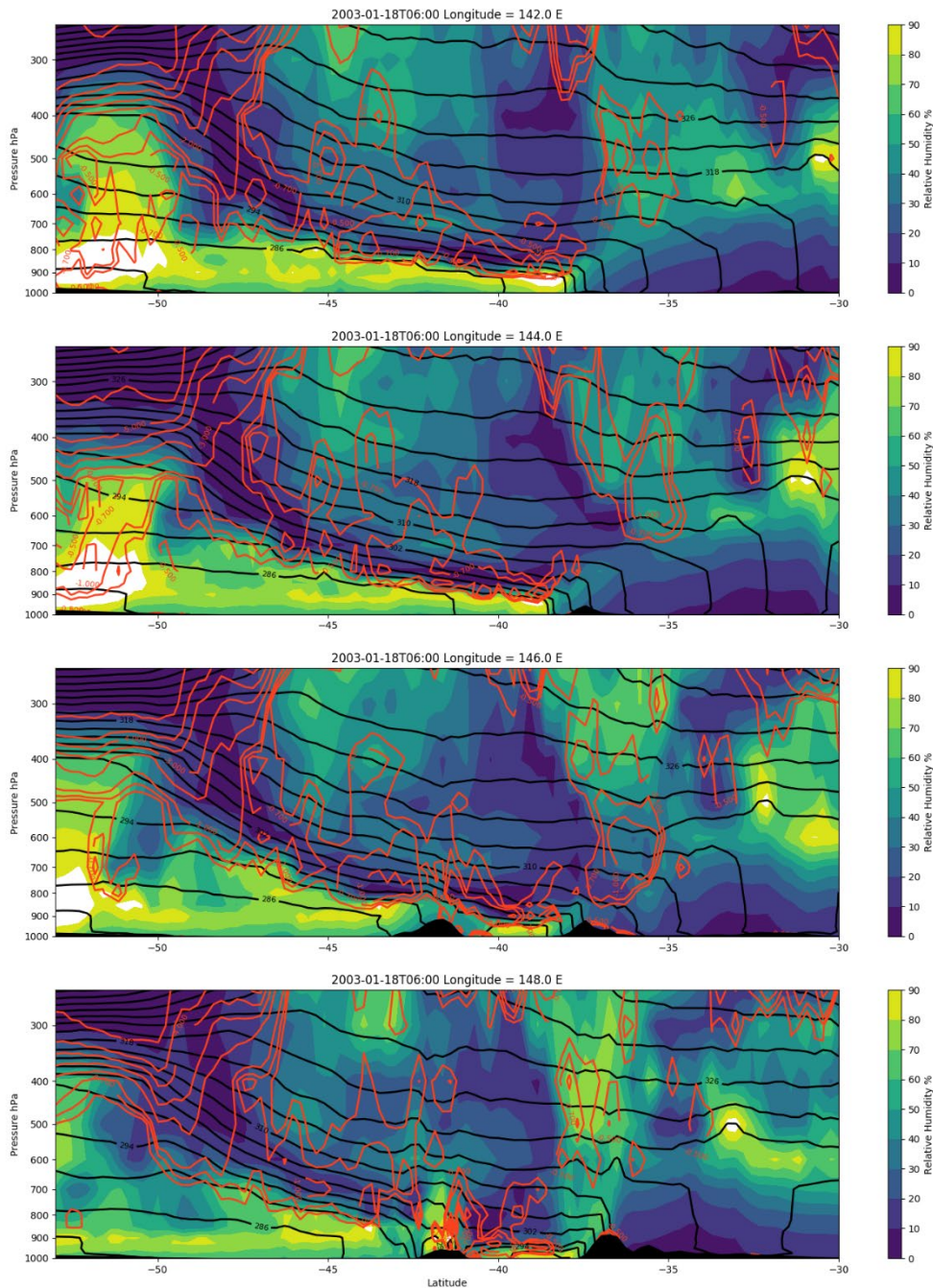
FIGURE 4-29 MERIDIONAL CROSS SECTIONS OF RELATIVE HUMIDITY (SHADED), POTENTIAL TEMPERATURE (BLACK CONTOURS) AND POTENTIAL VORTICITY (RED CONTOURS) AT 142, 144, 146 AND 148 °E AT 0000 UTC 18 JANUARY 2003.

Potential vorticity stronger than -0.7 PVU in the middle- to lower-troposphere on 17-18 January is shown in Figure 4-9. The very long downwards extension of enhanced PV (and low relative humidity) from the apex of the NTT over the south coast of the continent seen in Figures 4-4, 4-5, 4-7 and 4-8 can be seen in the northward progression of grey, blue and red regions between 50 °S and 40 °S in the bottom two panels. This was a coherent structure from the leading eastern edge of the NTT right around to its northwest flank and persisted throughout the development of the NTT.
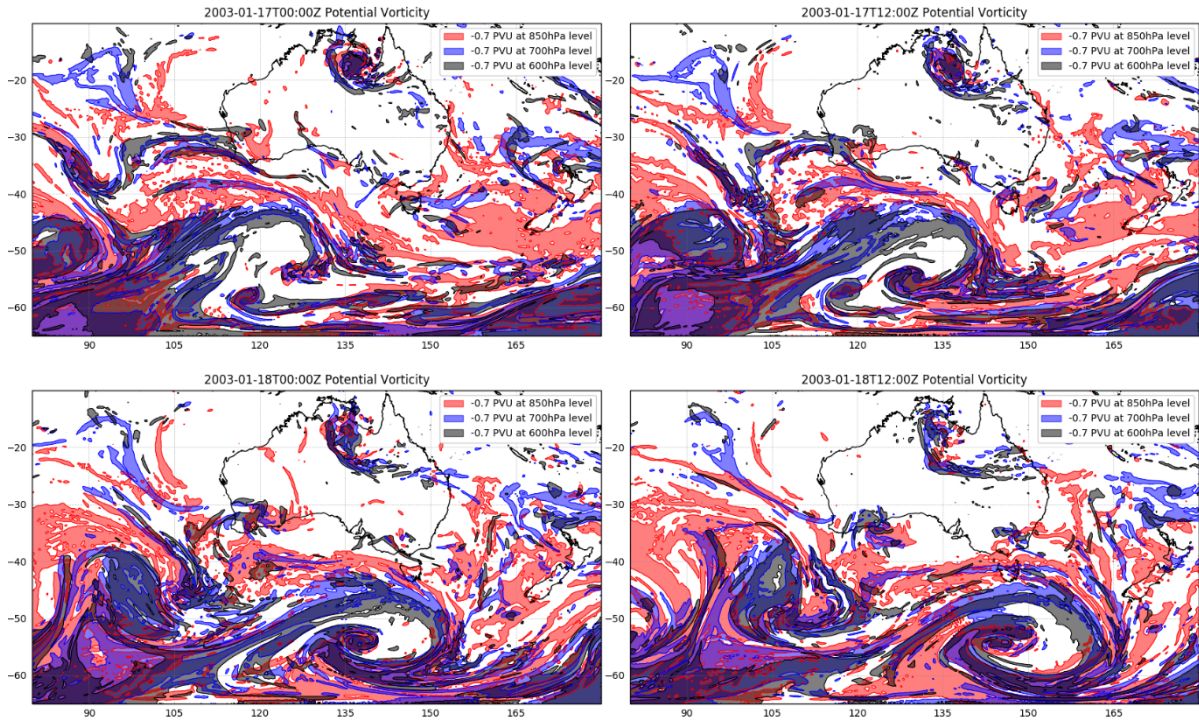
FIGURE 4-30 POTENTIAL VORTICITY GREATER THAN -0.7 PVU AT 850 HPA (RED), 700 HPA (BLUE) AND 600 HPA (GREY) AT 12 HOUR INTERVALS FROM 0000 UTC 17 JANUARY 2003 TO 1200 UTC 18 JANUARY 2003.

Figure 4-10 shows the ageostrophic wind in relation to the geopotential height field at 300 hPa. The ageostrophic wind shows divergence in the northeast region of the NTT and convergence in the northwest. The divergence field at 300 hPa is also shown in Figure 4-10, indicated by the shading. The divergence was calculated using unfiltered inputs and therefore is quite noisy. However, the regions of convergence and divergence associated with the NTT and indicated by the ageostrophic wind vectors were quite coherent, more so at earlier times. The region of convergence was consistent with the centroid of the 600 hPa -0.7 PVU arc in Figure 4-9.
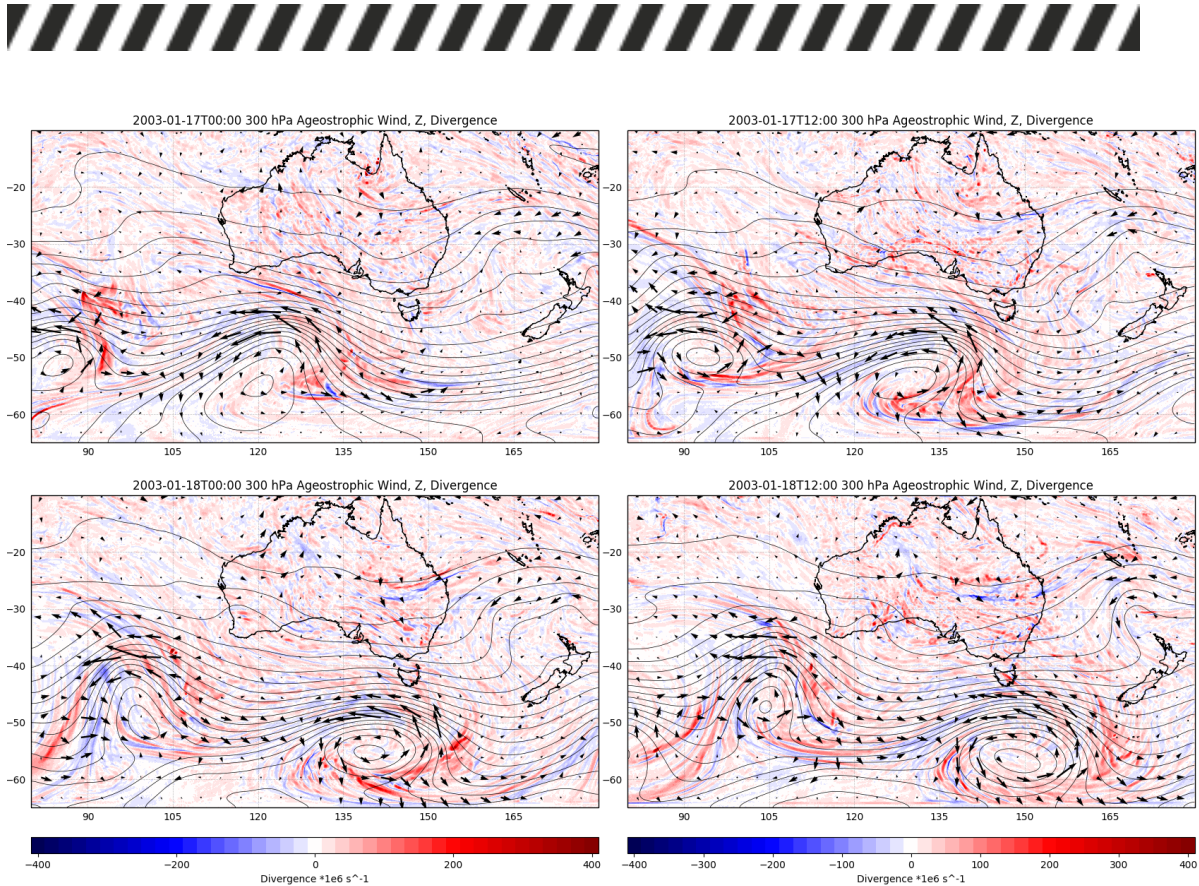
FIGURE 4-31 BARRA-R GEOPOTENTIAL HEIGHT CONTOURS (BLACK CONTOURS), AGEOSTROPHIC WIND VECTORS (BLACK ARROWS) AND DIVERGENCE (SHADED) AT 300 HPA AT 12 HOUR INTERVALS FROM 0000 UTC 17 JANUARY 2003 TO 1200 UTC 18 JANUARY 2003.

The ageostrophic wind is decomposed into components parallel and perpendicular to the geostrophic wind in the top panels of Figure 4-11. The associated stretching and diffluence components of the divergence are also indicated by shading. Down the entire western flank of the NTT, contraction was responsible for the main contribution to the divergence, counteracting some weaker diffluence. Along the right (southern) side of the weaker jet, a narrow band of strong confluence was coincident with the sharp northern boundary of a broad dry band visible in the satellite water vapour imagery (Figure 4-3 top left). As noted earlier, this dry band later crossed Bass Strait and contributed to the movement of dry air over the continent at low levels.

The band of confluence was also the northern boundary of a region of downward vertical velocity, evident in the bottom panels of Figure 4-11, that shared the same spatial extent as the dry band. The eastern extent of this downward motion/dry band was subject to weak divergence but also negative vorticity advection. The stronger vertical velocity in the western extent was in the region where the two jets merged, providing a combination of confluence on the northern extent, contraction west of the NTT apex, and cold advection behind the surface front.
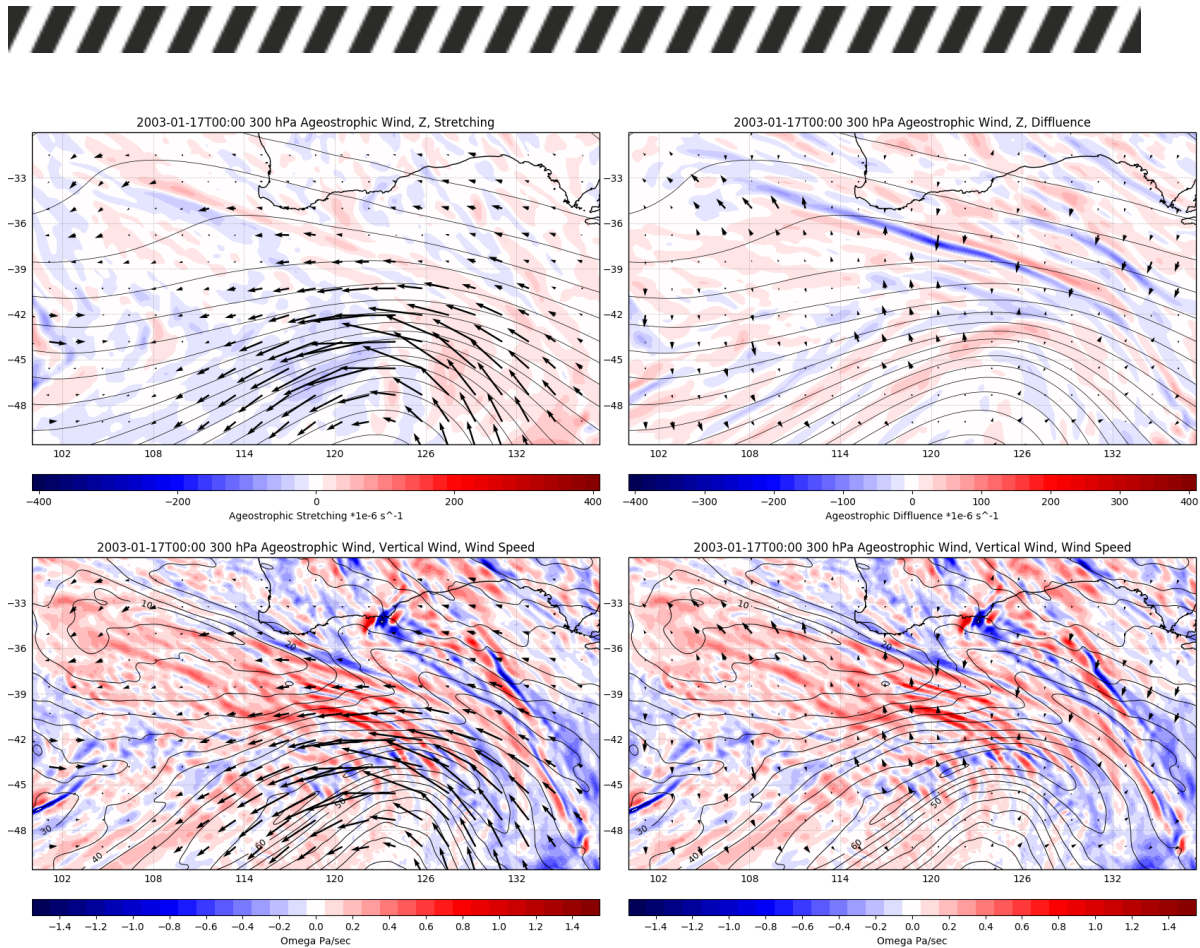
FIGURE 4-32 TOP ROW: BARRA-R GEOPOTENTIAL HEIGHT CONTOURS AGEOSTROPHIC WIND VECTORS PARALLEL TO GEOSTROPHIC WIND, AND AGEOSTROPHIC STRETCHING (LEFT) AND AGEOSTROPHIC WIND VECTORS PERPENDICULAR TO GEOSTROPHIC WIND, AND AGEOSTROPHIC DIFFLUENCE (RIGHT) AT 300 HPA AT 0000 UTC 17 JANUARY 2003. BOTTOM ROW: SCALAR WIND SPEED CONTOURS, VERTICAL WIND, AND AGEOSTROPHIC WIND VECTORS PARALLEL TO GEOSTROPHIC WIND (LEFT) AND AGEOSTROPHIC WIND VECTORS PERPENDICULAR TO GEOSTROPHIC WIND (RIGHT).

4.1.3 Discussion

It seems that despite the NTT occurring so far south, it is possible that it could have been responsible for an upper troposphere/lower stratosphere intrusion extending out to southeast Australia. It should be noted that this NTT was observed to be an uncharacteristically strong event in the climatological analysis (Section 5). Additionally, the interaction of the jet around the NTT apex and a weaker trough and jet to the north seems to have been responsible for the broad dry band that moved northwards over Bass Strait (and eventually right over the southeast coast). The proximity of the northern extent of both of these features to the top of the mixed layer over parts of southeast Australia implies that they could have played a role in the entrainment of exceptionally dry air into the mixed layer.

It is not clear that the NTT had any direct influence on the dry slot that passed directly over Canberra on the afternoon of 18 January and which was implicated by Mills (2005) as the leading cause of the first sudden drying episode on that day.

The morphology of the NTT in this event shows similar characteristics to that of the Wangary fire of 11 January 2005 (Mills, 2008a), another exceptionally strong NTT, with both NTT extending from deep in the Southern Ocean into a strong jet stream between 60°S and 40 °S (section 3.2.1). The comparison is also drawn, although

not explicitly in relation to NTT, by Mills (2008a) and in the classification of both of these events as abrupt drying events in relation to fire weather in the climatology of Mills (2008b). The NTT present in the 7 November 2002 Hobart event (Fox-Hughes, 2012) was also very similar (section 3.2.1), although this event was not as strong. In all three cases the apex of the NTT passed south of the Australian south coast.

Both Mills (2008a) and Fox-Hughes (2012) note the descent of air along isentropes from the northwest to the region above the observed extreme weather at the surface, similar to the present study. Investigation of the Hobart and Wangary events in the present study showed that the large-scale downward and outward sloping PV structure around the northern arc of the NTT seen in Figure 4-9 also occurred in those events (not shown). The Hobart event was revisited in some detail during the present study and it was found that the PV and relative humidity features were much more pronounced and well defined in BARRA-R than in the mesoLAPS model used by Fox-Hughes (2012). This indicates that despite both models having similar spatial resolution BARRA-R is doing a better job of resolving these dynamic processes.

A more detailed investigation of the evolution of these dry band features would help to improve predictability of such events. The situation described in this case is suggestive of the interaction of a weaker subtropical jet and the very strong polar jet feature. This is common with some significant severe weather events such as deep/explosive low development or severe thunderstorm outbreaks, but which is rarely discussed in connection with fire events.

The Ballandean fire event has not been examined in detail, however, the NTT present in this case showed similarities to the three cases discussed above with the exception that the trough axis crossed the south coast. The NTT associated with the Cobbler Road and Esperance fire events do not fit the same profile with both of these events becoming cut-off.

Lagrangian trajectory analysis of the upper-tropospheric dry air movement in these cases would help to resolve some of the ambiguity around the particular causes of sudden drying events at the surface. A climatological approach to this trajectory analysis, such as presented by Raveh-Rubin (2017), in combination with the climatology of NTT discussed in section 5, could establish any propensity for NTT to induce dry air intrusions and how this compares with other synoptic patterns. Regional and temporal trends could be assessed, with the possibility of extending the analysis to regional climate projections.

4.2 SEVERE THUNDERSTORMS, PERTH, WA 14 JULY 2014

4.2.1 Background

A number of tornadoes accompanied the passage of a cold front over Perth during the early morning of 14 July 2014. Houses were damaged in several suburbs, and many trees were uprooted or had branches snapped off in Perth suburbs including Hilton-O'Connor and Beeliar and in the Claremont-Nedlands area, while a further narrow damage path occurred in Yallingup. Similarly, a narrow damage path, consistent with a weak tornado was reported from Geraldton. The Perth Serpentine Doppler radar showed at least two potential

rotating couplets (indicative of rotating winds above the surface) at 0540 WST (2140 UTC). The Department of Fire and Emergency Services reported 87 calls for assistance as a result of house damage or fallen trees, and at the peak of the event, 14,000 customers lost power. Two men with muscular dystrophy died when power was lost to their respirators in the power failure.

Maximum observed winds were between 90-120 kmh-1 at several Bureau of Meteorology AWS, while a post-event survey by wind engineers indicated that the damage was done by winds of between 120-140 kmh-1.
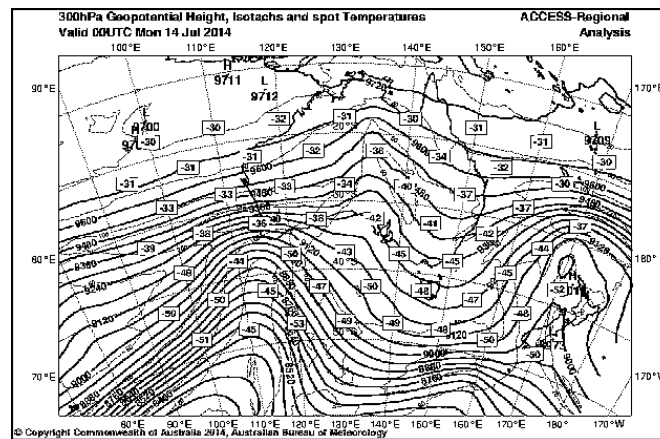
FIGURE 4-33. 300 HPA GEOPOTENTIAL HEIGHT (BOLD CONTOURS), ISOTACHS (THIN CONTOURS) AND SPOT TEMPERATURES FOR 0000 UTC 14 JULY 2014, FROM BUREAU OF METEOROLOGY NATIONAL OPERATIONS CENTRE.

An upper atmospheric trough is clearly evident over southwest Western Australia in the early morning of 14 July (Figure 4-12). The trough became increasingly negatively tilted as it crossed the coastline, enhancing its capacity generate severe weather.

Low-resolution water vapour imagery is readily available for this event from the US NOAA GIBBS (Global ISCCP B1 Browse System) website (Knapp, 2008). Figure 4-13 displays MTSAT WV imagery, with a clear dry slot (indicated in orange) near the tip of southwest Western Australia immediately to the west of the frontal band (blue/green).

Cool season severe thunderstorms are a common phenomenon in southern Australia, particularly in the southwest of Western Australia (Hanstrum et al., 2002). This case study offers a potential means to identify some of the more dangerous such events.
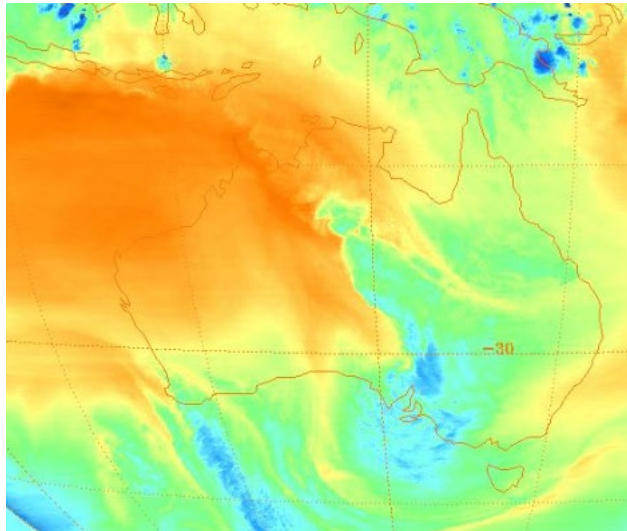
FIGURE 4-34. WATER VAPOUR SATELLITE IMAGE AT 2030 UTC 13 JULY 2014, SHOWING A WATER VAPOUR DRY SLOT (ORANGE) CLOSE TO THE SOUTHWEST WESTERN AUSTRALIAN COAST.

It is likely that the high windshear environment associated with the negatively tilted trough contributed to the likelihood of tornado occurrence, as cool-season tornadic thunderstorms are commonly associated with such environments (e.g. Childs et al., 2018). If this case study can better underpin this observation, it will be a useful addition to the research on forecasting cool-season tornadic thunderstorms as they are generally regarded as difficult to forecast with confidence (Sherburn et al., 2016).

4.2.2 Synoptic analysis

In the days preceding the event a long wave upper-tropospheric trough moved across the west coast associated with a surface trough and an extensive front. The surface front can be seen two days later in the top left panel of Figure 4-14 crossing the southeast coast of the continent. On 10 July the upper-tropospheric trough north of the northern extent of the surface front separated from the base of the trough, and a series of weak surface lows formed over the northwest Western Australian coast from early on 11 July. The longwave upper-tropospheric trough can be seen south of eastern Australia in Figure 4-15, with the now separated trough over Western Australia extending across the entire continent and across the north coast.
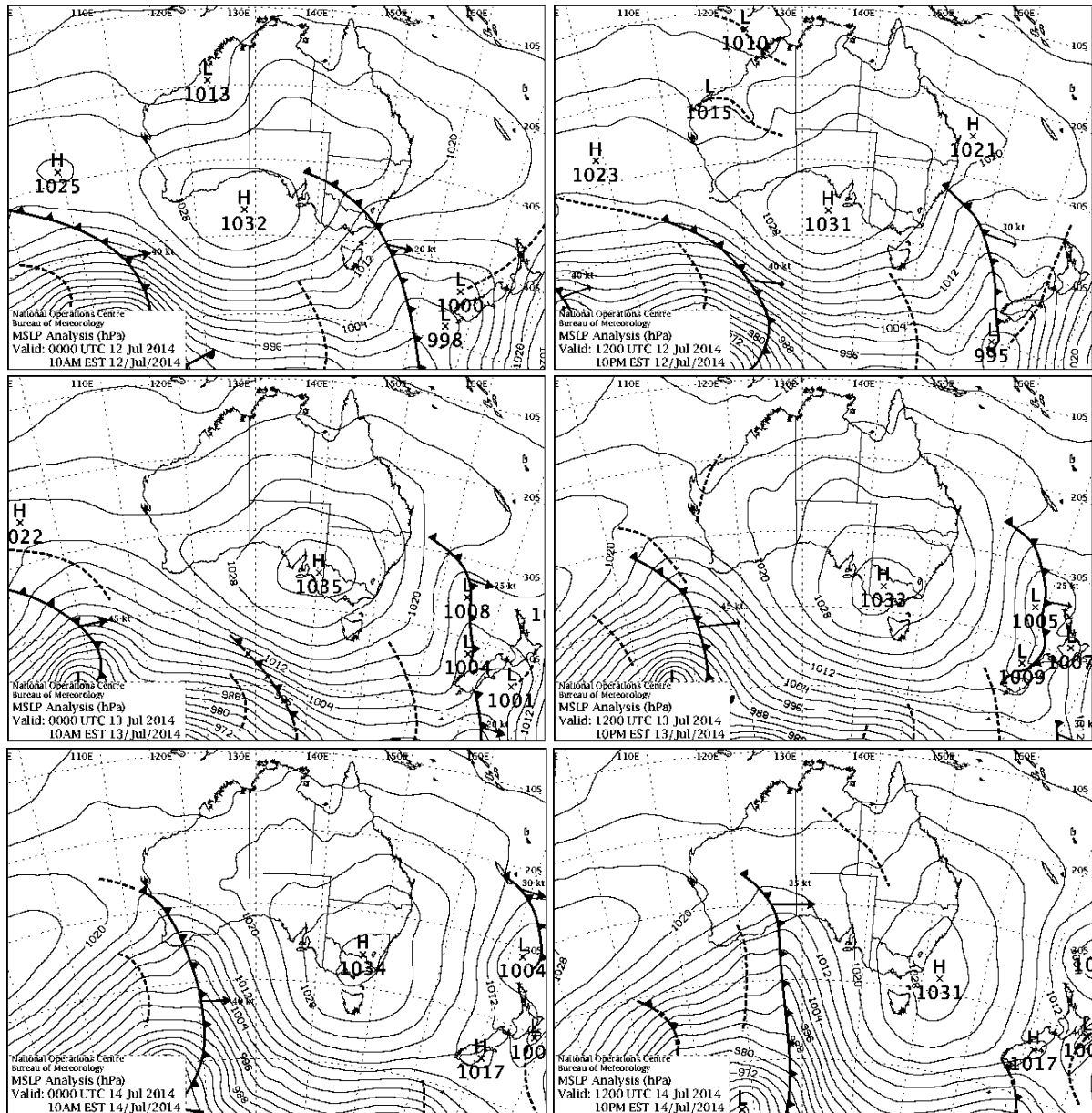
FIGURE 4-35 MEAN SEA LEVEL PRESSURE ANALYSIS CHARTS FROM THE BUREAU OF METEOROLOGY ARCHIVE AT 12-HOUR INTERVALS FROM 0000 UTC 12 JULY 2014 TO 1200 UTC 14 JULY 2014.

Over the next two days the upper-tropospheric trough moved eastwards only very slowly as it gradually assumed a near neutral tilt by 1800 UTC on 12 July. At this time a developing upper-tropospheric trough was approaching from the west and further to the south. This second trough had a strong jet across its apex at the latitude of the southwest tip of Western Australia, corresponding to the base of the first trough. The second trough continued to strengthen as it approached the slow moving first trough. The apex of the southern trough approached the base of the northern trough creating a highly diffluent region over southwest Western Australia by early on 13 July. Over the next 24 hours the southern trough became negatively tilted, crossing the tip of southwest Western Australia at 0000 UTC on 14 July.
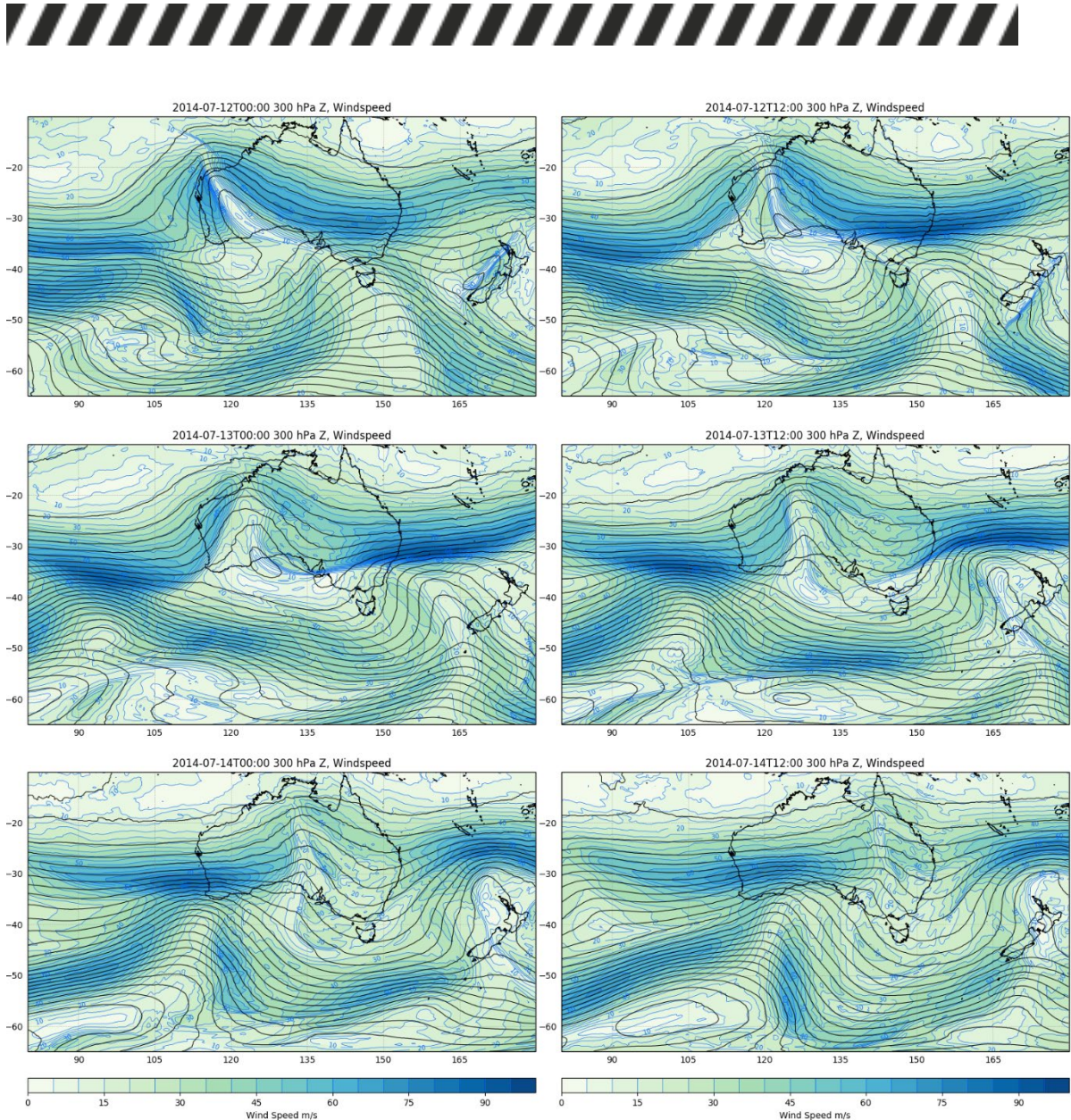
FIGURE 4-36 BARRA-R GEOPOTENTIAL HEIGHT CONTOURS AND SCALAR WIND SPEED (SHADED) AT 300 HPA AT 12 HOUR INTERVALS FROM 1200 UTC 12 JULY 2014 TO 1200 UTC 14 JULY 2014.

Following the passage of the surface front beginning on 10 July, the continent was dominated by a large high pressure system until a front embedded in a strong surface trough associated with the NTT crossed the southwest coast around 2100 UTC on 13 July.

The 300 hPa geopotential height field is plotted in the top left panel of Figure 4-16 at 1800 UTC 13 July, just prior to the tornado reports. Also plotted are the ageostrophic wind vectors and the divergence field. Red shading shows a band of strong divergence ahead of the NTT. The top right panel zooms in on the trough apex and southwest Western Australia. The ageostrophic wind vectors indicate that both stretching and diffluence were contributing significantly to the divergence field. These two terms are plotted separately in the second row of panels. In the left panel the component of the ageostrophic wind vectors parallel to the geostrophic wind highlights the stretching associated with acceleration in the entrance region of a jet on the southeast flank of the NTT. In the right panel the component of the ageostrophic wind vectors perpendicular

to the geostrophic wind indicates the sense of motion associated with the very strong diffluence at the southwest tip of the continent. Further concentrated regions of diffluence extended southward down the east flank of the NTT and across the NTT apex, while confluence occurred in the left jet exit just to the north. The third row of Figure 4-16 shows the stretching and diffluence again, but zoomed in over southwest Western Australia. Along the stretch of coast where the tornadoes were reported and over the ocean around the southwest tip of the continent it can be seen that the two terms cancel to some extent, although the positive areas tend to dominate combining to produce the coherent area of divergence shown in the top right panel.

In the bottom panel the same ageostrophic wind components are shown in relation to the scalar wind speed and the vertical wind. The region of strong upper-tropospheric divergence is associated with strong upward motion. While the ascent is quite consistent to the southwest of the continent, in the jet core to the north and across the west coast appears to be subject to some fairly strong gravity wave emission, as evidenced by the oscillations in the vertical wind motion field.
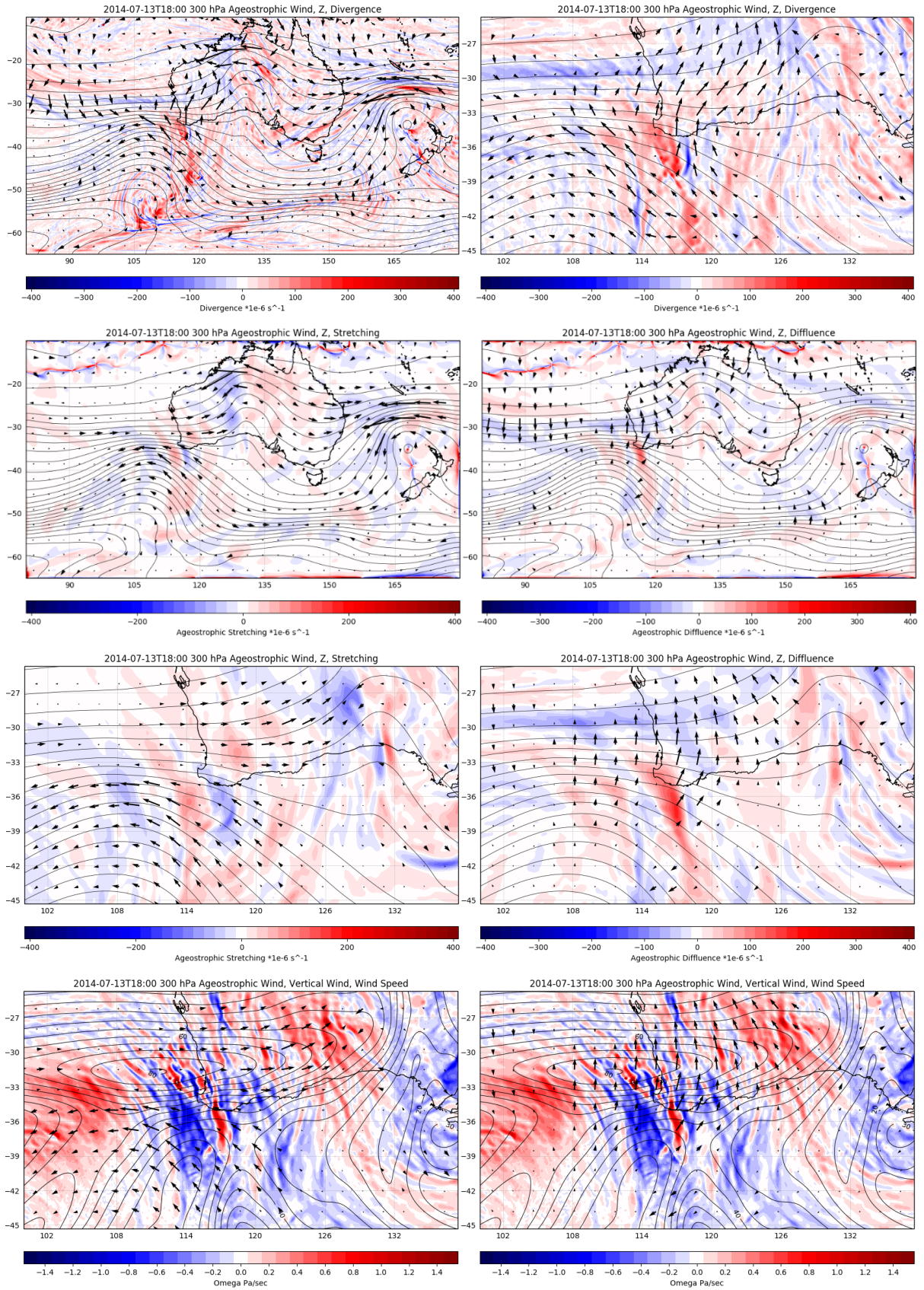
FIGURE 4-37 (PREVIOUS PAGE) TOP ROW: BARRA-R GEOPOTENTIAL HEIGHT CONTOURS, AGEOSTROPHIC WIND VECTORS (BLACK ARROWS) AND DIVERGENCE (SHADED) AT 300 HPA AT 1800 UTC 13 JULY 2014. SECOND AND THIRD ROWS: GEOPOTENTIAL HEIGHT CONTOURS, AGEOSTROPHIC WIND VECTORS PARALLEL TO GEOSTROPHIC WIND, AND AGEOSTROPHIC STRETCHING (LEFT) AND AGEOSTROPHIC WIND VECTORS PERPENDICULAR TO GEOSTROPHIC WIND, AND AGEOSTROPHIC DIFFLUENCE (RIGHT). BOTTOM ROW: SCALAR WIND SPEED CONTOURS, VERTICAL WIND, AND AGEOSTROPHIC WIND VECTORS PARALLEL TO GEOSTROPHIC WIND (LEFT) AND AGEOSTROPHIC WIND VECTORS PERPENDICULAR TO GEOSTROPHIC WIND (RIGHT).

4.2.3 Mesoscale Analysis

A sequence of 10-metre wind fields from BARRA-PH are plotted in Figure 4-17 for the hours preceding and just after the time of the tornadoes. Light northerly winds prevailed over the continent and to the south ahead of the cold front. Strong gradients in the screen level temperature and mean sea level pressure, also plotted, together with sharply backing winds over the ocean clearly indicate the position off the cold front, which crossed the coast at Perth at around 2200 UTC. Surface winds over the continent backed only slightly around this time.
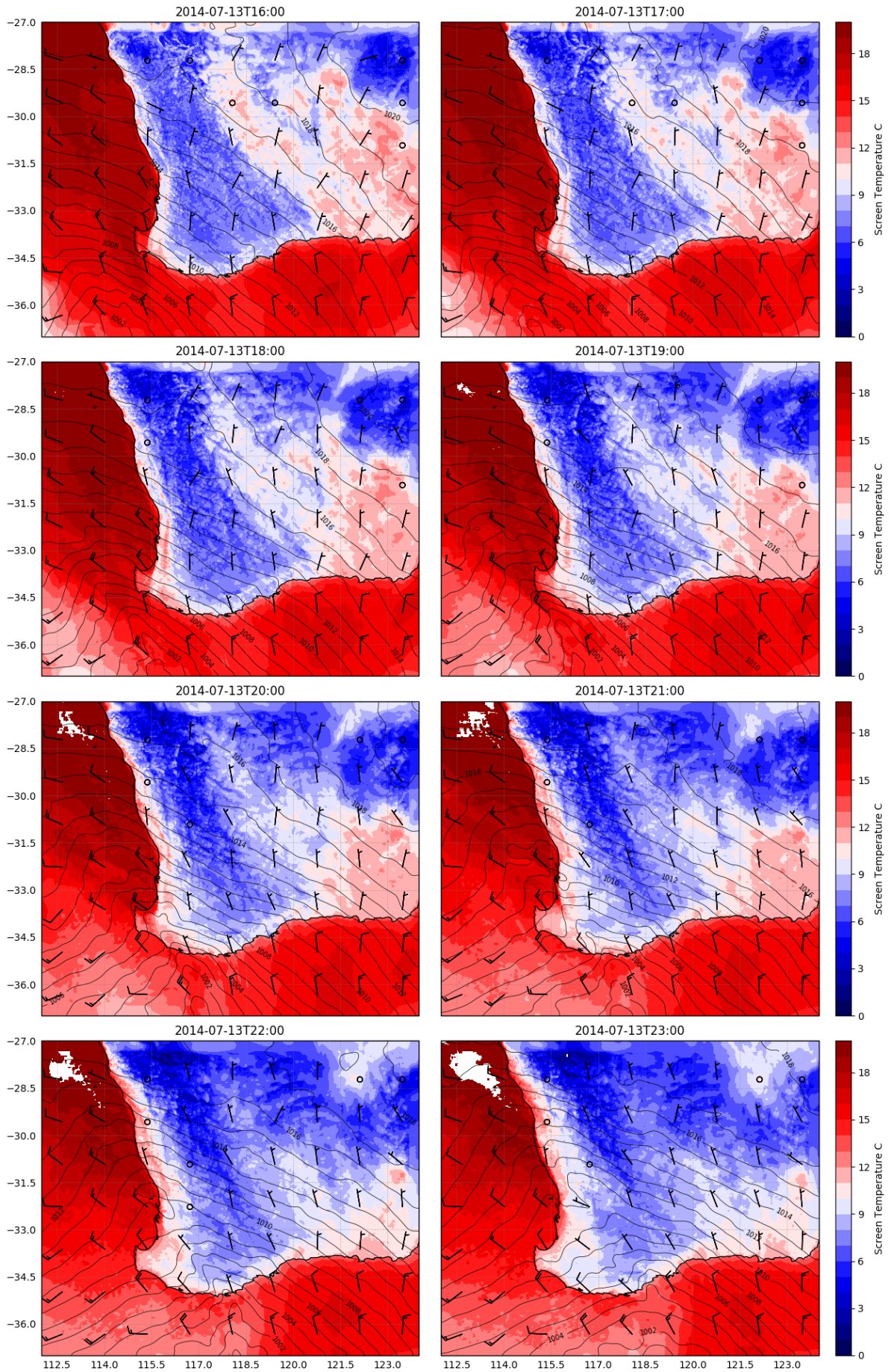
FIGURE 4-38 (PREVIOUS PAGE) BARRA-PH MEAN SEA LEVEL PRESSURE CONTOURS (HPA), SCREEN LEVEL TEMPERATURE (SHADED) AND 10-METRE WIND FIELD (BARBS) AT 1-HOUR INTERVALS FROM 1600 TO 2300 UTC 13 JULY 2014.

A comparison of the observed soundings from Perth Airport before and after the event with the simulated soundings from BARRA-PH in Figure 4-18 shows the level of detail in the vertical structure of the troposphere captured by the resolution of the dataset currently available. BARRA runs at higher vertical-resolution, but only a 21-level subset of the postprocessed data is available.
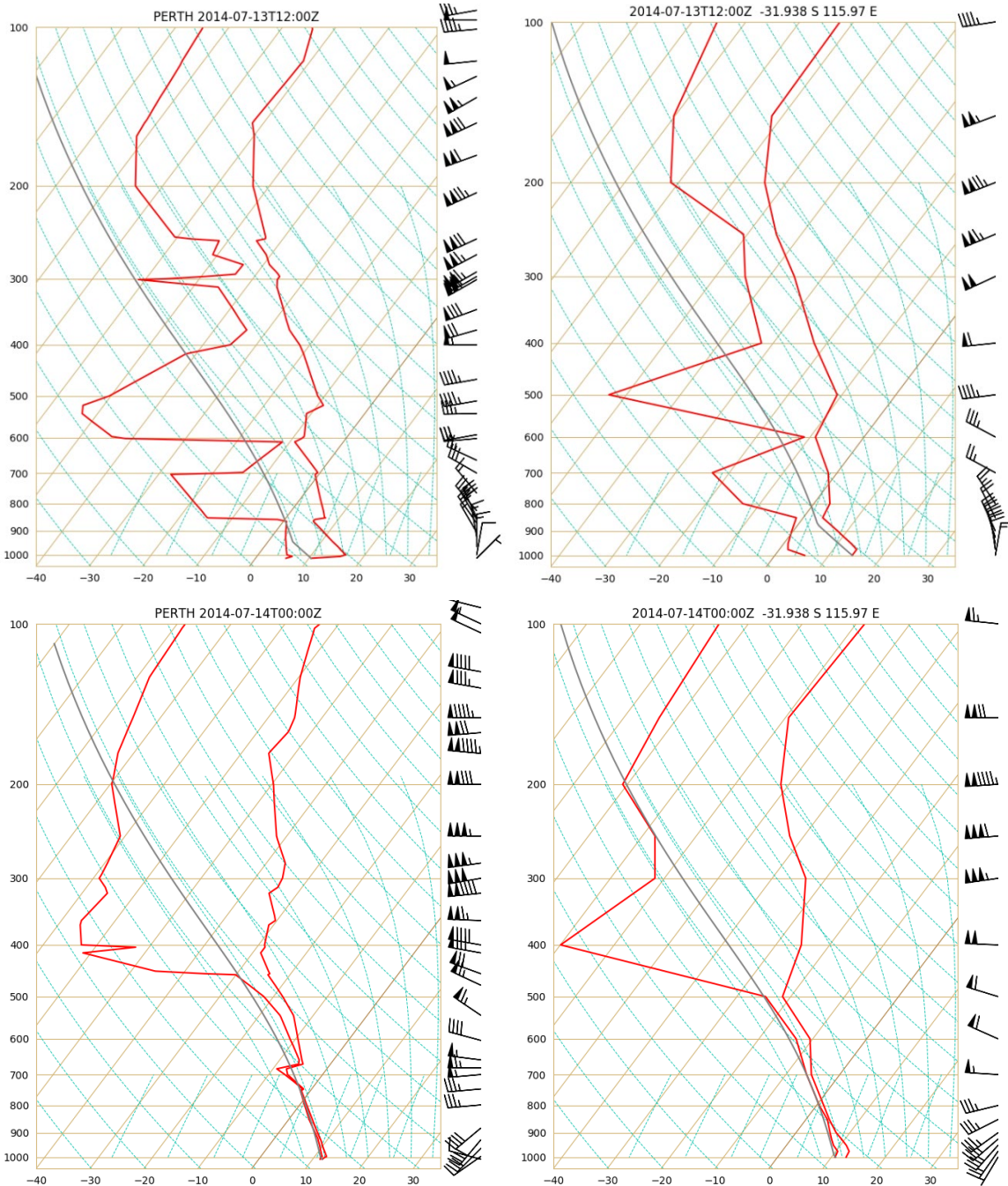
FIGURE 4-39 AEROLOGICAL DIAGRAMS FOR OBSERVATIONAL SOUNDINGS FROM PERTH AIRPORT (LEFT) AND BARRA-PH SIMULATIONS AT CORRESPONDING GRID CELL (RIGHT) AT NOMINAL 1200 UTC 13 JULY 2014 (TOP) AND 0000 UTC 14 JULY 2014 (BOTTOM).
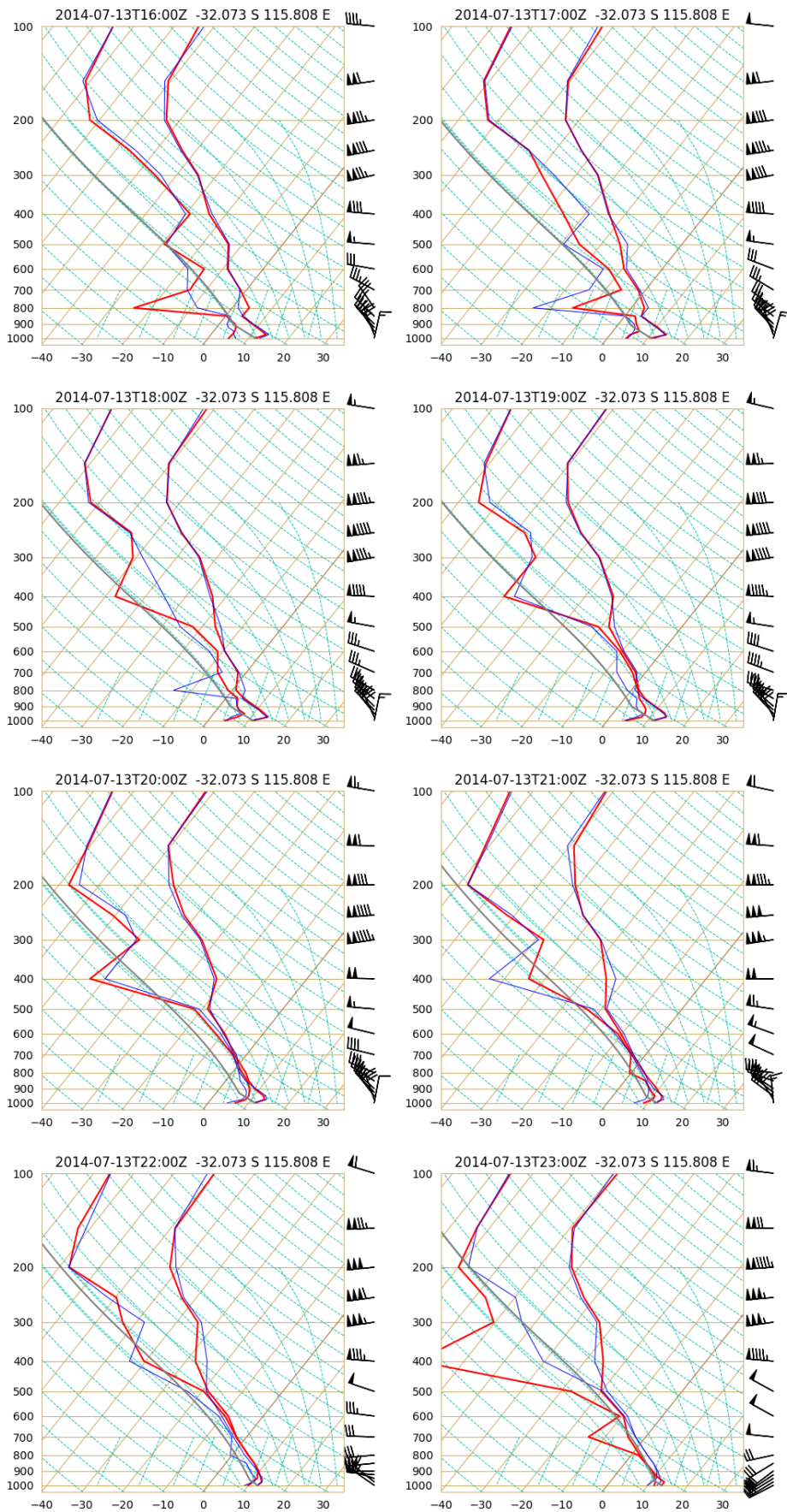
FIGURE 4-40 (PREVIOUS PAGE) AEROLOGICAL DIAGRAMS FROM BARRA-PH SIMULATIONS AT GRID CELL CORRESPONDING TO HILTON-O'CONNOR AREA OF PERTH SUBURBS AT 1-HOUR INTERVALS FROM 1600 TO 2300 UTC 13 JULY 2014. RED LINES ARE PROFILES FOR THE QUOTED DATE/TIME, BLUE LINES ARE PROFILES FOR THE PRECEDING HOUR.

Figure 4-19 gives a sequence of simulated soundings from BARRA-PH at the grid cell corresponding to the Hilton-O'Connor area the Perth, where one of the tornadoes was reported. The simulated soundings were very consistent across the Perth metropolitan area.

Throughout the period there was very strong, deep positive shear with the winds rotating anticyclonically and increasing in magnitude from the surface up to around 600 hPa and increasing in magnitude further up to the core of the jet at around 250 hPa. Similarly the bulk shear, or the magnitude of the wind vector difference between the surface and 850 hPa is very strong.

A strong surface inversion persists until the passage of the front. Above this the atmosphere becomes saturated to 500 hPa with the approach of the front, while higher still the upper troposphere becomes increasingly dry. There is little indication of any convective instability in the lower troposphere in either the observed or the simulated soundings. Convective available potential energy (CAPE) is zero throughout the period and 700 hPa surface lifted index (SLI) is positive in all soundings except the final sounding several hours after the event. However, Figure 4-20 shows that there is a sharp transition along the coast to negative SLI over the ocean as a result of slightly warmer and more moist surface conditions.
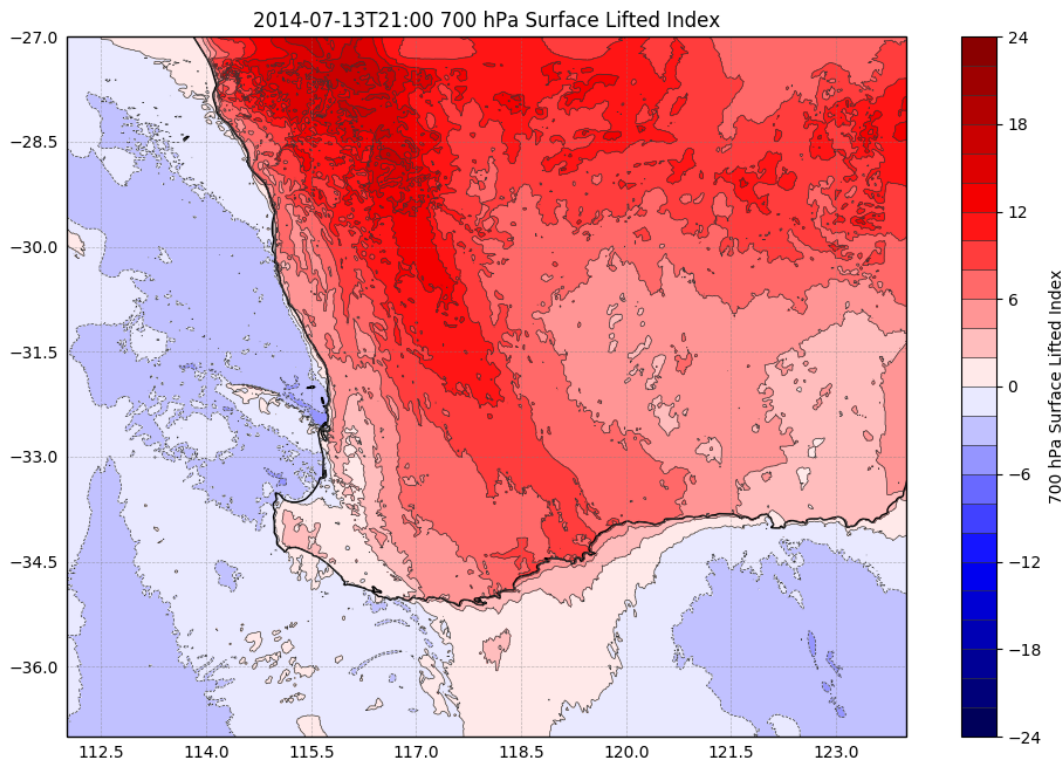
FIGURE 4-41 BARRA-PH SURFACE LIFTED INDEX AT 2100 UTC 13 JULY 2014.

In Figure 4-21 the wind field at 950 hPa highlights the sharpness of the windshear along the front. The divergence field is also plotted and the dark blue shading shows a line of strong convergence along the front where the southwesterly winds from the southern ocean meet the north-northwesterly winds over the

continent. A particularly strong stretch of this convergence line passes directly over Perth at 2200 UTC.
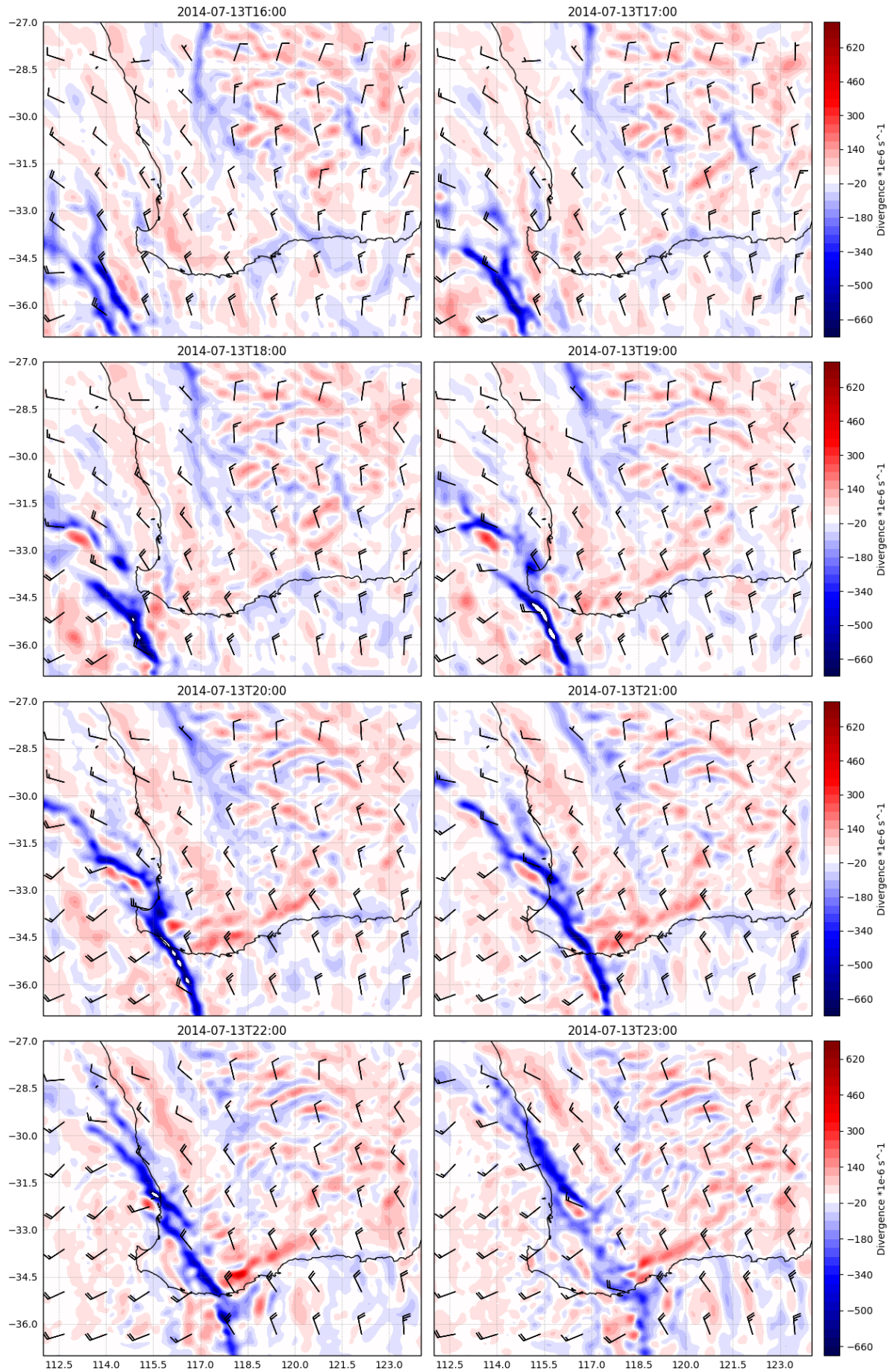
FIGURE 4-42 (PREVIOUS PAGE) BARRA-PH WIND FIELD (BARBS) AND DIVERGENCE AT 950 HPA AT 1-HOUR INTERVALS FROM 1600 TO 2300 UTC 13 JULY 2014.

Maps of the bulk shear, calculated as the magnitude of the wind vector difference between the 10-metre wind and 850 hPa wind, are given in Figure 4-22. These show wide spread strong bulk shear across southwest of the continent, and to the south in the lee of the continent. This intensifies with the approach of the front, particularly along the coast immediately ahead of the front. The contours indicate regions in the 950 hPa divergence field with convergence stronger than -140 × 10-6 s-1, as seen in Figure 4-21. These contours highlight the passage of the front and the coincidence of strong convergence with very high bulk shear as the front passes over Perth.

Cross sections along the line shown in the top left panel of Figure 4-22 are given in Figure 4-23 for the four hours immediately before and after the event. These cross sections run roughly southwest to northeast, perpendicular to the front. In these plots vertical velocity is shaded while the zonal wind is plotted in bold contours. Potential temperature is also plotted as thin black contours.

The zonal wind clearly shows the core of the upper-tropospheric jet moving further north as the apex of the NTT moves east, until it is positioned directly over Perth at 2200. At the longitude of the cross section this is in the exit region off the jet. As seen at 300 hPa in Figure 4-16, the cross sections show that in the cyclonic shear on the south side of the jet is associated with a broad region of upward motion between 500 and 150 hPa, more evident in the bottom three panels. This region of upward motion extends downward and northeastward to lower altitudes beneath the jet core, reaching all the way to the surface in the frontal zone. This is most notable at 2200 UTC after the front has crossed the coast and the regions of strongest vertical motion are directly above Perth.

As might be anticipated in the exit region of a strong jet, there appears to be gravity wave emission in the upper regions of the jet core. There are also fairly strong indications of this in the bottom panels of Figure 4-16. At 2200 UTC the upper-tropospheric wave pattern strengthens and appears to be coherent right down to the surface.
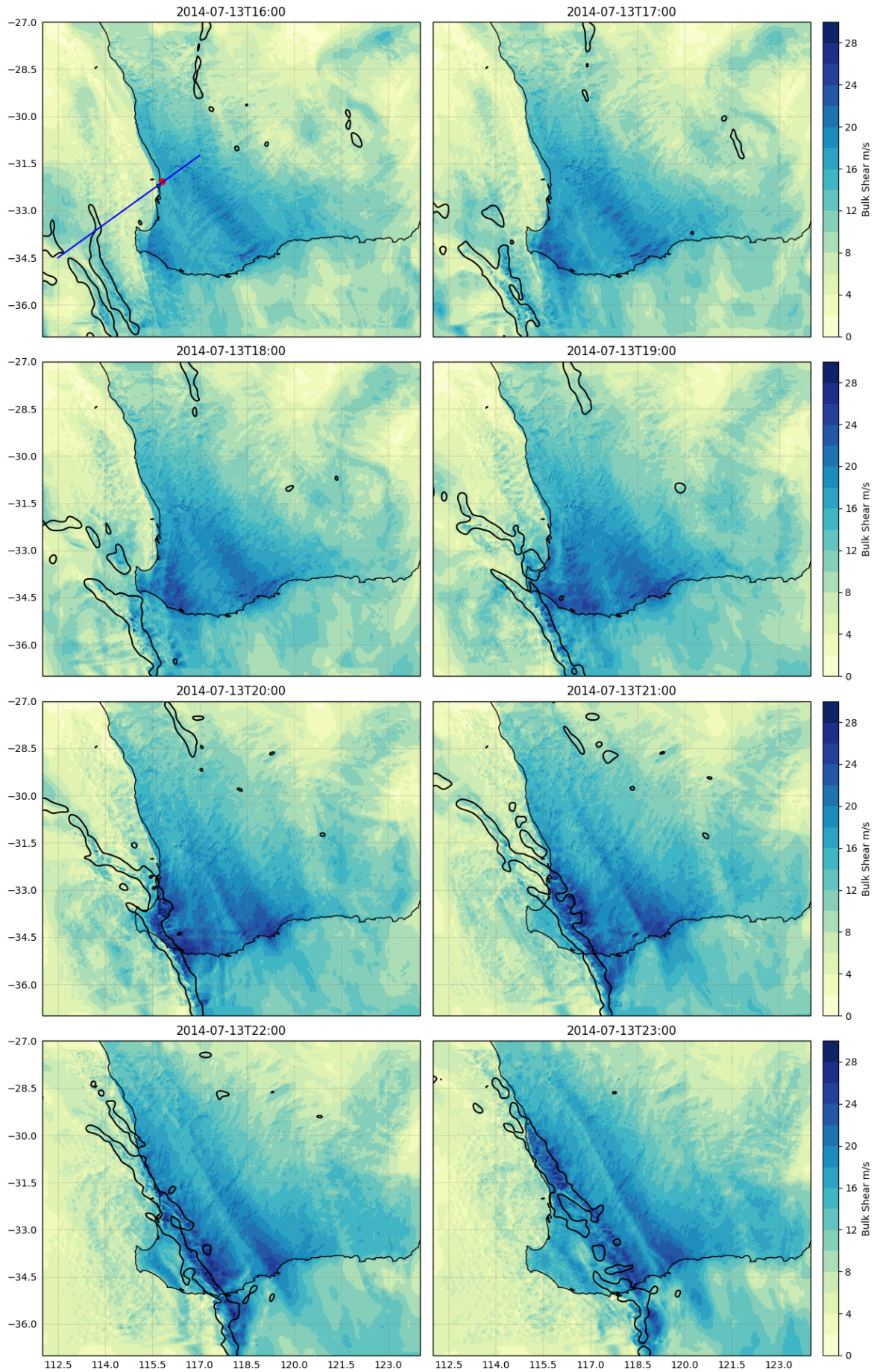
FIGURE 4-43 (PREVIOUS PAGE) BARRA-PH 10-METRE TO 850 HPA BULK SHEAR (SHADED) AND -140 × 10⁻⁶ S⁻¹ DIVERGENCE AT 950 HPA AT 1-HOUR INTERVALS FROM 1600 TO 2300 UTC 13 JULY 2014. THE LINE IN TOP LEFT PANEL INDICATES THE POSITION OF THE CROSS SECTION IN FIGURE 4-23. THE RED SPOT IN THE TOP LEFT PANEL INDICATES THE POSITION OF THE TORNADO REPORTED IN THE HILTON-O'CONNOR SUBURBS OF PERTH.
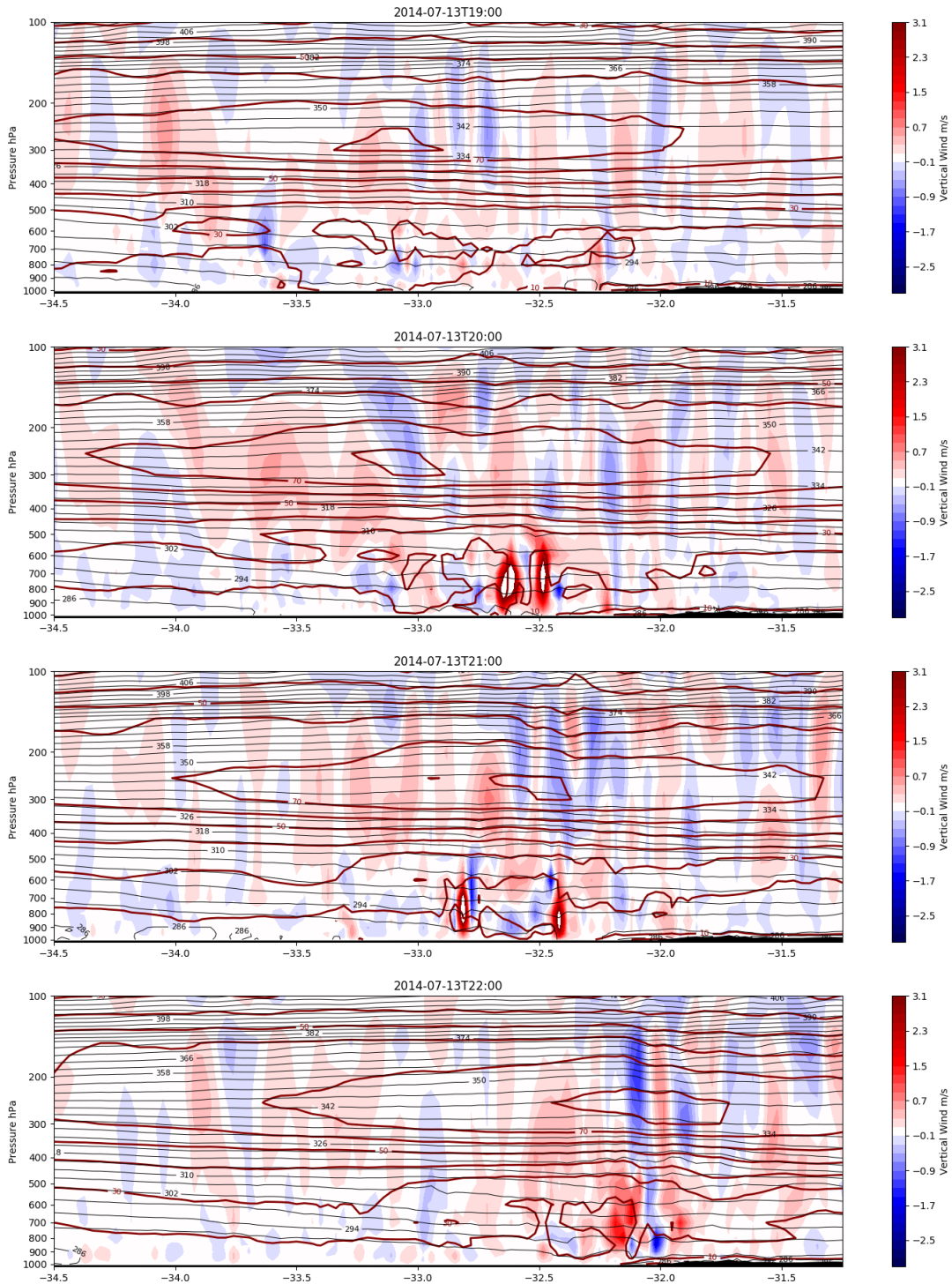
FIGURE 4-44 CROSS SECTIONS ALONG THE LINE SHOWN IN THE TOP LEFT PANEL OF FIGURE 4-22 OF VERTICAL WIND SPEED (SHADED), ZONAL WIND (RED CONTOURS, MS⁻¹) AND POTENTIAL TEMPERATURE (THIN BLACK CONTOURS, K) AT 1-HOURLY INTERVALS FROM 1900 TO 2200 UTC 13 JULY 2014.

The cross section in Figure 4-24 is a close up view of the cross section above the Perth region at 2200 UTC with an extended vertical domain showing the lower stratosphere. The region of strongest vertical wind is an updraft in the lower troposphere at 31.1 °S, directly above the coastal area of southern Perth. This is embedded in a broader region of mostly upward motion (at least in the plane

of the cross section) extending upward to the upper troposphere as discussed above. In close proximity to this are columns of rapidly descending air that could also be responsible for strong winds at the surface in addition to the tornadoes. The smaller more intense of these is likely the downdraft associated with the convection itself. The broader region to the northeast extends deep into the troposphere potentially bringing high momentum air from much higher in the vicinity of the jet. The depression of the 20 ms-1 zonal wind contour through these regions of downward motion indicate that BARRA is indeed resolving this process.
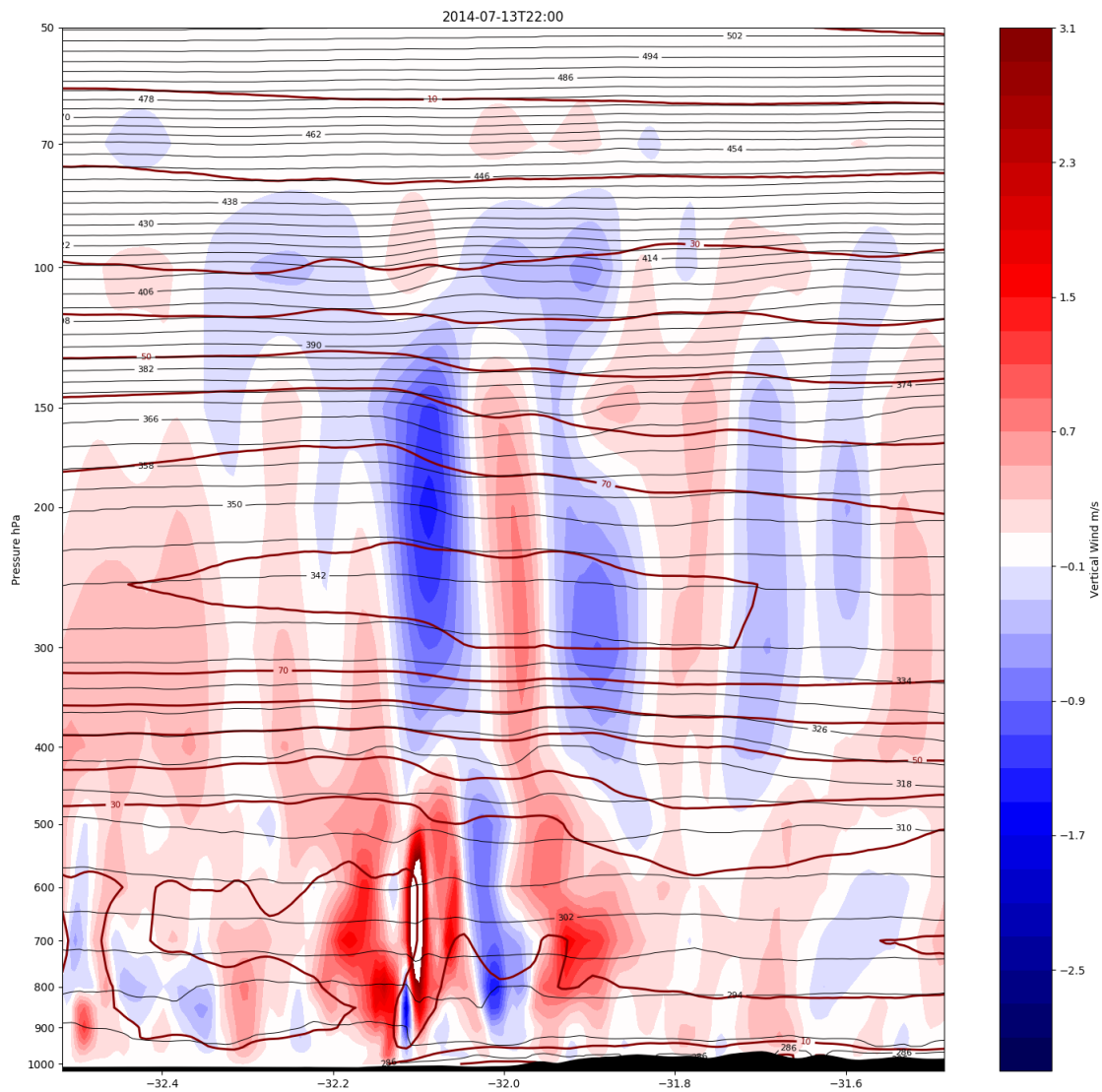
FIGURE 4-45 CROSS SECTION ALONG A RESTRICTED RANGE OF LINE SHOWN IN THE TOP LEFT PANEL OF FIGURE 4-22 OF VERTICAL WIND SPEED (SHADED), ZONAL WIND (RED CONTOURS, MS⁻¹) AND POTENTIAL TEMPERATURE (THIN BLACK CONTOURS, K) AT 2200 UTC 13 JULY 2014.

The quadrature phasing of the zonal and vertical wind perturbations in the upper troposphere is consistent with gravity wave motion, however, this relationship is not evident in the noisier lower troposphere. Nevertheless, the coherence of the vertical wind structure down to the surface is remarkable. The gravity wave does not appear to be propagating into the stratosphere indicating the possibility of reflection at the tropopause. The vertical wavelength, which appears to be of the order of the depth of the troposphere, and the slight discontinuity between 500 and 400 hPa are suggestive of a trapped mode. However, this is speculative and there could be other processes by which the wave is being coupled to the frontal circulation.

The coherence of this very deep circulation is not evident in the following hour (not shown), either rapidly breaking down or propagating out of the cross section examined.

4.2.4 Discussion

The analysis of the mesoscale meteorology near the surface has focussed largely on the parameters relating to the three criteria defined by Hanstrum et al. (2002) for the purpose of operationally identifying environments conducive to the occurrence of cool season tornadoes. While the low-level shear and convergence criteria were emphatically met at the locations of the tornadoes, the requirement of a negative SLI was not met in either the observed or simulated soundings. However, over the Indian Ocean to the west, across a sharp transition zone along the coast, SLI was negative while the bulk shear was low. Convergence associated with the passage of the surface front could have brought the instability and dynamic forcing together in coastal areas.

Regardless of the convective instability criteria, the lower-level dynamical forcing alone was very strong and with additional dynamical processes acting to reinforce this in the mid- to upper troposphere, little convective instability might have been required. With respect to the latter, diffluence in the right exit region of a strong jet, exacerbated by the interaction of the NTT with another trough downstream resulted in a broad region of ascending air. The negative tilt in the upper-tropospheric trough positioned this region of diffluence directly above the frontal zone. Gravity wave emission in the jet exit could also have played a role in establishing some very deep vertical circulation.

The deep tropospheric coherence of the vertical circulation was either highly transient, highly mobile or both. This highlights the difficulty of resolving high-end severe weather events and is an important aspect of what a modern numerical weather prediction (NWP) system can offer. Of further note in this regard is the value of BARRA in its ability capture such fine scale processes for research applications. The intention of this case study has been to highlight the dynamic forcing associated with NTT, and the value in taking the forecast of a NTT as a cue to look more closely for any atypical processes that might be triggered. There is broad scope to investigate this case in more detail in order to better characterise the coupling processes and provide further guidance for forecasting such events.

5 CLIMATOLOGY

5.1 INTRODUCTION

A climatology of NTT was compiled using the geopotential height fields of BARRA-R (section 2.1). The objective of the climatology was to record all of the NTT that occurred in southern Australia during the 1990-2018 period of the BARRA dataset. Additionally, it was noted whether each NTT event was associated with one or more entries in the SSA (section 2.2). Information on subregional occurrence was also included. Certain recurrent patterns enabled some NTT to be grouped accordingly for further discrimination.

The possibility of automating the identification of NTT in the BARRA-R data was explored. While various algorithms have been developed for the automated analysis of trough lines, Li et al. (2018) report that the most successful algorithms yield trough analysis success rates of around 80 %, and their measure of success necessarily permits some degree of inconsistency. The automated trough line outputs would need to be post-processed to determine the tilt, which as noted in section 3.1, is not always a simple analysis.

Based these ambiguities and the results of some preliminary attempts to implement such a scheme, this approach was abandoned in favour of visual inspection. For each six-hourly analysis in the BARRA-R data the 300 and 500 hPa geopotential height fields were inspected and the presence of an NTT recorded in a database. The locations of reported severe weather from the SSA for the six-hour period following the time of the analysis were also plotted on the geopotential height charts and a subjective assessment made of whether those reports were likely to be associated with any NTT present.

The process of compiling the climatology was iterative to some extent since it was not known what patterns in the morphology and regionality of NTT would emerge. The final result was a database of NTT occurrence on a six-hourly basis, recording the date, time, co-occurrence of one or more SSA entry, co-occurrence of any known severe fire event, any known publications describing the event, subregional location and any subgrouping based on recurrent patterns. The latter two of these will be discussed in section 5.2.

5.2 CLASSIFICATION OF SYNOPTIC PATTERNS INVOLVING NTT

The review of documented NTT events in section 3.2 was used as an initial guide for the scale of NTT events to be recorded and different morphologies that might be characteristic to particular surface impacts. After several iterations of analysis and review of the classifications, five subregional identifiers were chosen. Each event was classified as either eastern or western as determined by the longitude of the apex of the NTT. Each even was further classified as either Southern Ocean, south coastal or inland based on the extent of the trough axis. The criteria for each classification is summarised in Table 5-1.

TABLE 5-1 CRITERIA FOR ASSESSING REGIONAL CLASSIFICATIONS OF NEGATIVELY TILTED UPPER-TROPOSPHERIC TROUGHS.

Regional Classification	Criterion
Eastern Australia	NTT apex east of 135 °E
Western Australia	NTT apex west of 135 °E
Southern Ocean	NTT axis does not cross Australian continental south coast
South Coastal	NTT axis crosses Australian continental south coast
Inland	NTT axis entirely north of Australian continental south coast

Each NTT was assigned one of six further classifications which were defined based on the NTT scale and morphology of development. Each classification is described briefly below with a characteristic example.

5.2.1 Cut-off

In many cases, an upper-tropospheric instability developed into a positively tilted trough which subsequently became negatively tilted as it cut-off into a closed cyclonic system. In these cases surface impacts were often reported just prior to, or in the 12 hours following the system becoming cut-off. A typical example of this type of event is shown in the 300 hPa geopotential height fields on 24-25 February 1993, shown in Figure 5-1. At 1200 UTC on 24 February a shortwave trough south of the Great Australian Bight has just assumed a negative tilt (left panel). Twelve hours later the system has become a cut-off upper-tropospheric low (right panel).

This pattern had a tendency to occur frequently over southwest Western Australia and southeast Australia. In these cases the NTT would develop in the Southern Ocean, extending across the south coast as it became negatively tilted and cutting off over the south of the continent. Given the frequency with which these cases were observed, they were flagged as a sub-classification of the cut-off classification. Frequently the southeast Australian occurrence of this pattern would begin to develop but the NTT would not become cut-off and remained coherent as it propagated across the Tasman Sea, often not assuming a negative tilt until just off the east coast of Australia. This non-cut-off variation was also described as a sub-classification of the not cut-off classification described below in section 5.2.3.
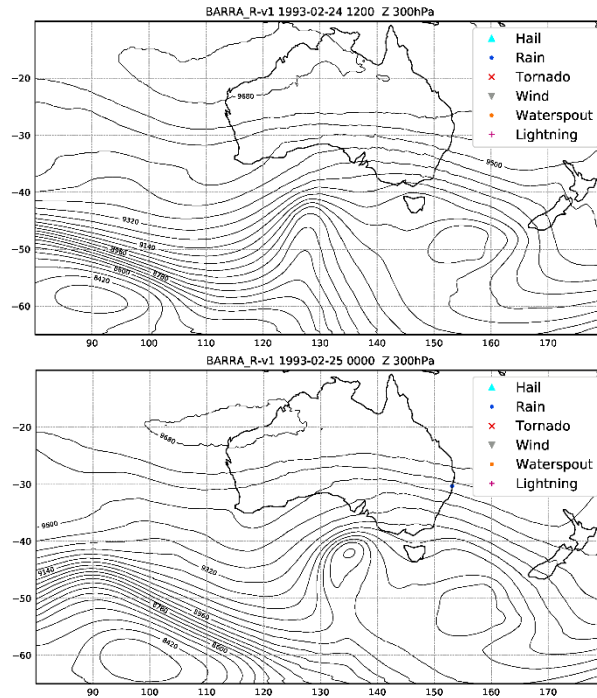
FIGURE 5-46 BARRA-R GEOPOTENTIAL HEIGHT CONTOURS (METRES) AT 300 HPA AT 1200 UTC 24 FEBRUARY 1993 (LEFT) AND AT 0000 UTC 25 FEBRUARY 1993 (RIGHT). SEVERE WEATHER REPORTED IN THE BUREAU OF METEOROLOGY SEVERE STORMS ARCHIVE DURING THE FOLLOWING 6 HOURS IS INDICATED BY THE MARKERS DEFINED IN THE LEGEND AT TOP RIGHT.

5.2.2 Well Developed Cut-off

In a number of cases where an upper-tropospheric cut-off low developed from either a positively or negatively tilted trough, the system became negatively tilted 24 or more hours later. An example of this was the 24 October 2005 event described by Feren (2008) in which large hail and heavy rain was reported along broad stretches of the east coast. In the left panel of Figure 5-2 this system can be seen originating three days earlier as an NTT in the Indian Ocean southwest of Western Australia just as it was beginning to cut off. In some cases the well developed cut-off low assumed a negative tilt as it reconnected with the jet stream to the south.
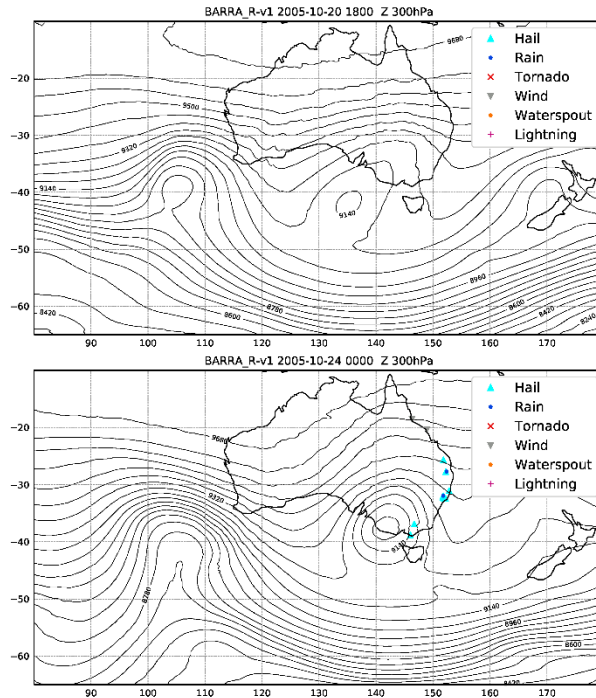
FIGURE 5-47 BARRA-R GEOPOTENTIAL HEIGHT CONTOURS (METRES) AT 300 HPA AT 1800 UTC 20 OCTOBER 2005 (LEFT) AND AT 0000 UTC 24 OCTOBER 2005 (RIGHT). SEVERE WEATHER REPORTED IN THE BUREAU OF METEOROLOGY SEVERE STORMS ARCHIVE DURING THE FOLLOWING 6 HOURS IS INDICATED BY THE MARKERS DEFINED IN THE LEGEND AT TOP RIGHT.

5.2.3 Not Cut-off

The majority of NTT did not become cut-off. The NTT associated with the 22 November 1992 Scottsdale tornado described by Fox-Hughes et al. (1996) is an example of such an event. In this case and many like it the NTT dissipated as it continued to move southeastward around the downstream flank of a longwave trough, as can be seen in Figure 5-3. In other cases where the NTT was embedded in a more uniform jetstream, the NTT relaxed back towards a neutral or positive tilt as it dissipated.
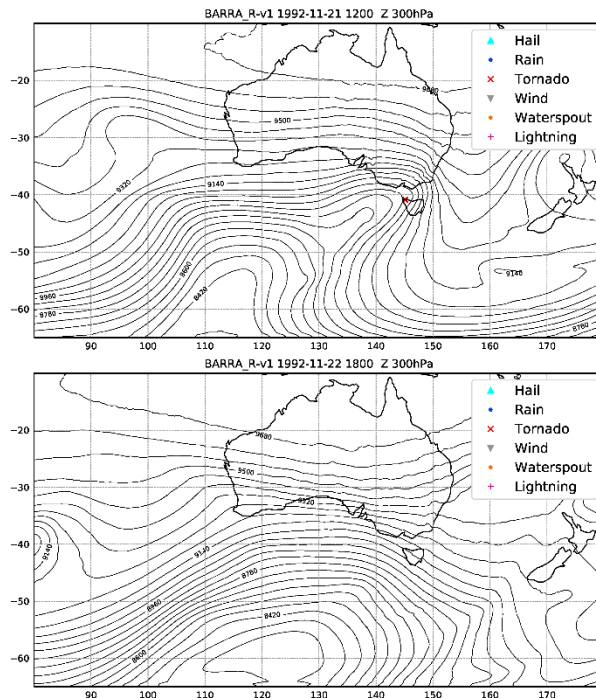
FIGURE 5-48 BARRA-R GEOPOTENTIAL HEIGHT CONTOURS (METRES) AT 300 HPA AT 1200 UTC 21 NOVEMBER 1992 (LEFT) AND AT 1800 UTC 22 NOVEMBER

2005 (RIGHT). SEVERE WEATHER REPORTED IN THE BUREAU OF METEOROLOGY SEVERE STORMS ARCHIVE DURING THE FOLLOWING 6 HOURS IS INDICATED BY THE MARKERS DEFINED IN THE LEGEND AT TOP RIGHT.

5.2.3 South Coastal

A less frequent but notable occurrence was the development of a medium scale NTT in the Great Australian Bight, typically crossing the southern coastline, and subsequent propagation along the southeast coast. The progression of such a NTT across along the southeast coast is given in Figure 5-4.
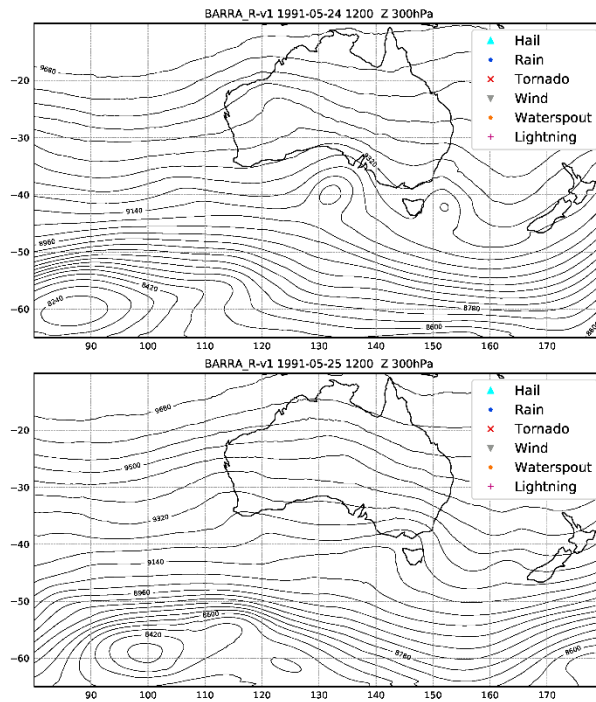
FIGURE 5-49 BARRA-R GEOPOTENTIAL HEIGHT CONTOURS (METRES) AT 300 HPA AT 1200 UTC 24 MAY 1991 (LEFT) AND AT 1200 UTC 25 MAY 1991 (RIGHT). SEVERE WEATHER REPORTED IN THE BUREAU OF METEOROLOGY SEVERE STORMS ARCHIVE DURING THE FOLLOWING 6 HOURS IS INDICATED BY THE MARKERS DEFINED IN THE LEGEND AT TOP RIGHT.

5.2.5 Small Scale

The 7 December 2005 Victorian hail event described by Feren (2008) is an example of a NTT of very small scale, but nevertheless significant impact. The passage of this NTT across Victoria can be seen in Figure 5-5. In general, the climatology was limited to synoptic scale NTT and excluded such events. However, a few events of this scale were recorded where it was evident that they were responsible for severe weather, although they were not included in the main climatological analysis.
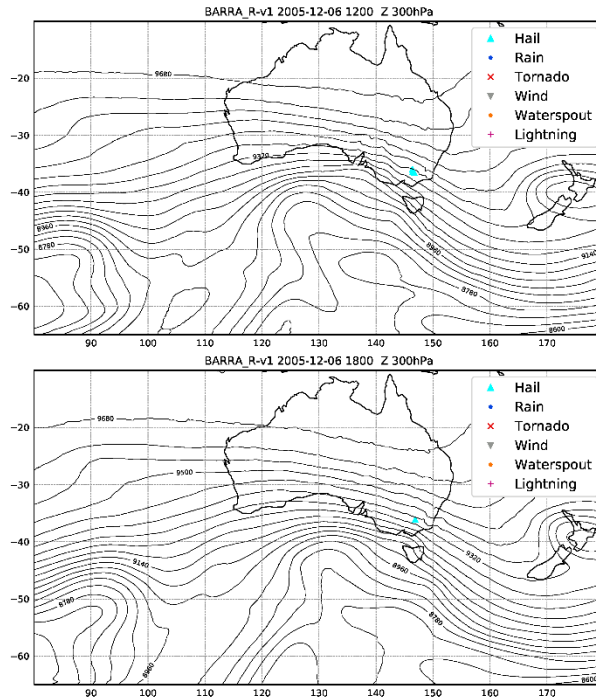
FIGURE 5-50 BARRA-R GEOPOTENTIAL HEIGHT CONTOURS (METRES) AT 300 HPA AT 1200 UTC 6 DECEMBER 2005 (LEFT) AND AT 1200 UTC 6 DECEMBER 2005 (RIGHT). SEVERE WEATHER REPORTED IN THE BUREAU OF METEOROLOGY SEVERE STORMS ARCHIVE DURING THE FOLLOWING 6 HOURS IS INDICATED BY THE MARKERS DEFINED IN THE LEGEND AT TOP RIGHT.

5.2.6 Eastern Inland

A broad shallow NTT over inland eastern Australia was noted on of 22 February 2013 by Louis (2018) in relation to the east coast low that caused tornadoes along the New South Wales south coast (Figure 5-6). NTT that occurred primarily over the continent were rare and were not the subject of climatological analysis since any associated severe weather was generally reported in northeast Australia, out of the scope of this study. However, for completeness they were recorded and broad shallow NTT events like that depicted in Figure 5-6 occurred over inland eastern Australia made up a sufficiently large proportion as to be noteworthy.
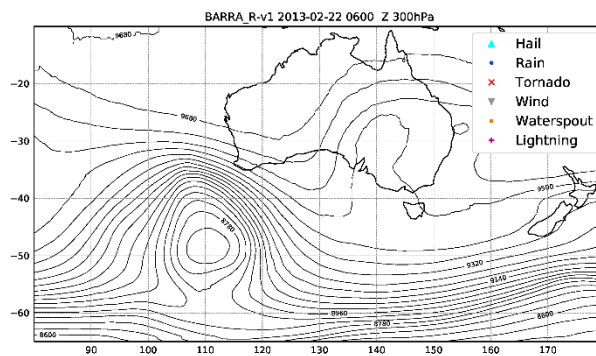
FIGURE 5-51 BARRA-R GEOPOTENTIAL HEIGHT CONTOURS (METRES) AT 300 HPA AT 0600 UTC 22 FEBRUARY 2013. SEVERE WEATHER REPORTED IN THE BUREAU OF METEOROLOGY SEVERE STORMS ARCHIVE DURING THE FOLLOWING 6 HOURS IS INDICATED BY THE MARKERS DEFINED IN THE LEGEND AT TOP RIGHT.

5.3 CLIMATOLOGY OF NTT

A climatological analysis is presented initially for all of the NTT events recorded in the BARRA-R data set from 1990-2018, with the exceptions of the inland regional, small scale, and eastern inland events described in section 5.2. Climatological

characteristics of note that are particular to regions or classifications are subsequently highlighted.

5.3.1 Frequency of NTT Events

Time series of monthly NTT occurrence is shown in Figure 5-7. The number of NTT events per month (hereafter NTT#) is plotted in blue, exhibiting significant variability on monthly time scales. In total 862 NTT events were identified in the 29 years of BARRA-R data analysed, just under 30 events per year. The monthly mean number of events is 2.5 with a standard deviation of 1.6.
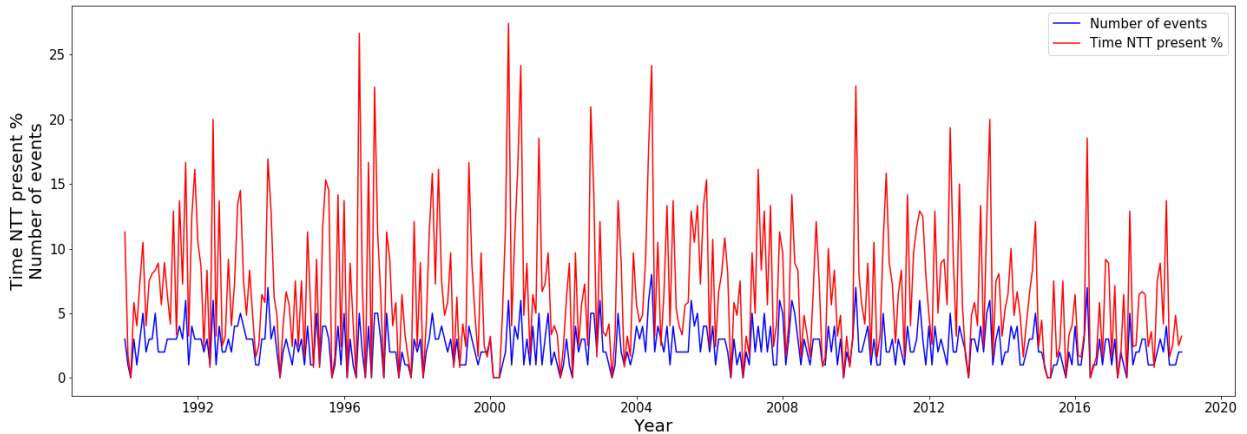
FIGURE 5-52 TIME SERIES OF NUMBER OF NEGATIVELY TILTED TROUGHS PER MONTH (BLUE) AND PERCENTAGE OF TIME THAT NEGATIVELY TILTED TROUGHS ARE PRESENT EACH MONTH (RED).

Also shown in Figure 5-7 is the percentage of time each month during which NTT were present (hereafter NTT%), showing greater variability than NTT# on monthly time scales as well as significant interannual variability. Over the 29 year period NTT were present 6.7 % of the time on average. The basic statistics are summarised in Table 5-2.

TABLE 5-2 SUMMARY STATISTICS FOR ALL NEGATIVELY TILTED TROUGH EVENTS IDENTIFIED IN THE BARRA-R DATASET DURING THE PERIOD OF 1990-2018.

Total events	862
Events per year	29.72
Events per month	2.48
Standard deviation of monthly events	1.58
Percentage of time NTT present	6.72 %
Standard deviation of monthly percentage of time NTT present	5.24 %

Visual inspection suggests that there has been a decrease in both NTT# and NTT% towards the end of the period. While the precise nature of this trend is difficult to discern, linear regression confirms a decrease in NTT# of 0.17 events per month per decade, which represents a reduction of 18 % over the 29 year period. Similarly, for NTT% there is a decrease of 0.72 % per decade, representing a reduction of 30 %.

5.3.2 Monthly Climatology

The climatological monthly mean annual cycle of NTT event occurrence is shown in Figure 5-8. The mean annual cycle over the full period, shown in blue, exhibits a distinct semi-annual pattern with a winter peak in June-July and a second peak

spanning late spring and early summer from November-January. The difference in the climatological means for the January maximum and February minimum is statistically significant at the 99.8% confidence level, as measured by Welch's t-test. The sudden drop from the maximum in January to the minimum in February represents a variability of more than 40% of the maximum.
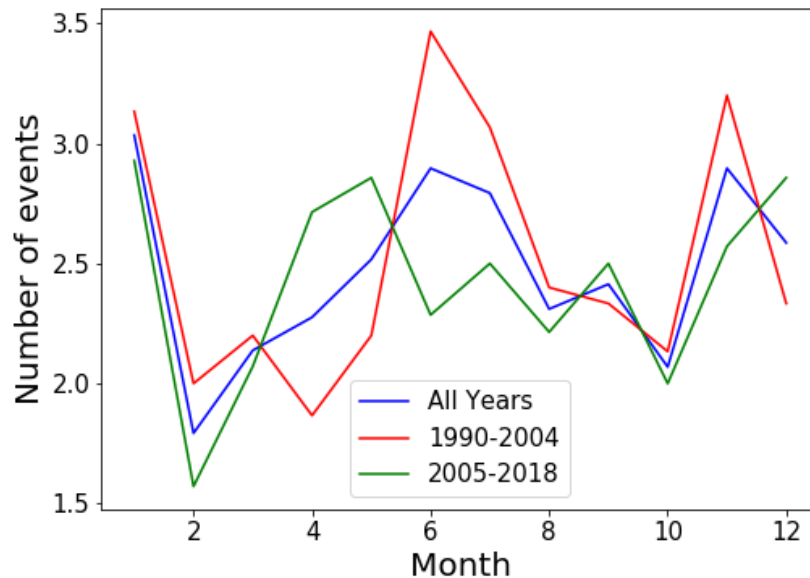
FIGURE 5-53 CLIMATOLOGICAL MONTHLY MEAN NUMBER OF NEGATIVELY TILTED TROUGH EVENTS PER MONTH FOR ALL YEARS (BLUE), FIRST 15 YEARS (RED), AND LAST 14 YEARS (GREEN).

The analysis was repeated for two sub-periods, 1990-2004 and 2005-2018, representing approximately the first and second halves of the dataset, in order to further characterise the trend observed in Figure 5-7. The climatologies for the two sub-periods are also plotted in Figure 5-8 showing lower values in general for the second sub-period (green line) than the first sub-period (red line). Also of note is a shift of the winter peak to a weaker autumn peak. While the differences between the sub-periods in April and June are not statistically significant they will be discussed further in the regional context later.

Figure 5-9 shows the same climatological analysis applied to NTT%. The same semiannual cycle evident in the NTT# analysis is again the dominant signal, with sharper peaks in June and November. Similar changes between the first and second sub-periods are also evident although the autumn peak in the second sub-period is later and less pronounced.

Results for the same analysis performed on a seasonal basis are presented in Table 5-3. The semiannual signal is not as well represented due to November to January span across spring and summer. Rather than attempting to capture this feature by assuming an offset basis for this and subsequent composite analyses, the contributions to the overall semiannual signal will be considered in the regional breakdown in later sections.
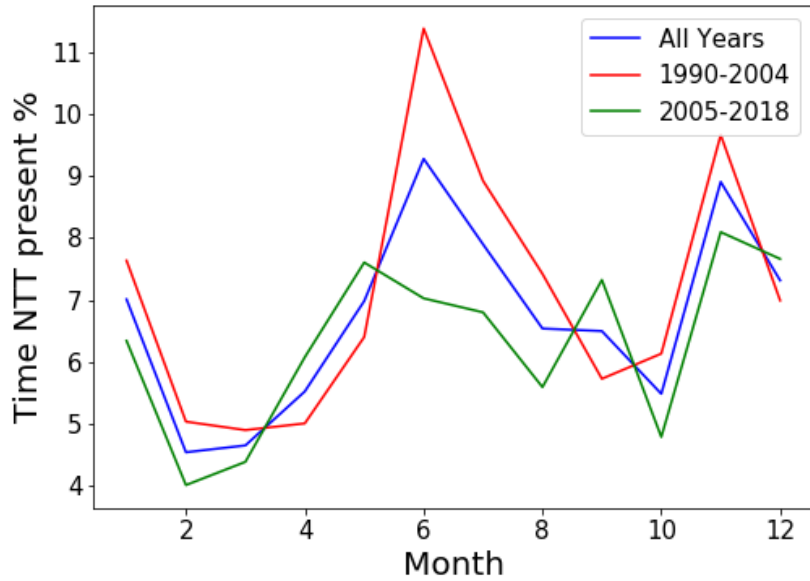
FIGURE 5-54 CLIMATOLOGICAL MONTHLY MEAN PERCENTAGE OF TIME THAT NEGATIVELY TILTED TROUGHS ARE PRESENT PER MONTH FOR ALL YEARS (BLUE), FIRST 15 YEARS (RED), AND LAST 14 YEARS (GREEN).

TABLE 5-3 CLIMATOLOGICAL SEASONAL MEANS OF MONTHLY PERCENTAGE OF TIME THAT NEGATIVELY TILTED TROUGHS ARE PRESENT (ALL %), AND MONTHLY MEAN NUMBER OF NEGATIVELY TILTED TROUGH EVENTS (ALL #) FOR ALL YEARS OF THE ANALYSIS (1990-2018).

Season	All %	All #
Autumn	5.71	2.31
Spring	6.96	2.46
Summer	6.28	2.47
Winter	7.90	2.67

5.3.3 Relationship with Regional Climate Drivers

The Spearman rank correlation of the monthly time series of NTT# and NTT% with the various climate indices described in section 2.3 was tested. The strongest relationship found was an anticorrelation of NTT% with the Southern Annular Mode (SAM) with a coefficient of -0.23. The next strongest anticorrelation was with the NIÑO1+2 index with a coefficient of -0.16. All other indices had coefficients of around -0.1 or smaller.

Cross correlation was also tested to investigate any potential predictability. The only indices to show any improved correlation with a lag of one month or more were the NIÑO3 and NIÑO3.4 at 2 and 3 months lag, although coefficients did not exceed -0.2.

Southern Annular Mode

Composite means of NTT# and NTT% for positive and negative phases of the SAM are given in Table 5-4. The strong preference for NTT occurrence during negative SAM (left panel) is statistically significant. The seasonal breakdown of this preference (right panel) generally follows the overall seasonal pattern observed

in Table 5-3, the only notable exception being a larger number of NTT events during autumn under negative SAM.

The synoptic scale weather systems of which upper-tropospheric troughs are a feature result from baroclinic instability in the persistent mid- to high-latitude westerly winds of the southern hemisphere. Hence, it is an intuitive result that southern Australia is subject to higher occurrences of NTT during the negative phase of the SAM when westerly winds extend further north than usual. The winter bias likely has a similar basis, since the seasonal variation in the northward extent of the westerlies maximises in winter. Thus, the negative SAM and winter biases compound to yield the strongest preference in Table 5-4 for NTT occurrence under these combined conditions.

TABLE 5-4 SOUTHERN ANNULAR MODE (SAM) PHASE COMPOSITE MEANS OF MONTHLY PERCENTAGE OF TIME THAT NEGATIVELY TILTED TROUGHS ARE PRESENT (ALL %), AND MONTHLY MEAN NUMBER OF NEGATIVELY TILTED TROUGH EVENTS (ALL #) FOR ALL YEARS OF THE ANALYSIS (1990-2018) (LEFT). COMPOSITE MEANS FOR SAM PHASE AND SEASON (RIGHT).

SAM Phase	All %	All #
Negative SAM	7.84	2.71
Positive SAM	5.89	2.30

SAM Phase	Season	All %	All #
Negative SAM	Autumn	7.51	2.81
	Spring	7.68	2.64
	Summer	7.75	2.58
	Winter	8.33	2.83
Positive SAM	Autumn	4.72	2.04
	Spring	6.23	2.28
	Summer	5.47	2.41
	Winter	7.53	2.52

Indian Ocean Dipole

Composite means of NTT# and NTT% for positive, neutral and negative phases of the Indian Ocean Dipole (IOD) are given in Table 5-5. Negative and neutral phases of the IOD have NTT occurrence slightly above average while a positive IOD results in a statistically significant reduction of more than 30% from neutral conditions (left panel).

The seasonal breakdown of the IOD phases (right panel) shows that during neutral and positive IOD the overall seasonality observed in Table 5-3 is maintained, while reflecting the low bias in the positive IOD. While the comparison of neutral and positive IOD seasonality is generally robust, the low

number of months that experience negative IOD in the 1990-2018 period results in large uncertainty in the associated statistics. In general, little weight can be placed on IOD influence outside of the winter-spring period, since the mechanism supporting development and maintenance of IOD breaks down with the onset of the Australian monsoon and Indonesian Throughflow.

TABLE 5-5 INDIAN OCEAN DIPOLE (IOD) PHASE COMPOSITE MEANS OF MONTHLY PERCENTAGE OF TIME THAT NEGATIVELY TILTED TROUGHS ARE PRESENT (ALL %), AND MONTHLY MEAN NUMBER OF NEGATIVELY TILTED TROUGH EVENTS (ALL #) FOR ALL YEARS OF THE ANALYSIS (1990-2018) (LEFT). COMPOSITE MEANS FOR IOD PHASE AND SEASON (RIGHT).

IOD Phase	All %	All #
Negative IOD	7.02	2.45
Neutral IOD	7.00	2.60
Positive IOD	4.86	1.77

IOD Phase	Season	All %	All #
Negative IOD	Autumn	3.85	2.00
	Spring	7.66	2.78
	Summer	11.29	5.00
	Winter	6.97	2.00
Neutral IOD	Autumn	6.00	2.42
	Spring	7.52	2.65
	Summer	6.29	2.46
	Winter	8.63	2.95
Positive IOD	Autumn	3.65	1.38
	Spring	4.40	1.56
	Summer	5.54	2.29
	Winter	5.63	1.94

El Niño Southern Oscillation

Composite means of NTT# and NTT% for positive, neutral and negative phases of the Oceanic Niño Index (ONI) are given in Table 5-6. NTT occurrence during neutral and La Niña conditions is slightly above average (left panel). There is an indication of a reduction in NTT occurrence during El Niño, however these differences are not statistically significant.

In the seasonal breakdown (right panel) the semiannual signal evident in Figure 5-9 is clear with the spring-summer peak shifting more towards spring than was shown in Table 5-3. This semiannual signal is statistically significant under La Niña conditions, while under neutral conditions NTT occurrence in much more uniform. During El Niño conditions the annual peak occurs in summer although this peak is not statistically distinct from the spring and winter values. In general only differences that are greater than around 3 between composite mean values of NTT% ("All %" column in Table 5-6) are statistically significant at 95 % confidence level. The difference between the annual cycles in El Niño and La Niña, and the summer difference in particular, could be related to the tendency for more frequent negative SAM during El Niño and more frequent positive SAM during La Niña.

TABLE 5-6 OCEANIC NIÑO INDEX (ONI) PHASE COMPOSITE MEANS OF MONTHLY PERCENTAGE OF TIME THAT NEGATIVELY TILTED TROUGHS ARE PRESENT (ALL %), AND MONTHLY MEAN NUMBER OF NEGATIVELY TILTED TROUGH EVENTS (ALL #) FOR ALL YEARS OF THE ANALYSIS (1990-2018) (LEFT). COMPOSITE MEANS FOR ONI PHASE AND SEASON (RIGHT).

ONI Phase	All %	All #
El Nino	6.00	2.32
La Nina	7.00	2.42
Neutral	6.88	2.57

ONI Phase	Season	All %	All #
El Nino	Autumn	2.46	1.38
	Spring	6.05	2.21
	Summer	7.42	2.76
	Winter	6.59	2.60
La Nina	Autumn	4.67	2.00
	Spring	8.22	2.70
	Summer	5.42	2.21
	Winter	9.61	2.65
Neutral	Autumn	6.66	2.58
	Spring	6.62	2.44
	Summer	6.16	2.47
	Winter	7.74	2.69

Multi-Index Analysis

Composite monthly means of NTT occurrence for the different phases of the SAM combined with the different phases of the IOD and ONI as well as season are given below. Given the larger range of combinations, results are shown only for NTT% which have more robust statistics, although results for NTT# are generally quite consistent (Appendix A.2).

Composite means of NTT% for various combinations of phases of the SAM and IOD are given in Table 5-7. The bias of NTT occurrence towards negative SAM (Table 5-4 left panel) is consistent across all phases of the IOD, although less so for positive IOD (left panel). The reduced NTT occurrence during positive IOD (Table 5-5 left panel) is consistent during negative SAM, but during positive SAM both negative and positive IOD favour reduced NTT occurrence. While the composite mean values for negative SAM-Negative IOD and negative SAM-neutral IOD are statistically indistinct, the difference between negative SAM-neutral IOD and all of the other combinations are statistically significant.

Including seasonal combinations reveals some larger differences with further concentration of the negative SAM-negative IOD bias to spring and summer (right panel). However, while the differences in the seasonal breakdown are quite large, they are in general not statistically significant.

TABLE 5-7 SOUTHERN ANNULAR MODE (SAM) AND INDIAN OCEAN DIPOLE (IOD) PHASE COMPOSITE MEANS OF MONTHLY PERCENTAGE OF TIME THAT NEGATIVELY TILTED TROUGHS ARE PRESENT (ALL %), AND MONTHLY MEAN NUMBER OF NEGATIVELY TILTED TROUGH EVENTS (ALL #) FOR ALL YEARS OF THE ANALYSIS (1990-2018) (LEFT). COMPOSITE MEANS FOR SAM, IOD PHASE AND SEASON (RIGHT).

		All %	
IOD Phase SAM Phase	Negative IOD	Neutral IOD	Positive IOD
Negative SAM	8.56	8.19	5.08
Positive SAM	4.80	6.16	4.72

			All %	
SAM Phase	IOD Phase Season	Negative IOD	Neutral IOD	Positive IOD
Negative SAM	Autumn	3.85	8.34	5.28
	Spring	12.47	7.97	3.55
	Summer	11.29	7.61	8.06
	Winter	7.71	8.82	5.87
Positive SAM	Autumn	0.00	4.93	2.03
	Spring	3.80	7.01	5.06
	Summer	0.00	5.56	4.53
	Winter	6.05	8.43	5.52

Composite means of NTT% for various combinations of phases of the SAM and ONI are given in Table 5-8. The preference for NTT occurrence during negative SAM (Table 5-4 left panel) is consistent across all phases of the ONI (left panel). During positive SAM the reduction in NTT occurrence during El Niño (Table 5-6) is enhanced, however, during negative SAM there is no appreciable variation across the ONI phases. The differences of positive SAM-El Niño from negative SAM-El Niño and Positive SAM-Neutral are both statistically significant.

Including seasons to the composite means shows that the summer difference between El Niño and La Niña NTT occurrence (Table 5-6 right panel) is more pronounced during negative SAM, while not evident during positive SAM. A further significant departure under negative SAM is the autumn difference between El Niño and La Niña, which is also not evident during positive SAM. The seasonality during positive SAM-La Niña is consistent with overall positive SAM seasonality. Seasonal variation during positive SAM-El Niño and during all neutral ONI conditions is not statistically significant.

TABLE 5-8 SOUTHERN ANNULAR MODE (SAM) AND OCEANIC NIÑO INDEX (ONI) PHASE COMPOSITE MEANS OF MONTHLY PERCENTAGE OF TIME THAT NEGATIVELY TILTED TROUGHS ARE PRESENT (ALL %), AND MONTHLY MEAN NUMBER OF NEGATIVELY TILTED TROUGH EVENTS (ALL #) FOR ALL YEARS OF THE ANALYSIS (1990-2018) (LEFT). COMPOSITE MEANS FOR SAM, ONI PHASE AND SEASON (RIGHT).

ONI Phase SAM Phase	El Nino	La Nina	Neutral
		All %	
Negative SAM	7.72	7.71	7.95
Positive SAM	4.13	6.65	6.10

SAM Phase	ONI Phase Season	El Nino	La Nina	Neutral
			All %	
Negative SAM	Autumn	3.09	9.46	7.94
	Spring	6.94	7.81	8.41
	Summer	10.49	4.49	7.23
	Winter	8.18	9.29	8.11
Positive SAM	Autumn	2.18	2.76	5.87
	Spring	3.89	8.55	5.35
	Summer	5.38	5.67	5.31
	Winter	4.21	9.83	7.42

5.3.4 Relationship with Severe Weather Events

The results in this section will be restricted to the analysis of the Australian Bureau of Meteorology (BoM) Severe Storms Archive (SSA), which as discussed in section 2.2, includes reports of severe wind gusts, damaging hail, tornadoes, heavy rain, lightning, waterspouts and damaging dust devils. Discussion of fire weather events will be treated separately.

Frequency of Severe Weather Associated with NTT

Just over 40 % of the 862 NTT events identified over the 1990-2018 period in the BARRA-R dataset were associated with a report in the SSA. Of the 5028 6-hour analysis periods when severe weather south of 25°S was reported in the SSA, 11.4 % were associated with NTT.

SSA reports were made during 11.9 % of all 6-hour analysis periods over the 1990-2018 period. During analysis periods when NTT were present the reporting rate increased to 20.1 %. The proportion of all 6-hour analysis periods that both NTT were present and a report was entered in the SSA was 1.4 %. A summary of the statistics describing the frequency of SSA report associated with NTT is given in Table 5-9.

TABLE 5-9 SUMMARY STATISTICS FOR ALL NEGATIVELY TILTED TROUGH EVENTS IDENTIFIED IN THE BARRA-R DATASET AND ASSOCIATED WITH SEVERE STORMS ARCHIVE REPORT DURING THE PERIOD OF 1990-2018.

Total NTT events	862
Total NTT events associated with SSA report	350
Percent of NTT events associated with SSA report	40.6 %
Total 6-hour analysis periods from 1990-2018	42368
Total 6-hour analysis periods with SSA report	5028
Percent of total time with SSA reports	11.9 %
Total 6-hour analysis periods with NTT present	2848
Percent total time with NTT present	6.7 %
Total 6-hour analysis periods with SSA report and NTT present	572
Percent total time with SSA report and NTT present	1.4 %
Percent of NTT occurrence associated with SSA report	20.1 %

Monthly Bias in Severe Weather Associated with NTT

In the previous section it was noted that the average amount of SSA reporting increased from 11.9 % over all conditions to 20.1 % given the occurrence of NTT (Table 5-9). The annual variation of the percentage of NTT occurrence that is associated with SSA reports is plotted in green in Figure 5-10 (left panel). There is

a roughly annual cycle with a maximum of 34.6 % in December and a minimum of 10.8 % in May. Thus, NTT are associated with severe weather significantly more often during summer and spring than autumn and winter.

For comparison, the annual variation in SSA reporting over all conditions is plotted in the same panel in blue. During all months of the year SSA reporting is significantly higher during the occurrence of NTT. From March to October the rate is double or more during the occurrence of NTT. Summer months have large absolute differences in reporting rates although relative differences are not as large. The differences for the majority of months are statistically significant at the 95 % confidence level using a weighted Welch's t-test.

The proportion of the total time that SSA reports are associated with NTT is plotted in red, although the features are difficult to discern since this represents only 11.9 % of all SSA reports (Table 5-9). In order to compare the seasonality of the three parameters, the climatology is plotted again (right panel) with each parameter normalised by their respective annual mean values. Here it can be seen that the proportion of the total time that NTT occurrence is associated with SSA reports has a semiannual cycle with a primary peak in December and a secondary peak in June. Seasonal composites are shown in Table 5-10.
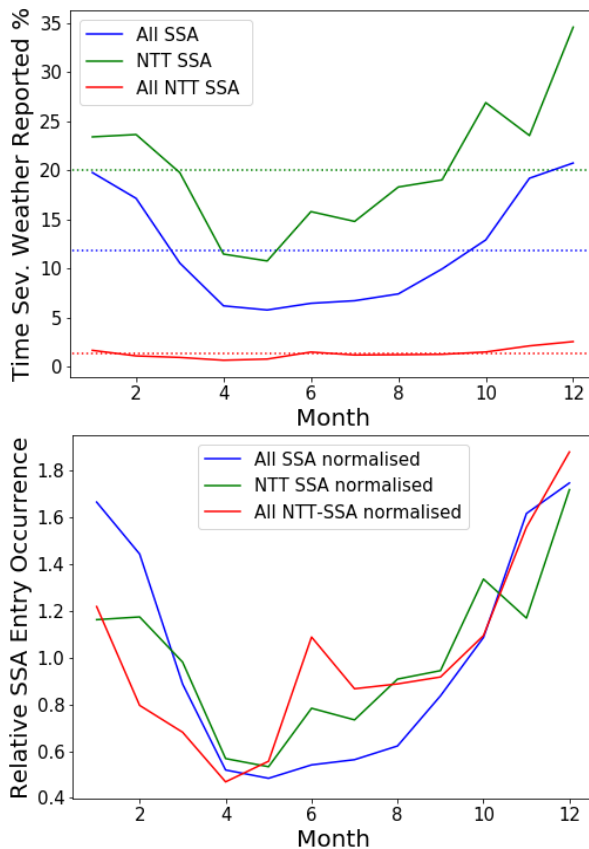
FIGURE 5-55 CLIMATOLOGICAL MONTHLY MEAN PERCENTAGE OF TIME IN EACH MONTH THAT SEVERE WEATHER IS REPORTED IN SSA (BLUE), PERCENTAGE OF NTT OCCURRENCE IN WHICH SEVERE WEATHER IS REPORTED IN SSA (GREEN) AND PERCENTAGE OF TIME IN EACH MONTH THAT SEVERE WEATHER IS REPORTED IN SSA WHILE NTT ARE PRESENT (RED) (LEFT). AS FOR (LEFT) BUT NORMALISED BY RESPECTIVE ANNUAL MEAN VALUES. DASHED LINES INDICATE ANNUAL WEIGHTED MEANS GIVEN IN TABLE 5-9.

TABLE 5-10 CLIMATOLOGICAL SEASONAL MEANS OF PERCENTAGE OF TIME IN EACH MONTH THAT SEVERE WEATHER IS REPORTED IN SSA (ALL SSA %), PERCENTAGE OF NTT OCCURRENCE IN WHICH SEVERE WEATHER IS REPORTED IN SSA (NTT SSA %) AND PERCENTAGE OF TIME IN EACH MONTH THAT

SEVERE WEATHER IS REPORTED IN SSA WHILE NTT ARE PRESENT (ALL SSA ENTRY %).

Season	All SSA %	NTT SSA %	All NTT SSA %
Autumn	7.51	13.44	0.77
Spring	14.00	23.06	1.60
Summer	19.28	27.90	1.77
Winter	6.85	16.15	1.27

Climate Drivers and Severe Weather Associated with NTT

Regional climate driver phase composite monthly means of severe weather reporting in relation to NTT are given in Table 5-11. The phase of SAM is seen to have no influence on the overall reporting of severe weather, however, there is a suggestion that when NTT are present severe weather is reported more often during positive SAM (left panel). Despite this small bias the overall percentage of time in each month that severe weather is reported in SSA while NTT are present is higher during positive SAM, reflecting the strong bias towards NTT occurrence during negative SAM (Table 5-4). Differences between severe weather reporting during difference phases of SAM are not statistically significant, so these results remain speculative.

TABLE 5-11 REGIONAL CLIMATE DRIVER PHASE COMPOSITE MEANS OF PERCENTAGE OF TIME IN EACH MONTH THAT SEVERE WEATHER IS REPORTED IN SSA (ALL SSA %), PERCENTAGE OF NTT OCCURRENCE IN WHICH SEVERE WEATHER IS REPORTED IN SSA (NTT SSA %) AND PERCENTAGE OF TIME IN EACH MONTH THAT SEVERE WEATHER IS REPORTED IN SSA WHILE NTT ARE PRESENT (ALL SSA ENTRY %).

SAM Phase	All SSA %	NTT SSA %	All NTT SSA %
Negative SAM	11.88	19.03	1.49
Positive SAM	11.86	21.11	1.25

IOD Phase	All SSA %	NTT SSA %	All NTT SSA %
Negative IOD	8.54	13.30	0.93
Neutral IOD	12.48	20.66	1.45
Positive IOD	9.78	19.71	0.96

ONI Phase	All SSA %	NTT SSA %	All NTT SSA %
El Nino	13.24	25.67	1.54
La Nina	13.54	22.01	1.55
Neutral	10.52	17.15	1.18

Severe weather reporting is lower in general during both positive and negative IOD than in neutral conditions (middle panel). This low bias does not occur during positive IOD when NTT are present. Regardless, the overall percentage of time in each month that severe weather is reported in SSA while NTT are present follows the same pattern as overall severe weather reporting. This is in contrast to the overall NTT occurrence bias towards neutral and negative IOD phases seen in Table 5-5. Differences between severe weather reporting during difference phases of SAM are statistically significant.

Both El Niño and La Niña conditions are associated with statistically significant increases in severe weather reports in comparison to neutral conditions. When NTT are present this pattern is maintained. A similar, but not statistically significant pattern is also seen in the overall percentage of time in each month that severe weather is reported in SSA while NTT are present. This differs from the overall bias in NTT occurrence towards neutral and La Niña conditions seen in Table 5-6.

5.3.5 Regional Variations

In the following analysis the regional breakdown has been carried out in two parts in order to maintain higher confidence in the statistics, given the ambiguity in some of the results of the full analysis in the section 5.3. NTT events were split first by Western Australia (WA) and Eastern Australia (EA) classifications, then by South Coastal (SC) and Southern Ocean (SO), however, the presentation of the results will be combined. Inland, Small Scale, and Eastern Inland classifications were excluded. Only notable differences from the overall results above will be presented.

Monthly Mean Climatology

The monthly mean climatologies of NTT events for each of the four regional classifications are plotted in Figure 5-11. In the top panels the complementary WA and EA events exhibit pronounced differences. NTT occurrence in the WA region has the same semi-annual cycle as seen in the overall results in Figure 5-8 while in the EA region there is only a weak annual cycle peaking in January. The decrease from the earlier period to the later period in the winter NTT occurrence is evident primarily in the WA events while the autumn increase is evident primarily in the EA events. The overall decrease in the annual number of NTT events noted in section 5.3.1 appears to be driven by the WA region and the winter peak in particular.

The difference in the annual variations of the complementary SC and SO events in the bottom panels of Figure 5-11 is equally dramatic. The SC region is subject to a strong annual cycle peaking in June-July while the SO region experiences a similarly strong annual cycle that peaks in January. Similar to the WA-EA comparison, the winter decrease from early to later periods is driven by the SC region while the autumn increase is driven primarily by the SO region. It is intuitive that the occurrence of NTT events that cross the south coast of Australia should peak in winter, since the mid- to high-latitude band of strong westerly winds in which NTT are typically embedded is positioned further north during winter. The corresponding southward position of the westerlies during summer explains the anti-phasing of the SO events. In the SC-SO comparison, it is the SC region that is driving the overall decrease in NTT occurrence from early to later periods.
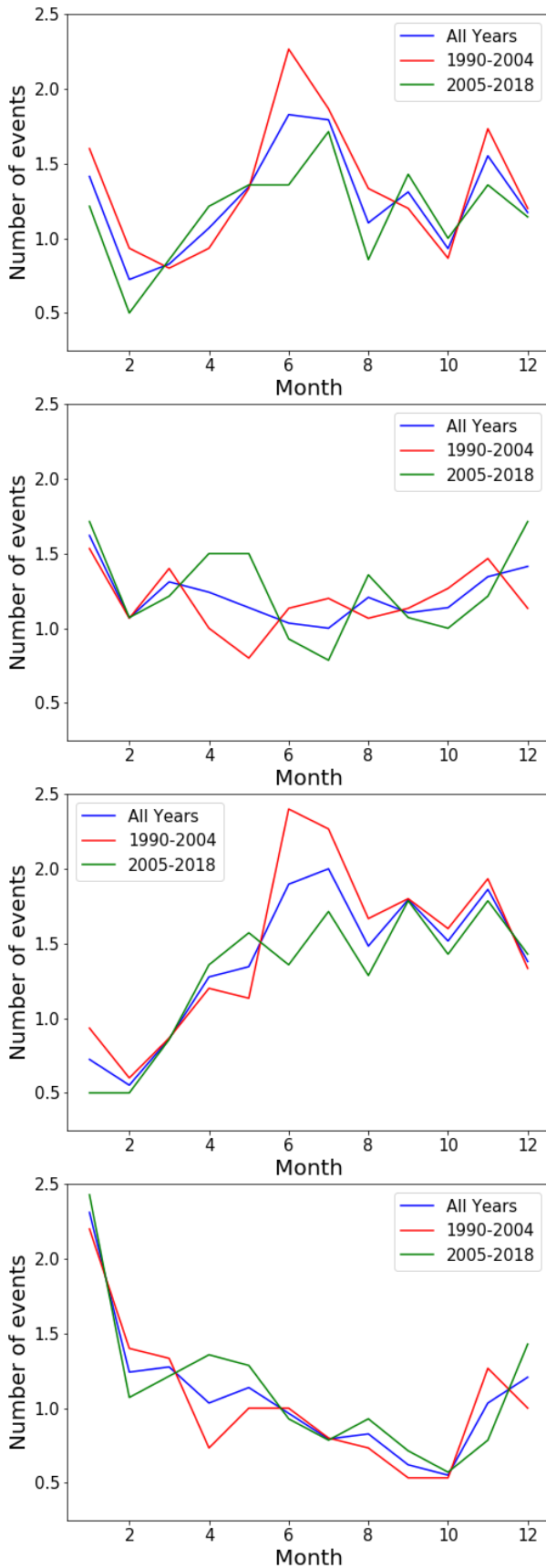
FIGURE 5-56 CLIMATOLOGICAL MONTHLY MEAN NUMBER OF NEGATIVELY TILTED TROUGH EVENTS PER MONTH FOR ALL YEARS (BLUE), FIRST 15 YEARS (RED), AND LAST 14 YEARS (GREEN), FOR WESTERN AUSTRALIA (TOP LEFT), EASTERN AUSTRALIA (TOP RIGHT), SOUTH COASTAL (BOTTOM LEFT) AND SOUTHERN OCEAN (BOTTOM RIGHT).

Regional Climate Drivers

There is no clear relationship between NTT occurrence and SAM in EA, while the biases associated with IOD and ENSO are consisted with the overall results.

In WA the bias towards negative SAM is stronger than in the overall results. Here, the relationship between NTT occurrence and IOD is similar to overall results but with a slightly stronger bias towards negative IOD.

As in WA, the relationship between NTT occurrence and IOD in CO is similar to overall results but with a slightly stronger bias towards negative IOD.

IN SO the bias against NTT occurrence during positive IOD is accompanied by a slight bias against negative IOD in comparison to neutral IOD. in general the relationship with ENSO is very weak, although it appears to have more influence during negative SAM than in the overall results.

5.4 DISCUSSION

The results in this climatology require some consideration of the inherent biases in the SSA noted in section 2.2. With the changes in reporting practices and frequency, it is likely that even if accounting for population increases and spread, the number of reports in the earlier parts of the archive is not consistent with more recent years. Thus, the overall frequency with which severe weather is associated with NTT in populated areas is very likely an underestimate.

Averaging the analysis over very broad subregions addresses to some extent the uneven spatial sampling that underlies the SSA. Regardless, in the first instance the results of the SSA analysis must be assumed to very strongly represent the statistics of NTT impacts on populated areas. However, the generality of the results is supported by the large scale of most of the NTT observed. As seen in the 2003 Canberra bushfires case study and the related events at Wangary and Hobart, the coherence of the impacts can extend over very large distances, a result supported by Mills (2008b).

To avoid the sampling issues inherent in the SSA, certain types of severe weather or severe weather potential could be diagnosed in BARRA, however, this is not without its own difficulties. Foremost still, the generic problem with using surface data pertaining to severe weather, whether SSA, BARRA, surface observations or other, is the ambiguity in its association with NTT. Without conducting detailed analysis of each case, it is often difficult to assess whether NTT are the likely cause of particular surface weather and the results are subjective based on interpretation of NTT characteristics and proximity of the surface impacts. In either case, the assessment requires a visual inspection of each NTT occurrence.

Use of the surface observational criteria applied climatologically by Mills (2008b) or Fox-Hughes (2015) is unlikely to be successful in identifying impacts of NTT, based on the representation by BARRA of observed meteograms recorded during some of the fire events discussed. However, if BARRA is resolving the relevant boundary layer mixing processes, but just not to the degree required to impact the surface, examining fire weather variables higher in the boundary layer might be informative. As mentioned above, Lagrangian trajectory

modelling could resolve much of the ambiguity around the direct connections between NTT and extreme fire weather at the surface.

A range of other severe weather or severe weather potential indicators could be applied. These could include direct measures such as vertical velocity or indices such as CAPE, DCAPE, CHaines index and the cool season tornado diagnostic of Hanstrum et al. (2002).

This study has identified some statistically significant biases towards the preferential occurrence of NTT during particular phases of regional climate drivers, most notably SAM and IOD. Since the SAM can vary on much shorter time scales than monthly, the definition of the SAM phase applied in this study did not attempt to characterise fully its variability given the monthly mean approach that was more appropriate for IOD and ENSO. It seems likely that a more detailed analysis at daily resolution could reveal stronger relationships than reported here. While it would not be a significant undertaking to repeat the analysis at higher temporal resolution, it is beyond the scope of the current project and should be the subject of further investigation.

The ability to extract NTT occurrence computationally would greatly enhance the ability to generalise this sort of analysis to other datasets and regions. In particular, it would be necessary to have automated analysis if there were to be any reasonable prospect of applying the analysis to climate projection ensembles. The development of automated NTT identification methods might be challenging and would probably be suitable only for statistical analysis given the unavoidable error rates likely to be involved. However, the prospects for this are reasonable, especially with the benefit from the completed BARRA climatology as a reference.

Due to the complexity of the subject, the duration of the project has not afforded the opportunity to explore a number of discriminating characteristics of NTT events that have been identified. Furthermore, the large spatial domain, the diverse range of events and impacts, and the broad range of influences from large scale climate variability provide broad scope for more targeted analysis. For example, it would be valuable to investigate in more detail the significant subregional variability observed across southern Australia including the differences in characteristic impacts and indications of subregional sensitivities to regional climate drivers.

SUMMARY AND CONCLUSIONS

PREVIOUSLY DOCUMENTED EVENTS

A review of documented cases where severe weather in southern Australia has been associated with negatively tilted upper-tropospheric troughs (NTT) has shown a diversity of morphology and surface impacts. Some authors simply note the presence of NTT in relation to the surface weather without investigating which particular aspects of the NTT distinguish the event from more commonly observed weather patterns. Several studies do note the pattern of a diffluent upper-tropospheric trough rapidly approaching a shortwave ridge downstream, and cite previous observational and theoretical studies of this situation. However, this phenomenon is not limited to the occurrence of NTT.

18 JANUARY 2003 CANBERRA BUSHFIRES AND OTHER FIRE EVENTS

Consistent with Fox-Hughes (2015), detailed analysis of the synoptic situation in the cases of three extreme fire weather events have shown very similar characteristics with a strong NTT extending from deep in the Southern Ocean northeastward into a strong jet stream between 60 °S and 40 °S and passing south of the continental coast without becoming cut-off. Strong evidence of upper-tropospheric dry air intrusions is very consistent across these cases. However, not all of the fire events noted in the present study fit this profile.

In the 18 January 2003 Canberra bushfires case study, it was found that despite the NTT occurring so far south there is compelling evidence that an upper-tropospheric dry air intrusion originating in the NTT apex region could have reached well over the continent and played a role in the sudden drying event observed in Canberra on the day. Furthermore, interactions between the NTT and a weaker trough to the northwest were likely the origin of a broad dry band positioned over Bass Strait during the fire event and which was connected at low levels to the dry intrusion and dry air over the continent. No clear connection was found between the NTT and the narrow dry slot which passed directly over Canberra during the event.

No association of particular patterns in NTT morphology with other specific severe weather phenomena have been noted in the present study, but the information in the climatology could be used to examine this further.

14 JULY 2014 PERTH TORNADOES

In the case study of the July 2014 Perth tornado outbreak, it was seen that a NTT southwest of Western Australia focussed an upper-tropospheric jet and created a highly diffluent jet exit region positioned over southwest Western Australia. This situation was compounded by the presence of another upper-tropospheric trough to the northeast over the continent reinforcing the diffluence. The resulting divergence in this region was associated with strong upward air movement directly above the surface frontal zone crossing the west coast at Perth. This enhanced strong dynamical forcing near the surface that was conducive to tornado formation. Gravity wave processes in the diffluent jet exit might also

have played a role in coupling lower- and upper-tropospheric circulation in the frontal zone.

This case study highlights the association of NTT with severe weather in situations where typical indicators might not flag the possibility of such severe impacts. In this case, only two of three criteria used for the prediction of cool season tornadoes were satisfied, however, despite the lack of convective instability the vertical circulation induced by the NTT together with the near surface dynamics were sufficient to cause the event.

The highly transient nature of some of the dynamic processes involved, even at the mesoscale, highlights the difficulty in forecasting such events and emphasises the worth in using a forecast of NTT occurrence as a flag to look closer at the associated fine-scale processes. The ability of the Australian Bureau of Meteorology (BoM) Atmospheric high-resolution Regional Reanalysis for Australia (BARRA) to resolve these features demonstrates the value of the dataset in applied research for improving meteorological understanding and forecasting.

CLASSIFICATIONS OF NTT REGIONALLY AND MORPHOLOGY

In the compilation of the climatology several distinct recurrent patterns of NTT development emerged. Most notable were the passage south of the Australian south coast of NTT embedded in a strong jet stream, the formation of cut-off upper-tropospheric lows over the western and eastern extremities of the south coast, and smaller scale NTT developing across the coast in the Great Australian Bight and propagating along the southeast coast. However, many other patterns were observed with the majority of NTT not developing into cut-off systems.

MONTHLY MEAN CLIMATOLOGY OF NTT OCCURRENCE

Across southern Australia the occurrence of NTT varies significantly on monthly and yearly time scales. NTT occurred roughly 2.5 times per month on average with NTT present in the region close to 7 % of the time. While not immediately evident in the time series, the monthly climatology shows a strong semi-annual cycle peaking in June-July and November-January. There was a slight decreasing trend in NTT occurrence over the 1990-2018 period and a statistically significant shift of the winter peak to autumn in the second half of the period. The attribution of this trend and change in seasonality is currently unresolved. Both could be related to the relatively low occurrence of certain combinations of climate drivers during the first and second halves of the analysis period. This should be the subject of further analysis.

SUBREGIONAL BREAKDOWN OF MONTHLY MEAN CLIMATOLOGY

When grouped by Australian south coastal and Southern Ocean regions the monthly mean NTT occurrence exhibited strong annual cycles with the two regions anti-phased, presumably the result of the annual migration of the southern hemisphere mid- to high-latitude belt of westerly winds. When grouped by western and eastern regions of Australia the western region exhibited a semi-annual oscillation seen in the overall results, apparently combining the sharp anti-phased peaks of the south coastal and Southern Ocean regions. In the eastern

region only a weak annual signal matching the Southern Ocean region was evident.

NTT OCCURRENCE IN DIFFERENT PHASES OF REGIONAL CLIMATE DRIVERS

Composite means of NTT occurrence during different phases of three regional climate drivers revealed some statistically significant biases. A strong preference was observed for NTT occurrence during the negative phase of the Southern Annular Mode (SAM). A similarly strong preference was noted for NTT occurrence during the negative and neutral phases of the Indian Ocean Dipole (IOD) over the positive phase. There was an indication of a reduction in NTT occurrence during El Niño, however, these differences were not statistically significant.

Repeating the composite monthly analysis by both regional climate driver phase and season highlighted some stronger biases. The bias towards negative SAM is consistent across all seasons with the strongest bias towards negative SAM in winter. Similarly, the bias against positive IOD is consistent across the seasons during neutral IOD with the strongest bias occurring during neutral IOD in winter, however, the seasonality of IOD implies that results outside of winter-spring bear little weight. The seasonality of NTT occurrence during different phases of El Niño-Southern Oscillation (ENSO) varied significantly with a much more pronounced semi-annual cycle during La Niña and the strongest bias during La Niña in winter.

Multi-index composite analysis was also performed. A statistically significant bias towards NTT occurrence during the combination of negative SAM and neutral IOD was found. A larger bias was observed towards combined negative SAM and negative IOD, however, due to the low number of IOD events, particularly in summer, this was not statistically significant. The bias against positive SAM is enhanced during El Niño and reduced during La Niña. Very strong differences between El Niño and La Niña NTT occurrence in summer and autumn was observed during negative SAM but were not evident during positive SAM.

The strongest correlation of monthly time series of NTT occurrence with monthly regional climate driver indices was -0.23 with SAM. Weak anticorrelation of -0.16 was also found with the NIÑO1+2 index.

SEVERE WEATHER REPORTING IN ASSOCIATION WITH NTT OCCURRENCE

Over 40 % of the 862 NTT events identified over the 1990-2018 period in the BARRA dataset were associated with a report in the Bureau of Meteorology Severe Storms Archive (SSA). When SSA entries were grouped in 6-hourly periods to match the BARRA-R analysis times, 11.4% of all severe weather reporting was associated with NTT.

The average amount of SSA reporting south of 25 °S increased from 12 % of the time over all conditions to 20 % given the occurrence of NTT.

A strong annual cycle peaking in summer was observed in the reporting of all severe weather south of 25 °S. Severe weather reporting when NTT are present is consistently higher in all months. NTT are associated with severe weather,

excluding fire, significantly more often during summer and spring than autumn and winter.

The phase of SAM had no impact on reporting of all severe weather south of 25 °S, while severe weather reporting associated with NTT generally followed the preferential occurrence of NTT during negative SAM, but was not statistically significant.

Reporting of all severe weather south of 25 °S was higher during neutral IOD than positive or negative IOD, however, the low bias did not occur during positive IOD when NTT were present.

Both El Niño and La Niña conditions were associated with increases in all severe weather south of 25 °S in comparison to neutral conditions. When NTT were present this pattern was maintained.

Applying BARRA to the systematic analysis of a range of quantitative severe weather diagnostics in relation to the NTT climatology could provide highly valuable information on the association of different patterns of NTT occurrence with particular severe weather phenomena without the spatial sampling biases intrinsic to SSA. This could include, for example, stability indices relating to thunderstorm formation and severe fire weather effects. However, without assessing each case in detail, the issue of subjectively assigning a severe weather event with association to a NTT remains. This would be less of an issue for certain diagnostics. For example, in the case of extreme fire weather impacts, Lagrangian trajectory analysis could resolve much of the ambiguity around the association of NTT with intrusions of dry high momentum air at or near the surface.

CONCLUDING REMARKS

While modern numerical weather prediction (NWP) systems are increasingly capable of resolving the surface weather parameters associated with severe weather events, there are known deficiencies. An example of this is the over-estimation of low winds and under-estimation of high winds common to numerous models. Better understanding of the role of features such as NTT in generating surface weather helps interpretation and refinement of the NWP output, particularly for users of weather data such as emergency services agencies. Furthermore, as products from NWP such as sub-seasonal to seasonal outlooks become more refined, there is value in recognising the occurrence of potential impacts of NTT that may be resolved at the synoptic or sub-synoptic scale in such model configurations even if the potential severity of the weather parameters are note explicitly resolved. For example, if a sub-seasonal to seasonal model ensemble shows a high probability of a NTT occurrence in a particular region a certain number of weeks in advance, that is useful information for planning and preparedness for emergency services managers. Thus, this sort of synoptic climatological study in combination with detailed analyses of particular events continues to be of great relevance to natural hazard prediction and management.

FUTURE WORK

The material in the case studies and climatology sections of this report would each form the basis for manuscripts to be published in peer-reviewed literature for the benefit of enhanced scrutiny, credibility and broad dissemination of the results.

During the analysis of the vertical circulations that occurred during the case study events, a climatology of vertical motions across the entire BARRA-R domain was compiled. A more detailed analysis of this climatology would be of significant value to the understanding of geophysical processes in the region as well as to the development of BARRA and other NWP models. The climatology will be shared with the meteorological community and could be the subject of further publications in peer-reviewed literature.

Further analysis of the relationship between NTT and surface weather impacts could be pursued with the benefit of BARRA by systematically analysing quantitative metrics used to predict severe weather. Thus, climatologies of parameters such as convective available potential energy (CAPE), Downwards CAPE (DACAP), C-Haines index, cool season tornado diagnostics and Lagrangian trajectory analysis, could be combined with the NTT climatology to establish more specific relationships between particular severe weather phenomena with the distinct NTT morphologies and locations observed.

With the benefit of the historical climatology generated in this project, the representation of NTT occurrence in climate models could be assessed and, if verified, a further assessment made of the projected changes in NTT occurrence in the future.

REFERENCES

1   Bjerknes, J. (1954), The difluent upper trough, Arch. Met. Geoph. Biokl. A., 7, 41–46, doi:10.1007/BF02277903.

2   Bureau of Meteorology (2016a), Extensive early June rainfall affecting the Australian east coast, Special Climate Statement 57, Australian Bureau of Meteorology, Melbourne, Australia, http://www.bom.gov.au/climate/current/statements/scs57.pdf.

3   Bureau of Meteorology (2016b), Severe thunderstorm and tornado outbreak South Australia 28 September 2016, Tech. rep., Australian Bureau of Meteorology, Melbourne, Australia, http://www.bom.gov.au/announcements/sevwx/sa/Severe Thunderstorm and Tornado Outbreak 28 September 2016.pdf.

4   Bureau of Meteorology (2017), Bushfire Predictive Services Final Report: An evaluation of fire spread simulators used in Australia, Tech. rep., Australian Bureau of Meteorology, Melbourne, Australia.

5   Burrows, N. (2015), Fuels, weather and behaviour of the Cascade Fire (Esperance Fire #6) 15-17 November 2015, Tech. rep., Western Australia Department of Parks and Wildlife, Perth, Western Australia, doi:10.13140/RG.2.1.5027.5927.

6   Childs, S. J., R. S. Schumacher, and J. T. Allen (2018), Cold-season tornadoes: Climatological and meteorological insights, Weather Forecast., 33(3), 671–691, doi:10.1175/WAF-D-17-0120.1.

7   Davies, T., M. J. P. Cullen, A. J. Malcom, M. H. Mawson, A. Staniforth, A. A. White, and N. Wood (2005), A new dynamical core for the Met Office's global and regional modelling of the atmosphere, Q. J. R. Met. Soc., 131(608), 1759–1782, doi:10.1256/qj.04.101.

8   Evenson, E. C., and R. H. Johns (1995), Some climatological and synoptic aspects of severe weather development in the northwestern United States, Natl. Wea. Dig., 20(1), 34–50.

9   Feren, G. (2008), Characteristics of eastern Australian-western Tasman Sea enhanced-Vs and their connection to severe weather, in 24th Conference on Severe Local Storms, American Meteorological Society.

10   Fox-Hughes, P. (2012), Springtime fire weather in Tasmania, Australia: Two case studies, Weather Forecast., 27(2), 379–395, doi:10.1175/WAF-D-11-00020.1.

11   Fox-Hughes, P. (2014), Severe winds in south-east Tasmania, 9th February 2014, B. Aust. Met. Ocean. Soc., 27(3), 48–49.

12   Fox-Hughes, P. (2015), Characteristics of some days involving abrupt increases in fire danger, J. Appl. Meteorol. Clim., 54(12), 2353–2363, doi:10.1175/JAMC-D-15-0062.1.

13   Fox-Hughes, P., J. Bally, and G. Hubbert (1996), A tornadic thunderstorm in northwest Tasmania: 22 November 1992, Aust. Meteorol. Mag., 45(2), 161–175.

14   Fox-Hughes, P., I. Barnes-Keoghan, and A. Porter (2018), Observations of a tornado at an automatic weather station in northern Tasmania, J. South. Hemisph. Earth Syst. Sci., 68, 2015–2030, doi:10.22499/3.6801.012.

15   Fromm, M., A. Tupper, D. Rosenfeld, R. Servranckx, and R. McRae (2006), Violent pyroconvective storm devastates Australia's capital and pollutes the stratosphere, Geophys. Res. Lett., 33(5), L05,815, doi:10.1029/2005GL025161.

16   Glickmann, T. S., N. J. MacDonald, and F. Sanders (1977), New findings on apparent relationship between convective activity and shape of 500 mb troughs, Mon. Wea. Rev., 105(8), 1060–1061, doi:10.1175/1520-0493(1977)105<1060:NFATAR>2.0.CO;2.

17   Gong, D., and S. Wang (1999), Definition of Antarctic oscillation index, Geophys. Res. Lett., 26(4), 459–462, doi:10.1029/1999GL900003.

18   Hanstrum, B. N., G. A. Mills, A. Watson, J. P. Monteverdi, and C. A. Doswell (2002), The cool-season tornadoes of California and southern Australia, Weather Forecast., 17(4), 705–722, doi:10.1175/1520-0434(2002)017<0705:TCSTOC>2.0.CO;2.

19   Hendon, H. H., D. W. J. Thompson, and M. C. Wheeler (2007), Australian rainfall and surface temperature variations associated with the Southern Hemisphere annular mode, J. Clim., 20(11), 2452–2467, doi:10.1175/JCLI4134.1.

20   Jeffreys, H. (1926), On the dynamics of geostrophic winds, Q. J. R. Met. Soc., 52(217), 85–104, doi:10.1002/qj.49705221708.

21   Johns, R. H. (1993), Meteorological conditions associated with bow echo development in convective storms, Weather Forecast., 8(2), 294–299, doi:10.1175/1520-0434(1993)008<0294:MCAWBE>2.0.CO;2.

22   Knapp, K. R. (2008), Scientific data stewardship of international satellite cloud climatology project B1 global geostationary observations, J. Appl. Remote Sens., 2(10.1117/1.3043461), 023,548.

23   Louis, S., E. Couriel, G. Lewis, M. Glatz, M. Kulmar, J. Golding, and J. Hanslow (2016), NSW east coast low event 3 to 7 June 2016 weather, wave and water level matters, in 25th NSW Coastal Conference.

24   Louis, S. A. (2018), A warm-front triggered nocturnal tornado outbreak near Kiama, NSW, Australia, J. South. Hemisph. Earth Syst. Sci., 68, 147–164, doi:10.22499/3.6801.008.

25   MacDonald, N. J. (1976), Apparent relationship between convective activity and shape of 500 mb troughs, Mon. Wea. Rev., 104(12), 1618–1622, doi:10.1175/1520-0493(1976)104<1618:OTARBC>2.0.CO;2.

26   MacDonald, N. J., and F. W. Ward (1974), Possible association between convection and tilting troughs, Riv. Ital. Geofis. Sci., 23(1-2), 79–81.

27   Machta, L. (1949), Dynamic characteristics of a tilted-trough model, J. Meteor., 6(2), 261–265, doi:10.1175/1520-0469(1949)006<0261:DCOATT>2.0.CO;2.

28   McLeod, R. (2003), Inquiry into the operational response to the January 2003 bushfires in the ACT, Tech. rep., Australian Capital Territory, Canberra, ACT.

29   Mills, G. A. (2001), Mesoscale cyclogenesis in reversed shear - the 1998 Sydney to Hobart yacht race storm, Aust. Meteorol. Mag., 50(1), 29–52.

30 Mills, G. A. (2005), On the subsynoptic-scale meteorology of two extreme fire weather days during the Eastern Australian fires of January 2003, Aust. Meteorol. Mag., 54(4), 265–290.

31 Mills, G. A. (2008a), Abrupt surface drying and fire weather Part 1: overview and case study of the South Australian fires of 11 January 2005, Aust. Meteorol. Mag., 57(4), 299–309.

32 Mills, G. A. (2008b), Abrupt surface drying and fire weather Part 2: a preliminary synoptic climatology in the forested areas of southern Australia, Aust. Meteorol. Mag., 57(4), 311–328.

33 Mills, G. A., and I. Russell (1992), The April 1990 floods over eastern Australia: Synoptic description and assessment of regional NWP guidance, Weather Forecast., 7(4), 636–668, doi:10.1175/1520-0434(1992)007<0636:TAFOEA>2.0.CO;2.

34 Milrad, S. (2018), Synoptic Analysis and Forecasting: An Introductory Toolkit, Elsevier, doi:10.1016/C2015-0-05604-0.

35 Moore, T. J., and W. A. Abeling (1988), A diagnosis of unbalanced flow in upper levels during the AYE-SESAME I period, Mon. Wea. Rev., 116(12), 2425–2436, doi:10.1175/1520-0493(1988)116<2425:ADOUFI>2.0.CO;2.

36 Peace, M., and G. A. Mills (2012), A case study of the 2007 Kangaroo Island bushfires, CAWCR Technical Report 053, The Centre for Australian Weather and Climate Research, Melbourne, Australia.

37 Peace, M., T. Mattner, and G. A. Mills (2011), The Kangaroo Island bushfires of 2007 A meteorological case study and WRF-fire simulation, in MODSIM2011. 19th International Congress on Modelling and Simulation, Perth, Australia, December 2011, edited by F. Chan, D. Marinova, and R. Anderssen, pp. 228–234, iSBN: 978-0-9872143-1-7. www.mssanz.org.au/modsim2011/D10/wongsosaputro.pdf.

38 Przybylinski, R. W. (1995), The bow echo: Observations, numerical simulations, and severe weather detection methods, Weather Forecast., 10(2), 203–218, doi:10.1175/1520-0434(1995)010<0203:TBEONS>2.0.CO;2.

39 Raveh-Rubin, S. (2017), Dry intrusions: Lagrangian climatology and dynamical impact on the planetary boundary layer, J. Clim., 30(17), 6661–6682, doi:10.1175/JCLI-D-16-0782.1.

40 Rawlins, F., S. P. Ballard, K. J. Bovis, A. M. Clayton, D. Li, G. W. Inverarity, A. C. Lorenc, and T. J. Payne (2007), The Met Office global four-dimensional variational data assimilation scheme, Q. J. R. Met. Soc., 133(623), 347–362, doi:10.1002/qj.32.

41 Rossby, C. G., and Collaborators (1939), Relation between variations in the intensity of the zonal circulation of the atmosphere and the displacements of the permanent centers of action, J. Mar. Res., 2(1), 38–55.

42 Saji, N. H., and T. Yamagata (2003), Possible impacts of Indian Ocean Dipole mode events on global climate, Clim. Res., 25(2), 151–169, doi:10.3354/cr025151.

43 Sgarbossa, D., J. Fischer, M. Boss, and J. Taylor (2018), The end-to-end convective hazard risk forecast process developed by the Australian extreme weather desk for the South Australian 28 September 2016 tornado outbreak, in 29th Severe Local Storms Conference, American Meteorological Society.

44 Sherburn, K. D., M. D. Parker, J. R. King, and G. M. Lackmann (2016), Composite environments of severe and nonsevere high-shear, low-CAPE convective events, Weather Forecast., 31(6), 1899–1927, doi:0.1175/WAF-D-16-0086.1.

45 Speer, M. S., and L. M. Leslie (2000), A comparison of five flood rain events over the New South Wales north coast and a case study, Int. J. Climatol., 20(5), 543–563, doi:10.1002/(SICI)1097-0088(200004)20:5<543::AID-JOC498>3.0.CO;2-C.

46 Starr, V. P. (1948), An essay on the general circulation of the Earth's atmosphere, J. Meteor., 5(2), 39–43, doi:10.1175/1520-0469(1948)005<0039:AEOTGC>2.0.CO;2.

47 Su, C. -H., N. Eizenberg, P. Steinle, D. Jakob, P. Fox-Hughes, C. J. White, S. Rennie, C. Franklin, I. Dharssi, and H. Zhu (2018), BARRA v1.0: The Bureau of Meteorology Atmospheric high-resolution Regional Reanalysis for Australia, Geosci. Model Dev. Discuss, 12(5), 2049–2068, doi:10.5194/gmd-12-2049-2019.

48 Taylor, J. C., K. C. Xuereb, and W. J. Taylor (2013), Extreme rainfall at Wilsons Promontory 22-23 March 2011, B. Aust. Met. Ocean. Soc., 26(5), 91–106.

49 Uccellini, L. W., P. J. Kocin, R. A. Petersen, C. H. Wash, and K. F. Brill (1984), The Presidents' Day cyclone of 18-19 February 1979: Synoptic overview and analysis of the subtropical jet streak influencing the pre-cyclogenetic period, Mon. Wea. Rev., 112(1), 35–55, doi:10.1175/1520-0493(1984)112<0031:TPDCOF>.0.CO;2.

50 Velden, C. S., and G. A. Mills (1990), Diagnosis of upper-level processes influencing an unusually intense extratropical cyclone over southeast Australia, Weather Forecast., 5(3), 449–482, doi:10.1175/1520-0434(1990)005<0449:DOULPI>2.0.CO;2.

STATISTICAL ANALYSIS SUMMARIES

NTT REGIONAL FREQUENCY AND SEVERE WEATHER ASSOCIATIONS

	All	East	West	South	Coast
Total events	862	(423)	437	(377)	(483)
Events per year	29.72	(14.59)	15.07	(13.00)	(16.66)
Events per month	2.48	(1.22)	1.26	(1.08)	(1.39)
Standard deviation of monthly events	1.58	(1.11)	1.15	(1.11)	(1.22)
Percentage of time NTT present	6.72 %	3.83 %	2.88 %	2.88 %	3.83 %
Standard deviation of monthly percentage of time NTT present	5.24 %	3.3 %	3.15 %	3.02 %	3.98 %

	All	East	West	South	Coast
Total NTT events	862	(423)	437	(377)	(483)
Total NTT events associated with SSA report	350	(205)	135	(98)	(247)
Percent of NTT events associated with SSA report	40.6 %	(48.5 %)	30.9 %	(26.0 %)	(51.1 %)
Total 6-hour analysis periods from 1990-2018	42368	42368	42368	42368	42368
Total 6-hour analysis periods with SSA report	5028	3907	1121	5028	5028
Percent of total time with SSA reports	11.9 %	9.2 %	2.6 %	11.9 %	11.9 %
Total 6-hour analysis periods with NTT present	2848	1622	1221	1219	1624
Percent total time with NTT present	6.7 %	3.8 %	2.9 %	2.9 %	3.8 %
Total 6-hour analysis periods with SSA report and NTT present	572	386	182	138	430
Percent total time with SSA report and NTT present	1.4 %	0.9 %	0.4 %	0.3 %	1.0 %
Percent of NTT occurrence associated with SSA report	20.1 %	23.8 %	14.9 %	11.3 %	26.5 %

ALL – SOUTHERN AUSTRALIA

Season	All %	All #
Autumn	5.71	2.31
Spring	6.96	2.46
Summer	6.28	2.47
Winter	7.90	2.67

SAM Phase	All %	All #
Negative SAM	7.84	2.71
Positive SAM	5.89	2.30

IOD Phase	All %	All #
Negative IOD	7.02	2.45
Neutral IOD	7.00	2.60
Positive IOD	4.86	1.77

ONI Phase	All %	All #
El Nino	6.00	2.32
La Nina	7.00	2.42
Neutral	6.88	2.57

SAM Phase	Season	All %
Negative SAM	Autumn	7.51
	Spring	7.68
	Summer	7.75
	Winter	8.33
Positive SAM	Autumn	4.72
	Spring	6.23
	Summer	5.47
	Winter	7.53

IOD Phase	Season	All %
Negative IOD	Autumn	3.85
	Spring	7.66
	Summer	11.29
	Winter	6.97
Neutral IOD	Autumn	6.00
	Spring	7.52
	Summer	6.29
	Winter	8.63
Positive IOD	Autumn	3.65
	Spring	4.40
	Summer	5.54
	Winter	5.63

ONI Phase	Season	All %	A
El Nino	Autumn	2.46	
	Spring	6.05	
	Summer	7.42	
	Winter	6.59	
La Nina	Autumn	4.67	
	Spring	8.22	
	Summer	5.42	
	Winter	9.61	
Neutral	Autumn	6.66	
	Spring	6.62	
	Summer	6.16	
	Winter	7.74	

IOD Phase / SAM Phase	Negative IOD	Neutral IOD	Pos
Negative SAM	2.92	2.80	
Positive SAM	1.78	2.45	

All #

IOD Phase / SAM Phase	Negative IOD	Neutral IOD	Pos
Negative SAM	8.56	8.19	
Positive SAM	4.80	6.16	

All %

ONI Phase / SAM Phase	El Nino	La Nina	Neu
Negative SAM	2.75	2.52	
Positive SAM	1.86	2.37	

All #

ONI Phase / SAM Phase	El Nino	La Nina	Ne
Negative SAM	7.72	7.71	
Positive SAM	4.13	6.65	

All %

SAM Phase	Season	IOD Phase: Negative IOD	Neutral IOD	Pos
Negative SAM	Autumn	2.00	3.04	
	Spring	3.75	2.70	
	Summer	5.00	2.54	
	Winter	2.40	2.97	
Positive SAM	Autumn	0.00	2.13	
	Spring	2.00	2.59	
	Summer	0.00	2.41	
	Winter	1.50	2.94	

All #

SAM Phase	Season	IOD Phase: Negative IOD	Neutral IOD	Pos
Negative SAM	Autumn	3.85	8.34	
	Spring	12.47	7.97	
	Summer	11.29	7.61	
	Winter	7.71	8.82	
Positive SAM	Autumn	0.00	4.93	
	Spring	3.80	7.01	
	Summer	0.00	5.56	
	Winter	6.05	8.43	

All %

SAM Phase	Season	ONI Phase: El Nino	La Nina	Neutral
Negative SAM	Autumn	1.75	4.00	2.78
	Spring	2.41	2.50	3.00
	Summer	3.20	1.50	2.60
	Winter	3.33	2.57	2.72
Positive SAM	Autumn	1.22	1.20	2.46
	Spring	1.71	2.87	2.05
	Summer	2.47	2.41	2.37
	Winter	1.50	2.70	2.67

All #

SAM Phase	Season	ONI Phase: El Nino	La Nina	Neutra
Negative SAM	Autumn	3.09	9.46	7.94
	Spring	6.94	7.81	8.41
	Summer	10.49	4.49	7.23
	Winter	8.18	9.29	8.11
Positive SAM	Autumn	2.18	2.76	5.87
	Spring	3.89	8.55	5.35
	Summer	5.38	5.67	5.31
	Winter	4.21	9.83	7.42

All %

Season	All SSA %	NTT SSA %	All N SSA
Autumn	7.51	13.44	0
Spring	14.00	23.06	1
Summer	19.28	27.90	1
Winter	6.85	16.15	1

SAM Phase	All SSA %	NTT SSA %	All NTT SSA %
Negative SAM	11.88	19.03	1.49
Positive SAM	11.86	21.11	1.25

IOD Phase	All SSA %	NTT SSA %	All NTT SSA %
Negative IOD	8.54	13.30	0.93
Neutral IOD	12.48	20.66	1.45
Positive IOD	9.78	19.71	0.96

ONI Phase	All SSA %	NTT SSA %	All NTT SSA %
El Nino	13.24	25.67	1.54
La Nina	13.54	22.01	1.55
Neutral	10.52	17.15	1.18

EASTERN AUSTRALIA – EAST OF 135°E

EASTERN AUSTRALIA – EAST OF 135°E

Season	All %	All #
Autumn	3.44	1.22
Spring	3.89	1.20
Summer	4.05	1.37
Winter	3.90	1.08

SAM Phase	All %	All #
Negative SAM	4.09	1.10
Positive SAM	3.62	1.30

IOD Phase	All %	All #
Negative IOD	3.66	1.05
Neutral IOD	3.99	1.30
Positive IOD	2.88	0.79

ONI Phase	All %	All #
El Nino	3.44	1.10
La Nina	3.84	1.16
Neutral	3.97	1.29

SAM Phase	Season	All %
Negative SAM	Autumn	4.27
	Spring	4.13
	Summer	4.48
	Winter	3.63
Positive SAM	Autumn	2.99
	Spring	3.64
	Summer	3.81
	Winter	4.15

IOD Phase	Season	All %
Negative IOD	Autumn	0.27
	Spring	4.43
	Summer	7.26
	Winter	3.61
Neutral IOD	Autumn	3.70
	Spring	4.19
	Summer	4.06
	Winter	4.07
Positive IOD	Autumn	2.23
	Spring	2.43
	Summer	3.43
	Winter	3.43

ONI Phase	Season	All %	A
El Nino	Autumn	1.00	0
	Spring	3.50	1
	Summer	5.00	1
	Winter	2.88	0
La Nina	Autumn	2.62	1
	Spring	4.37	1
	Summer	3.66	1
	Winter	4.30	0
Neutral	Autumn	4.17	1
	Spring	3.79	1
	Summer	3.66	1
	Winter	4.06	1

IOD Phase SAM Phase	Negative IOD	Neutral IOD	Po
			All #
Negative SAM	1.08	1.16	
Positive SAM	1.00	1.40	

IOD Phase SAM Phase	Negative IOD	Neutral IOD	Po
			All %
Negative SAM	4.36	4.26	
Positive SAM	2.63	3.80	

ONI Phase SAM Phase	El Nino	La Nina	N
			All #
Negative SAM	1.02	0.83	
Positive SAM	1.19	1.33	

ONI Phase SAM Phase	El Nino	La Nina	N
			All %
Negative SAM	3.89	3.54	
Positive SAM	2.97	3.99	

SAM Phase	IOD Phase Season	Negative IOD	Neutral IOD	P
				All #
Negative SAM	Autumn	0.00	1.42	
	Spring	2.00	1.21	
	Summer	3.00	1.07	
	Winter	0.60	0.97	
Positive SAM	Autumn	0.00	1.29	
	Spring	1.20	1.41	
	Summer	0.00	1.53	
	Winter	0.75	1.39	

SAM Phase	IOD Phase Season	Negative IOD	Neutral IOD	P
				All %
Negative SAM	Autumn	0.27	4.94	
	Spring	7.06	4.23	
	Summer	7.26	4.41	
	Winter	4.09	3.64	
Positive SAM	Autumn	0.00	3.12	
	Spring	2.32	4.14	
	Summer	0.00	3.87	
	Winter	3.02	4.50	

SAM Phase	ONI Phase Season	El Nino	La Nina	Neutral
				All #
Negative SAM	Autumn	0.25	1.25	1.35
	Spring	1.18	0.92	1.47
	Summer	1.20	0.83	1.07
	Winter	0.89	0.43	1.08
Positive SAM	Autumn	0.78	0.90	1.43
	Spring	0.71	1.53	1.10
	Summer	1.73	1.50	1.42
	Winter	1.00	1.10	1.30

SAM Phase	ONI Phase Season	El Nino	La Nina	Neutral
				All %
Negative SAM	Autumn	0.40	4.09	4.97
	Spring	3.97	3.73	4.64
	Summer	5.94	2.61	4.25
	Winter	3.00	3.71	3.83
Positive SAM	Autumn	1.27	2.03	3.66
	Spring	2.36	4.88	3.18
	Summer	4.38	3.95	3.20
	Winter	2.69	4.72	4.26

Season	All SSA %	NTT SSA %	All N SSA
Autumn	5.60	14.13	0
Spring	11.44	29.02	1
Summer	16.42	33.96	1
Winter	3.58	16.79	0

SAM Phase	All SSA %	NTT SSA %	All NTT SSA %
Negative SAM	9.15	22.62	0.93
Positive SAM	9.27	24.77	0.90

IOD Phase	All SSA %	NTT SSA %	All NTT SSA %
Negative IOD	5.83	17.35	0.63
Neutral IOD	9.83	24.01	0.96
Positive IOD	7.24	25.90	0.75

ONI Phase	All SSA %	NTT SSA %	All NTT SSA %
El Nino	10.45	32.51	1.12
La Nina	11.01	25.81	0.99
Neutral	7.88	19.75	0.79

WESTERN AUSTRALIA – WEST OF 135°E

WESTERN AUSTRALIA – WEST OF 135°E

Season	All %	All #
Autumn	2.25	1.08
Spring	3.06	1.26
Summer	2.23	1.10
Winter	3.99	1.57

SAM Phase	All %	All #
Negative SAM	3.73	1.62
Positive SAM	2.26	0.99

IOD Phase	All %	All #
Negative IOD	3.37	1.41
Neutral IOD	3.00	1.29
Positive IOD	1.98	0.98

ONI Phase	All %	All #
El Nino	2.53	1.22
La Nina	3.16	1.24
Neutral	2.90	1.28

SAM Phase	Season	All %
Negative SAM	Autumn	3.22
	Spring	3.53
	Summer	3.25
	Winter	4.70
Positive SAM	Autumn	1.72
	Spring	2.59
	Summer	1.66
	Winter	3.36

IOD Phase	Season	All %
Negative IOD	Autumn	3.58
	Spring	3.23
	Summer	4.03
	Winter	3.36
Neutral IOD	Autumn	2.28
	Spring	3.32
	Summer	2.22
	Winter	4.55
Positive IOD	Autumn	1.42
	Spring	1.97
	Summer	2.11
	Winter	2.20

ONI Phase	Season	All %	A
El Nino	Autumn	1.46	
	Spring	2.52	1
	Summer	2.39	1
	Winter	3.71	1
La Nina	Autumn	2.05	
	Spring	3.86	1
	Summer	1.76	0
	Winter	5.26	1
Neutral	Autumn	2.47	1
	Spring	2.83	1
	Summer	2.50	1
	Winter	3.67	1

IOD Phase SAM Phase	Negative IOD	Neutral IOD	Po	All #
Negative SAM	1.85	1.65		
Positive SAM	0.78	1.04		

IOD Phase SAM Phase	Negative IOD	Neutral IOD	Po	All %
Negative SAM	4.20	3.90		
Positive SAM	2.17	2.35		

ONI Phase SAM Phase	El Nino	La Nina	Ne	All #
Negative SAM	1.73	1.69		
Positive SAM	0.68	1.02		

ONI Phase SAM Phase	El Nino	La Nina	Ne	All %
Negative SAM	3.79	4.17		
Positive SAM	1.16	2.64		

SAM Phase	IOD Phase Season	Negative IOD	Neutral IOD	Po	All #
Negative SAM	Autumn	2.00	1.62		
	Spring	1.75	1.48		
	Summer	2.00	1.46		
	Winter	1.80	2.00		
Positive SAM	Autumn	0.00	0.83		
	Spring	0.80	1.17		
	Summer	0.00	0.88		
	Winter	0.75	1.52		

SAM Phase	IOD Phase Season	Negative IOD	Neutral IOD	Po	All %
Negative SAM	Autumn	3.58	3.36		
	Spring	5.42	3.72		
	Summer	4.03	3.17		
	Winter	3.62	5.19		
Positive SAM	Autumn	0.00	1.79		
	Spring	1.48	2.87		
	Summer	0.00	1.70		
	Winter	3.02	3.91		

SAM Phase	ONI Phase Season	El Nino	La Nina	Neutral	All #
Negative SAM	Autumn	1.50	2.75	1.43	
	Spring	1.24	1.58	1.53	
	Summer	2.00	0.67	1.53	
	Winter	2.44	2.14	1.64	
Positive SAM	Autumn	0.44	0.30	1.00	
	Spring	1.00	1.33	0.95	
	Summer	0.73	0.91	0.95	
	Winter	0.50	1.50	1.37	

SAM Phase	ONI Phase Season	El Nino	La Nina	Neutral	All %
Negative SAM	Autumn	2.69	5.37	2.93	
	Spring	2.93	4.09	3.76	
	Summer	4.47	1.88	2.99	
	Winter	5.17	5.59	4.29	
Positive SAM	Autumn	0.91	0.73	2.18	
	Spring	1.53	3.67	2.17	
	Summer	1.00	1.73	2.11	
	Winter	1.52	5.03	3.17	

Season	All SSA %	NTT SSA %	All NTT SSA %
Autumn	1.90	12.08	0.2
Spring	2.56	15.22	0.4
Summer	2.86	16.60	0.3
Winter	3.27	15.33	0.6

SAM Phase	All SSA %	NTT SSA %	All NTT SSA %
Negative SAM	2.73	14.86	0.55
Positive SAM	2.59	14.95	0.34

IOD Phase	All SSA %	NTT SSA %	All NTT SSA %
Negative IOD	2.71	8.89	0.30
Neutral IOD	2.66	15.91	0.48
Positive IOD	2.54	10.62	0.21

ONI Phase	All SSA %	NTT SSA %	All NTT SSA %
El Nino	2.79	15.68	0.40
La Nina	2.52	17.17	0.54
Neutral	2.64	13.48	0.39

//

SOUTHERN OCEAN – SOUTH OF CONTINENTAL AUSTRALIAN COASTLINE

SOUTHERN OCEAN – SOUTH OF CONTINENTAL AUSTRALIAN COASTLINE

Season	All %	All #
Autumn	2.82	1.15
Spring	2.37	0.74
Summer	4.04	1.59
Winter	2.30	0.86

SAM Phase	All %	All #
Negative SAM	3.24	1.14
Positive SAM	2.62	1.04

IOD Phase	All %	All #
Negative IOD	2.54	0.95
Neutral IOD	3.09	1.17
Positive IOD	1.78	0.64

ONI Phase	All %	All #
El Nino	2.70	1.05
La Nina	2.84	1.02
Neutral	2.97	1.12

SAM Phase	Season	All %
Negative SAM	Autumn	3.34
	Spring	2.89
	Summer	5.11
	Winter	2.14
Positive SAM	Autumn	2.53
	Spring	1.84
	Summer	3.45
	Winter	2.43

IOD Phase	Season	All %
Negative IOD	Autumn	2.19
	Spring	3.59
	Summer	5.65
	Winter	1.27
Neutral IOD	Autumn	2.99
	Spring	2.38
	Summer	4.08
	Winter	2.66
Positive IOD	Autumn	1.42
	Spring	1.61
	Summer	3.32
	Winter	1.46

ONI Phase	Season	All % A
El Nino	Autumn	0.88
	Spring	2.10
	Summer	4.64
	Winter	2.00
La Nina	Autumn	2.39
	Spring	2.87
	Summer	3.40
	Winter	2.26
Neutral	Autumn	3.34
	Spring	2.17
	Summer	4.12
	Winter	2.39

All #

IOD Phase / SAM Phase	Negative IOD	Neutral IOD	Po
Negative SAM	1.23	1.20	
Positive SAM	0.56	1.15	

All %

IOD Phase / SAM Phase	Negative IOD	Neutral IOD	Po
Negative SAM	3.24	3.44	
Positive SAM	1.54	2.85	

All #

ONI Phase / SAM Phase	El Nino	La Nina	Ne
Negative SAM	1.25	0.86	
Positive SAM	0.84	1.11	

All %

ONI Phase / SAM Phase	El Nino	La Nina	Ne
Negative SAM	3.41	2.84	
Positive SAM	1.93	2.85	

All #

SAM Phase	IOD Phase / Season	Negative IOD	Neutral IOD
Negative SAM	Autumn	1.33	1.21
	Spring	1.75	0.82
	Summer	2.00	1.82
	Winter	0.60	1.03
Positive SAM	Autumn	0.00	1.21
	Spring	0.80	0.59
	Summer	0.00	1.53
	Winter	0.25	0.94

All %

SAM Phase	IOD Phase / Season	Negative IOD	Neutral IOD	Po
Negative SAM	Autumn	2.19	3.73	
	Spring	5.83	2.76	
	Summer	5.65	5.02	
	Winter	1.32	2.49	
Positive SAM	Autumn	0.00	2.65	
	Spring	1.80	1.95	
	Summer	0.00	3.57	
	Winter	1.21	2.83	

All #

SAM Phase	ONI Phase / Season	El Nino	La Nina	Neutral
Negative SAM	Autumn	1.00	1.50	1.09
	Spring	0.76	0.75	1.20
	Summer	2.10	1.00	1.87
	Winter	1.33	0.57	0.84
Positive SAM	Autumn	0.33	0.90	1.43
	Spring	0.57	1.00	0.24
	Summer	1.27	1.50	1.63
	Winter	0.83	0.60	0.90

All %

SAM Phase	ONI Phase / Season	El Nino	La Nina	Neutral
Negative SAM	Autumn	1.64	4.32	3.46
	Spring	2.38	2.56	3.71
	Summer	6.88	3.25	4.67
	Winter	2.26	2.09	2.11
Positive SAM	Autumn	0.54	1.62	3.27
	Spring	1.42	3.11	1.07
	Summer	3.14	3.44	3.70
	Winter	1.61	2.38	2.62

Season	All SSA %	NTT SSA %	All N SSA
Autumn	7.51	4.32	0
Spring	14.00	9.24	0
Summer	19.28	17.65	0
Winter	6.85	11.07	0

SAM Phase	All SSA %	NTT SSA %	All NTT SSA %
Negative SAM	11.88	9.84	0.32
Positive SAM	11.86	12.66	0.33

IOD Phase	All SSA %	NTT SSA %	All NTT SSA %
Negative IOD	8.54	7.35	0.19
Neutral IOD	12.48	11.44	0.35
Positive IOD	9.78	12.75	0.23

ONI Phase	All SSA %	NTT SSA %	All NTT SSA %
El Nino	13.24	16.27	0.44
La Nina	13.54	14.72	0.42
Neutral	10.52	7.93	0.24

COASTAL – INLAND OF CONTINENTAL AUSTRALIAN COASTLINE

COASTAL – INLAND OF CONTINENTAL AUSTRALIAN COASTLINE

Season	All %	All #
Autumn	2.87	1.15
Spring	4.58	1.72
Summer	2.24	0.89
Winter	5.60	1.79

SAM Phase	All %	All #
Negative SAM	4.58	1.58
Positive SAM	3.27	1.25

IOD Phase	All %	All #
Negative IOD	4.48	1.50
Neutral IOD	3.90	1.42
Positive IOD	3.08	1.13

ONI Phase	All %	All #
El Nino	3.28	1.27
La Nina	4.15	1.38
Neutral	3.90	1.44

SAM Phase	Season	All %
Negative SAM	Autumn	4.15
	Spring	4.77
	Summer	2.62
	Winter	6.19
Positive SAM	Autumn	2.17
	Spring	4.39
	Summer	2.02
	Winter	5.08

IOD Phase	Season	All %
Negative IOD	Autumn	1.67
	Spring	4.06
	Summer	5.65
	Winter	5.70
Neutral IOD	Autumn	2.99
	Spring	5.12
	Summer	2.20
	Winter	5.95
Positive IOD	Autumn	2.23
	Spring	2.78
	Summer	2.21
	Winter	4.17

ONI Phase	Season	All %
El Nino	Autumn	1.58
	Spring	3.92
	Summer	2.76
	Winter	4.59
La Nina	Autumn	2.28
	Spring	5.35
	Summer	2.02
	Winter	7.30
Neutral	Autumn	3.29
	Spring	4.45
	Summer	2.04
	Winter	5.35

IOD Phase / SAM Phase	Negative IOD	Neutral IOD	Po...	All #
Negative SAM	1.69	1.60		
Positive SAM	1.22	1.29		

IOD Phase / SAM Phase	Negative IOD	Neutral IOD	Po...	All %
Negative SAM	5.32	4.73		
Positive SAM	3.26	3.30		

ONI Phase / SAM Phase	El Nino	La Nina	Ne...	All #
Negative SAM	1.50	1.66		
Positive SAM	1.03	1.25		

ONI Phase / SAM Phase	El Nino	La Nina	Ne...	All %
Negative SAM	4.28	4.88		
Positive SAM	2.19	3.78		

SAM Phase	IOD Phase / Season	Negative IOD	Neutral IOD	All #
Negative SAM	Autumn	0.67	1.83	
	Spring	2.00	1.88	
	Summer	3.00	0.71	
	Winter	1.80	1.94	
Positive SAM	Autumn	0.00	0.90	
	Spring	1.20	2.00	
	Summer	0.00	0.88	
	Winter	1.25	1.97	

SAM Phase	IOD Phase / Season	Negative IOD	Neutral IOD	All %
Negative SAM	Autumn	1.67	4.57	
	Spring	6.64	5.19	
	Summer	5.65	2.56	
	Winter	6.39	6.34	
Positive SAM	Autumn	0.00	2.26	
	Spring	2.00	5.05	
	Summer	0.00	2.00	
	Winter	4.84	5.57	

SAM Phase	ONI Phase / Season	El Nino	La Nina	Neutral	All #
Negative SAM	Autumn	0.75	2.50	1.70	
	Spring	1.65	1.75	1.80	
	Summer	1.10	0.50	0.73	
	Winter	2.00	2.00	1.88	
Positive SAM	Autumn	0.89	0.30	1.00	
	Spring	1.14	1.87	1.81	
	Summer	1.20	0.91	0.74	
	Winter	0.67	2.00	1.77	

SAM Phase	ONI Phase / Season	El Nino	La Nina	Neutral	All %
Negative SAM	Autumn	1.45	5.13	4.44	
	Spring	4.51	5.25	4.69	
	Summer	3.53	1.24	2.57	
	Winter	5.91	7.20	6.00	
Positive SAM	Autumn	1.64	1.13	2.58	
	Spring	2.47	5.44	4.28	
	Summer	2.24	2.23	1.62	
	Winter	2.59	7.37	4.81	

Season	All SSA %	NTT SSA %	All N... SSA...
Autumn	7.51	22.15	0...
Spring	14.00	30.02	1...
Summer	19.28	45.99	1...
Winter	6.85	18.09	1...

SAM Phase	All SSA %	NTT SSA %	All NTT SSA %
Negative SAM	11.88	25.33	1.16
Positive SAM	11.86	27.65	0.91

IOD Phase	All SSA %	NTT SSA %	All NTT SSA %
Negative IOD	8.54	16.67	0.74
Neutral IOD	12.48	27.73	1.08
Positive IOD	9.78	23.73	0.73

ONI Phase	All SSA %	NTT SSA %	All NTT SSA %
El Nino	13.24	32.90	1.08
La Nina	13.54	26.83	1.12
Neutral	10.52	24.06	0.94